Chapter 1

Introduction

1.1 Background

The existence of wave groups has been known to sailors for a long time. These wave groups produce long waves, so called infragravity waves and are also often referred to as “surf beat". Munk (1949) and Tucker (1950) were the first to report field measurements of these low frequency motions. After they had been reported for the first time they were confirmed in a number of field experiments. These long waves are known to cause ship-mooring problems in harbours through-out the world. That the wave groups can cause long wave excitation at the harbour entrance, was first shown theoretically by Bowers (1977). More research on this phenomenon was carried out by Mei and Agnon (1989). During storms wave motions induced by these wave groups may result in damage to the ship itself or the surrounding mooring facilities, as the ships are more susceptible to the time scale of the wave groups than to that of the individual carrier waves. As this may have a bad influence on loading and unloading operations, research is needed on the generation and propagation of these waves in and near harbours. For the construction of new ports a rule of thumb should result for the prediction of these long waves from a number of research studies on the long wave action in harbours and the resulting vessel response. This specific study focuses on the generation of long waves generated by wave grouping inside Saldanha Bay (South Africa). The computer program Surf Beat as described by Reniers et al. (2000) is used to model generation and propagation of these long waves on a stretch of coastline and inside the harbour areas. It has been tested in harbours, like Barbers Point Harbour (Hawaii,USA) or Tomakomai Port (Japan), giving quite good results for the prediction of long waves in port areas.

1.2 Problem Definition

Mooring problems are one of the most important issues in port construction and port operation when harbours are facing the open sea. Operational standards usually define that cargo handling for large vessels is possible when significant wave height is below some level, i.e., 0.5 [m]. However, several ports have reported mooring problems when the wave condition is below the operational level. Many authors have related this problem with the action of long waves inside the port areas.
Long waves are known to be the cause of mooring problems in the Saldanha Bay. These waves have periods between 50 and 500 s. This is a range of natural oscillation for the horizontal motions of the moored ships. Therefore, moored vessels at the jetty experience conditions of resonance for these motions during the occurrence of these long waves. Such ship motions can be up to several meters and cause adverse conditions, both for vessels and the fender system. Long waves have been noticed to occur usually together with the storm conditions and the passing of weather fronts. If the occurrence and magnitude of these long waves could be predicted, measures can be taken to mitigate or prevent conditions of large moored ship motions at the jetty.

1.3 Objectives

The program Surf Beat will be used to model the long wave generation and propagation inside Saldanha Bay. Main objectives can be summarized in:

- Sensibility analysis of the model for the main parameters (inputs).
- Study of the best situation of a new jetty in the main bay.
- Selection of the best place to get good and reliable long waves measures.

Secondary research objectives are:

- Determine the most important parameters needed for the input data for the hydrodynamic model and point the procedure required for that by analyzing the data available and identifying the different inputs for the model and selecting the cases to treat in the research.
- Determine the parameters and variables necessaries for a fast and precise calibration of the hydrodynamic model of the existing harbour using Delft-3D and SURFBEAT computer programs.

1.4 Description of Modeled Harbour

Saldanha Bay is placed in the southwestern area of South Africa (Western Cape area). It faces the Atlantic Ocean in an area where swell action becomes remarkable when weather fronts are passing this area of the Atlantic Ocean. Some bulk carriers have reported mooring problems under these conditions, caused by large surging motion due long wave action at the ore loading jetty. Two wave buoys have been installed in the bay for the measuring of the wave action.

1.5 Outline

This thesis is divided in eight chapters. Chapter 2 contains the literature study performed for the study. Chapter 3 deals with the description and analysis of data. Chapter 4 provides an overview of the translation of the boundary conditions into usable model input parameters. The calibration, sensitivity analysis and validation of the model is explained in chapter 5. Chapter 6 presents the different runs made with the hydrodynamic model SURFBEAT and the analysis to get the best new buoy location to get good and real measurements. Chapter 7 has the different runs made with the hydrodynamic model SURFBEAT and the analysis to get the best new jetty location. Chapter 8 contains the conclusions and recommendations.

Chapter 2

Literature Study

2.1 Chapter Overview

This chapter summarizes the most important results from the literature study performed before the start of the thesis project and during it. Underlying basic theories, as linear wave theory, have been assumed to be known by the reader. The chapter is organized in two parts; the first one includes a definition of the long waves, its classification and action in a harbour basin; at the end some other effects found by another researchers in similar investigations are mentioned and their application in this specific case is analyzed. The second part contains the strip theory for ships and its modulation.
It is important to note that most of the papers and publications about the long wave action deals mainly with the observation and the description of the phenomena. Only a few authors propone explications about the observable fact, then among the different effects described in the following sections, there are some that can be theoretically and numerically accurate enough treated; other effects can not be modeled and are mentioned with the purpose of recognized them as sources of error.

2.2 Wave Classification and Definition

Ocean waves can be classified in different ways. One classification uses the forces which generate the waves, another classification considers the restoring forces responsible for returning the water particles to their average position in the water column, and another classification is based on the frequency spectrum representation of all oceanic waves (characteristic periods) and distinguishes between capillary waves, gravity waves, long period waves, tides and transtidal waves. Naturally, according every generation process involved, waves have different characteristics as frequency, length and amplitude (see Figure 2.1).

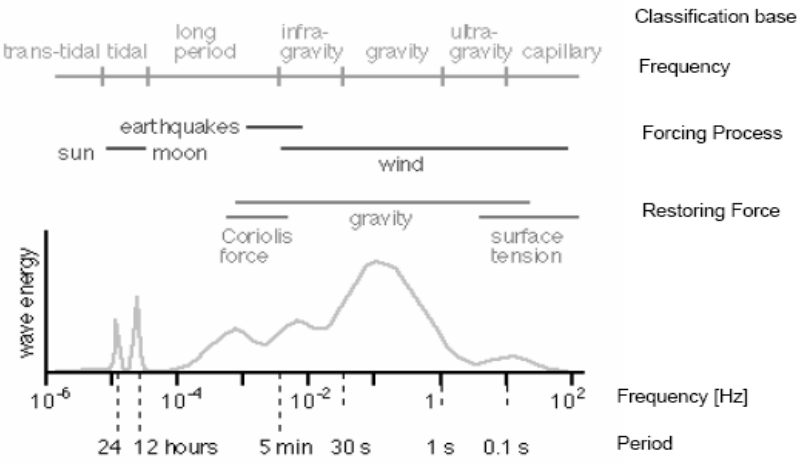

Figure 2.1: Ocean waves classification

2.2.1 Sea and Swell Waves

The highest energy content of the wave spectrum corresponds to the gravity waves generated by wind, and this group contains the sea and swell waves.

Sea waves are produced by local winds. Their periods are in between 1 [sec] and 8 [sec].Measurements show they are composed of a chaotic mix of height and period. In general, the stronger the wind the greater the amount of energy transfer and thus larger the waves produced. As sea waves move away from where they are generated they change in character and become swell waves.

Swell waves are generated by winds and storms in another area. As the waves travel from their point of origin, they organize themselves into groups or wave trains of similar heights and periods. These groups of waves are able to travel thousands of kilometers unchanged in height and period, which is in between 8 [sec] and 30 [sec]. Swell waves are uniform in appearance, have been sorted by period, and have a longer wavelength and longer period than sea waves.
Because these waves are generated by winds in a different location, it is possible to experience high swell waves even when the local winds are calm.

2.2.2 Definition of Infragravity long-waves

Long waves are those with periods higher than 30 [sec], they include tides, different oceanic waves and other second order waves with wave periods between 30 second and 5 minutes known as *infragravity waves*; they play an important factor in several near shore processes, and are discussed below.

2.2.2.1 Bound Infragravity Waves

This type of waves is generated by the grouped short wind waves (swell waves).They propagate at the group velocity, they are 180º out of phase with the short-wave envelope and the amplitudes are proportional to the square of the short wave heights.
The development of the theory that describes these waves started with the first observations made by Munk [1949] and Tucker [1950] that the temporal variation of incident short-wave heights in groups of waves is responsible for the presence of infragravity waves in the near shore. Munk introduced the term ***surfbeat*** to describe the long waves that propagate back out to sea when groups of ordinary waves break on a beach (see Figure 2.2)

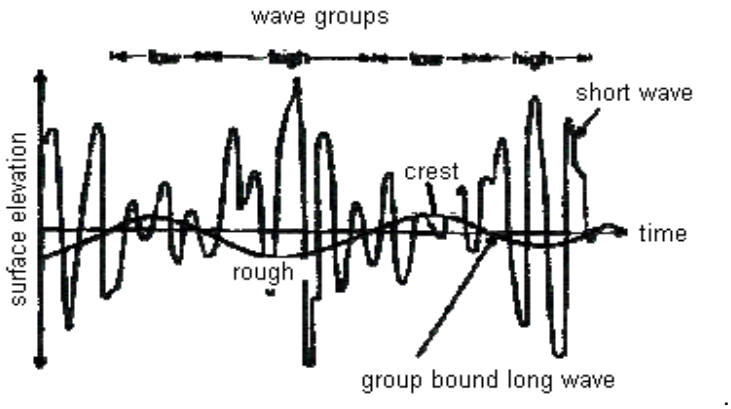

Figure 2.2 Bound long wave

Longuet-Higgins and Stewart [1962,1964] suggested that bound infragravity waves are forced by the spatial changes of *momentum flux* associated with normally incident short wave groups. Within the surf zone the wave group modulation is destroyed by wave breaking, consequently the bound infragravity wave is released as a free wave. In case of small incidence angles, the free infragravity wave reflects and is able to escape (or leake) to deeper water. However, for increased angles of incidence the free infragravity wave may become trapped (See Figure 2.4).

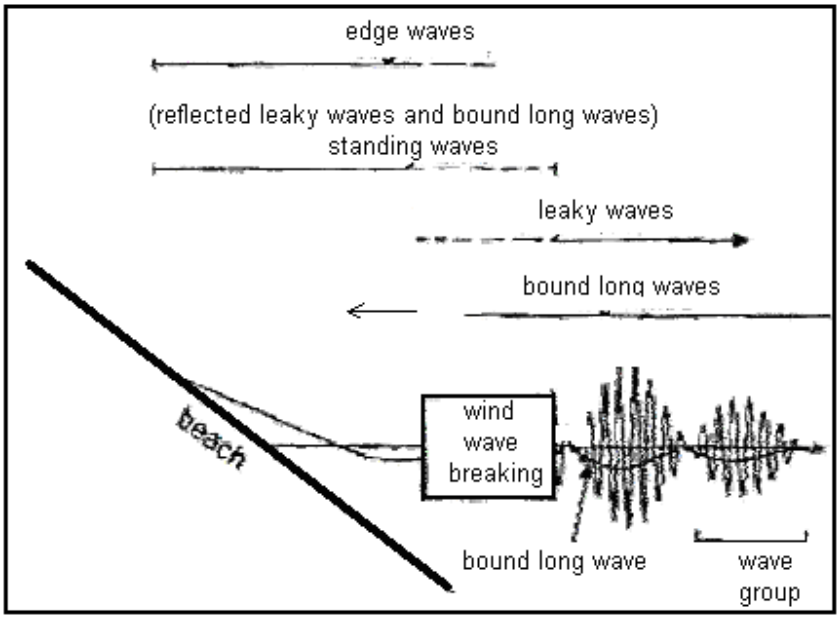

Figure 2.3 Bound and free infragravity waves

2.2.2.2 Leaky or Free Infragravity Waves

As described in section 2.1.2.1, when the group of short waves moves towards the shoreline with a small approach angle and breaks in the surf zone, then the bound infragravity wave is released, reflecting in the shoreline and traveling seaward as the leaky or free wave. Similarly, bound waves traveling over an uneven bathymetry can be partially released as free waves (Dingemans et al [1991])

2.2.2.3 Edge Waves

The outgoing free infragravity wave may be trapped in shallow water by reflection and refraction effects when the angle of incidence of the short wave group is large enough. Gallagher [1971] showed theoretically that certain directional distribution of the incident wave field could resonantly excite edge waves; if the difference wave number of the interaction includes a long shore component, edge waves can be generated either by the same nonlinearities described before in the shoaling region.

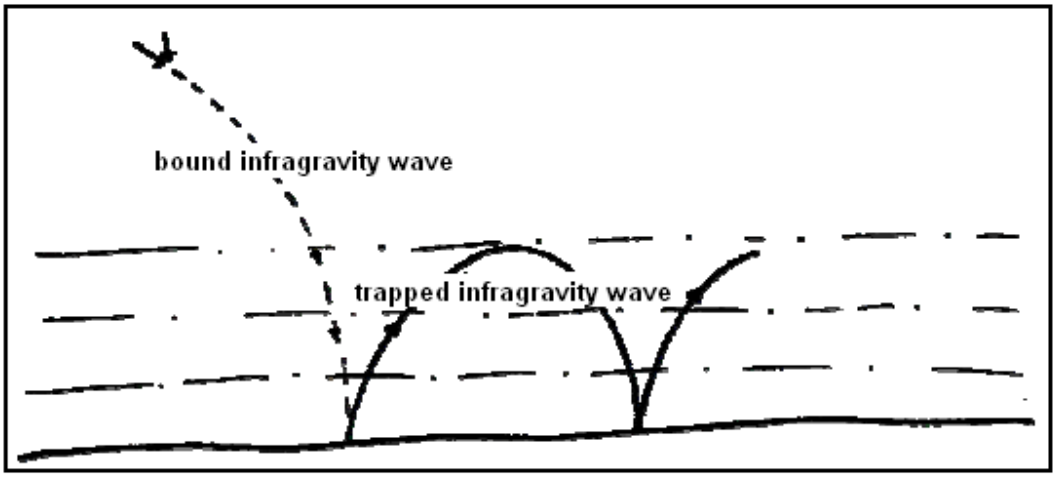

Figure 2.4 Edge Waves (from Reniers, Roelvink and van Dongeren [2000])

2.2.3 Long infragravity waves: Saldanha Bay

As we can see in Figure 2.1, waves can be classified by characteristic period (frequency). Natural periods for the ships moored in the jetty in surge, varies between 70 - 150 seconds depending on the ship. The problem is that infragravity long waves periods are very close to these natural periods of ship's motions, which are excited for these ones, causing the presence of resonance.

Other kind of waves, do not cause any problem for different reasons. First and common reason for all the waves is their period. Moreover, for short waves (sea and swell), breaking process takes place at shallow water, so just some short waves reach the ore jetty area.

For the sway motion, don not exist this problem because there is not much wave activity in the ore jetty perpendicular direction and the fender systems natural periods are smaller than long wave periods in the area.

2.3 Wave properties

2.3.1 Waves in general

If the surface elevation is assumed to vary sinusoidally the wave period T is the time between the passing of a wave trough and a wave crest. The wave height H is the vertical distance between this wave crest and wave trough.
Next to this characterization, waves can be divided into two general categories, namely short waves and long waves. The first type is a wave of which the length is much smaller than or comparable to the water depth at that specific location. A wind-generated wave is generally a short or deep water wave. In general a wave is a deep water wave if the water depth exceeds half the wavelength.
The tidal elevation on the other hand is also a wave phenomenon, which behaves like a long or shallow water wave. The expression shallow water wave tells us that there is a lot of interaction between the bottom and the wave. If the water depth is smaller than 1/20th of the wavelength the wave behaves much like a long wave. There is of course a large range of waves that belong to neither category. These are called waves in intermediate water depth.

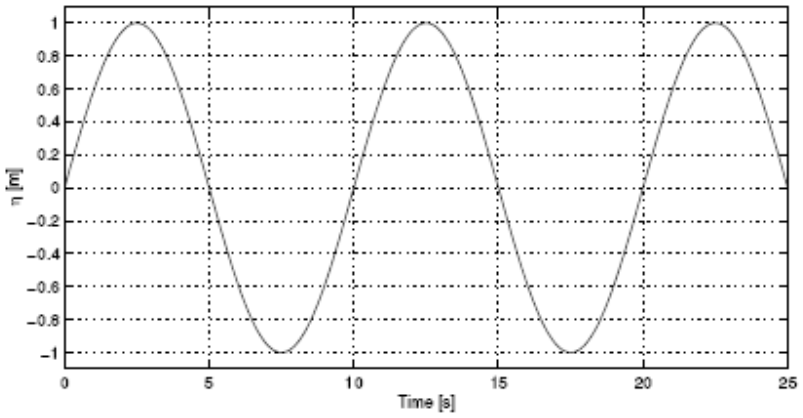

Figure 2.5: Sine waveform

2.3.2 Linear wave theory

A number of theories exist for the purpose of understanding the wave hydromechanics. Just the linear theory applicable for waves with small surface elevation will be briefly mentioned. It is based on the assumption of an incompressible fluid with no rotation. These assumptions result in the Laplace equation shown in equation 2.1.

$$\frac{\partial^2 \phi}{\partial x^2} + \frac{\partial^2 \phi}{\partial y^2} = 0 \qquad (2.1)$$

Here Φ is the velocity potential. If the boundary conditions near the surface are linearized (valid for small values of H / L and H / h), equation 2.2 describes these boundary condition.

$$\frac{\partial^2 \phi}{\partial t^2} + g \frac{\partial\ \phi}{\partial z} = 0 \leftarrow z = 0 \quad (2.2)$$

A sine shaped surface elevation is now introduced:

$$\eta(x,t) = a\ \sin(\omega t - kx) \quad (2.3)$$

In which:

η	= the surface elevation.
a = ½ H	= the amplitude of the surface elevation
W = 2π/T	= the angular frequency
k = 2π/L	= the wave number

This equation describes a sine shaped wave form, that moves along the x-axis with a constant speed c = w/k. This is the so called celerity of the wave. For this wave form the flow potential can be described as follows for constant depth h:

$$\phi(x,z,t) = \frac{\omega a}{k}\ \frac{\cosh\ \mathrm{k}(h+z)}{\sinh\ \mathrm{kh}}\ \cos(\omega t - kx) \quad (2.4)$$

Equation 2.4 can be differentiated in x or in z to find the velocity components in these directions. If the wave is freely propagating, the relationship between wave number and frequency can be described by the dispersion relation (see equation 2.5). This relation is in the linearized form independent of the wave height.

$$\eta = \frac{S_{xx}}{\rho(gh - c_{g^2})} + \text{constant}\ \omega^2 = gk \tanh\ kh \quad (2.5)$$

2.3.3 Energy and energy flux

A striking feature of gravity waves is that they can transfer energy in space. This section will deal with the energy contained by a certain wave field. The accompanying energy transfer is also described here.

Energy: The total energy present in a wave consists of two contributions, kinetic energy E_k and potential energy E_p. For purposes of simplicity they have been averaged over time. The potential energy is the energy needed to raise a certain mass above a certain reference level. The kinetic energy on the other hand is the energy of a mass at a certain speed and is equal to the potential energy. The total energy in a gravity wave can be calculated with equation 2.6 and is proportional to the square of the wave height.

$$E_{tot} = E_k + E_p = \frac{1}{4}\rho g a^2 + \frac{1}{4}\rho g a^2 = \frac{1}{2}\rho g a^2 = \frac{1}{8}\rho H^2 \quad (2.6)$$

Where:

H = 2a = wave height
P = density

Energy flux: The energy flux represents the transfer of energy through a vertical plane in the spatial domain. It is composed of the following contributions:

1. Advection of energy of water particles travelling through the plane.
2. Work done by pressure exerted on particles moving through the plane.

If the components shown above are summed and integrated from the bottom to the free surface the result is the total instantaneous transfer of energy through a plan with constant x and a width of ∂y. The mean value of this total energy transfer in the propagation direction per time and width is then given by:

$$F = \int_{-h}^{\eta} (p + \rho g z + \frac{1}{2}\rho q^2) u dz \quad (2.7)$$

$$F = \int_{-h}^{\eta} (\frac{1}{2}\rho g a^2)(\frac{1}{2} + \frac{kh}{\sinh\ 2\mathrm{kh}})(\frac{\omega}{k}) = Enc \quad (2.8)$$

In which:

n = ratio group velocity / phase velocity
c = phase velocity
F = energy flux
u = velocity

2.3.4 Momentum flux

A general expression for the instantaneous flux of momentum across a unit area of a vertical plane in a fluid is:

$$p + \rho u^2 \quad (2.9)$$

Equation 2.9 shows that the momentum flux consist of two parts, namely a pressure part and a part due to bodily transfer of momentum ρu at a rate u. If this instantaneous flux is integrated between the bottom (z = -h) and the free surface (z = η), the total momentum flux across a plane x = constant is obtained as shown in equation 2.10.

$$\int_{-h}^{\eta} (p + \rho u^2) dz \quad (2.10)$$

2.3.5 Wave groups

The first plot in figure 2.6 shows a phenomenon caused by two interacting sine wave functions. The group pattern clearly emerges from this graph. The group pattern for a typical wind wave spectrum is less distinct, but through various transformations wave grouping can be extracted from the time series generated from the filtered spectrum. A typical wave train showing "wave groups" is shown in the bottom graph in figure 2.6.

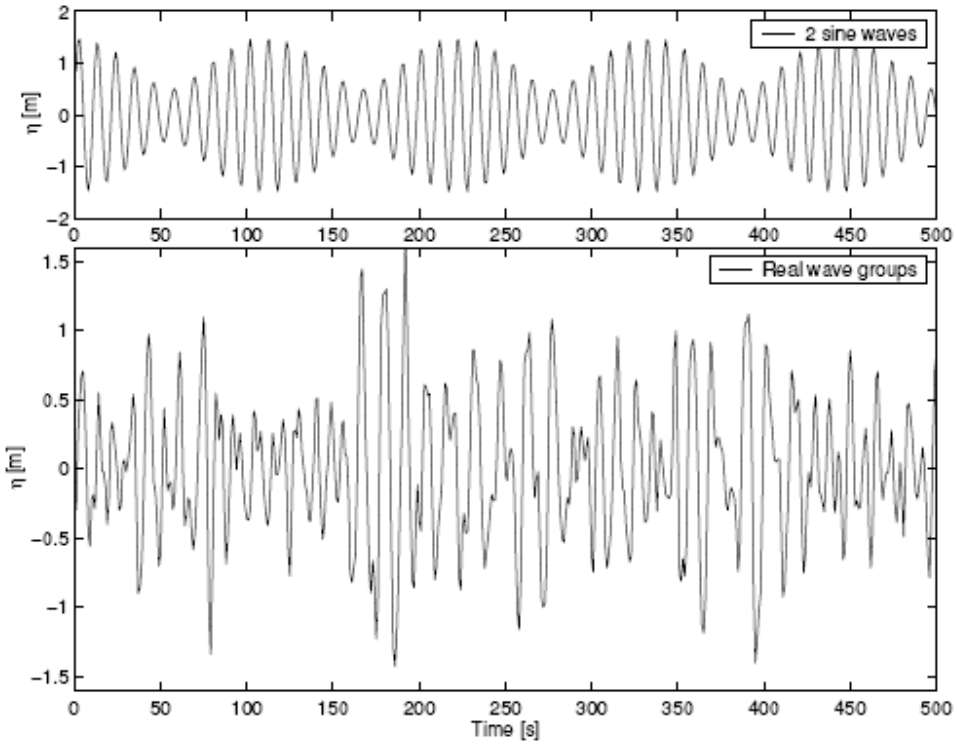

Figure 2.6: Bi-chromatic wave groups and wave groups observed at Barbers Point

Much research has been done on wave group statistics. Many parameters have been devised to give a reliable measure for wave groupiness. The most successful model has been developed by Kimura (1980). This model is based on the correlation between successive wave heights. Goda (1970) also related certain statistical properties of the spectrum to wave groupiness in the parameter Q_p. Many of the earlier parameters are based on intuitive grounds rather than on theoretical ones. To the author's knowledge Battjes and Vledder (1984) were the first to show a theoretical relationship between spectral height and wave groupiness based on Kimura's earlier work. This research resulted in a parameter to describe wave groupiness, which is shown in equation 2.11.

$$k^2(\tau)m^2{}_0 = \left[\int_0^\infty S(f)\cos(2\pi f\tau)df\right]^2 + \left[\int_0^\infty S(f)\sin(2\pi f\tau)df\right]^2 \quad (2.11)$$

Where:

f = frequency
m_0 = the zero$_{th}$ moment of the spectral density function S(f)
T = is the mean wave period.

Hudspeth and Medina (1991) developed a wave groupiness parameter based on statistical parameters of the envelope of the wave train (namely the mean value and the variance). This parameter tends to a certain constant value as record size increases. This parameter will therefore produce no useful results for wave groupiness analysis.

2.4 Forced long waves

2.4.1 General

To the author's knowledge Biesel (1952) was the first to show the existence of non-linear interactions at the difference frequency of wave groups. Munk (1949) and Tucker (1950) were the first scientists to truly measure the phenomenon known as “surf beat" in a real sea. From the 1960's on extensive research has been done on the subject of generation of long waves by wave groups. Most conspicuous research on the generation of forced long waves and some introductory theory have been set down in this section.

2.4.2 Radiation stress

Longuet-Higgins and Stewart (1962) derived a theory based on radiation stress to explain the generation of long waves by short waves. Radiation stress provides for a straightforward model to explain a number of interesting non-linear properties of waves. This theory is briefly depicted here for the one-dimensional case. Subsequently the existence of a set-down beneath a group of waves is explained according to this theory.

Radiation stress S_{xx} is actually defined as the mean value of the total momentum flux (See equation 2.10), minus the momentum flux in the absence of waves:

$$S_{xx} = \int_{-h}^{\eta} (p + \rho u^2) dz - \int_{-h}^{0} (p_0) dz \quad (2.12)$$

For a sinusoidal, progressive wave this can be shown to be given by:

$$S_{xx} = \frac{1}{8} \rho g H^2 \left(\frac{2kh}{\sinh 2\mathrm{kh}} + \frac{1}{2} \right) = E(2n - \frac{1}{2}) \quad (2.13)$$

So in deep water ($kh \geq 1$, $n = 1/2$) the radiation stress tends to $1/2E$ and in shallow water ($n = 1$) the resulting radiation stress is equal to $3/2E$. In transitional water the radiation stress will lie somewhere in between.

2.4.3 Bound waves

This section describes the generation of bound waves by the theory of radiation stress as described in the previous section. As there is a difference between the derivation for the long wave generation in shallow and in deep water, they will be treated separately here.

Carrier waves in deep water to avoid certain non-linear effects the envelope of the energy density of the wave groups is assumed to vary sinusoidally instead of the envelope of the wave group amplitude. The radiation stress is then given by:

$$S_{xx} = \frac{1}{2}E = \frac{1}{2}E_0\left[1 + b\cos\Delta k(x - c_g t)\right] \qquad (2.14)$$

Longuet-Higgins and Stewart (1962) state that a variation in radiation stress will cause convergences in an upper layer. This upper layer has an approximate thickness of D ~ K^{-1} all radiation stress is concentrated in this layer. The lower layer only responds to deviations in the mean water level, caused by the radiation stress. The pressure in the lower layer is assumed to be hydrostatic and it should also satisfy the Bernoulli equation. Using the equation of continuity and the horizontal momentum equation, the surface elevation can be derived. The result is given in equation 2.15.

$$\eta = -\frac{(a^2 - a_0{}^2)\Delta k}{4\left[\tanh\ h\Delta k - \Delta k / h\right]} \qquad (2.15)$$

If the approximation is taken one step further, by assuming that h∆k » 1 and ∆k=k « 1, equation 2.15 becomes:

$$\eta = -\frac{(a^2 - a_0{}^2)\Delta k}{4} \qquad (2.16)$$

This expression shows that the long wave elevation is always 180 degrees out of phase with a^2. So the water will be depressed under the highest waves.

Carrier waves in shallow water The assumption of concentration of radiation stress in the upper layer is no longer valid in shallow water. We may however assume that the group length is large compared to the water depth, i.e. that h∆k « 1. There is also a tendency for waves to be expelled from under regions with high energy density. The following equation describes the rate of change of momentum M.

$$\frac{\partial M}{\partial t} = -\frac{\partial}{\partial x}(S_{xx} + \rho g h\eta) \qquad (2.17)$$

$$-\frac{\partial M}{\partial x} = \frac{\partial}{\partial t}(\rho\eta) \qquad (2.18)$$

Solving these equations for $\frac{\partial \eta}{\partial x}$ and integrating with respect to x we find:

$$\eta = \frac{S_{xx}}{\rho(gh - c_{g^2})} + \text{constant} \qquad (2.19)$$

As can be seen in figure 2.7 there is a depression under the highest waves in the group, so a 180 degrees phase difference. Also, there is a rise in the water level under relatively low waves.

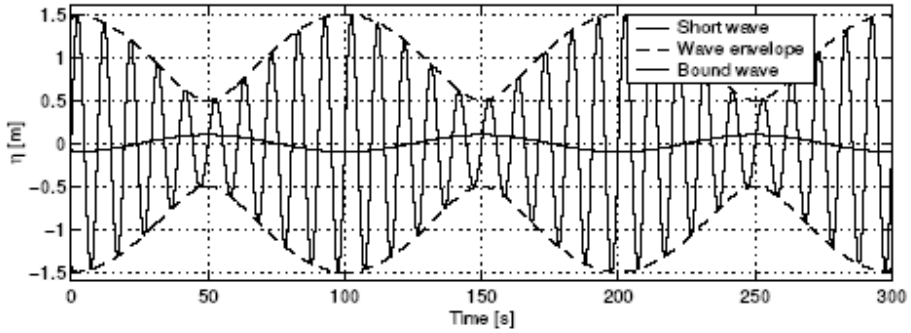

Figure 2.7: Wave groups with corresponding bound wave

2.5 Seiches in Harbours

In order to analyze the effects of infragravity waves in ports, the concept of *seiche* is incorporated. A seiche is the oscillating response of an enclosed or semi-enclosed water body to external forcing; in harbours, they can be of two different types: free seiches and forced seiches. Its frequency band includes both infragravity waves, with periods between 0.5 to 10 minutes, and shelf waves, with periods between 10 to 30 minutes.

2.5.1 Seiche Bands Definition

Okihiro and Guza [1996] defined a seiche band between frequencies of 0.0005 and 0.03 [Hz] (0.5 to 30 [min] in period) and split it into three broad frequency bands corresponding to the degree of correlation between energy measurements inside the harbour and offshore swell energy. The lowest frequency band (0.0005 - 0.002[Hz] in frequency and 10 - 30 [min] in period) is weakly correlated with the swell energy. The midfrequency band (0.002-0.01[Hz] in frequency and 10 [min] to 100 [sec] in period) is highly correlated with the swell energy. The high-frequency band (0.01-0.03 [Hz] in frequency and 30 – 100 [sec] in period) shows some correlation with the swell energy. These definitions are used in this research.

2.5.2 Free Seiches

A free seiche occurs when an initial force disturbs the water level in a system. When the initial force stops, the water level changes in the opposite direction to that imposed by the initial force, in an attempt to return the equilibrium in to the system. However, the inertia of the water carries the system past equilibrium, the water level then continues to oscillate about the equilibrium level at a period characteristic of the system, which depends on the length and depth of the basin (Sorensen, [1978]). These free seiche decay exponentially due friction, if the forcing is not repeated.
Okihiro and Guza [1996] made extensive field observation in three small harbours and found that energy at the resonant periods is amplified within the harbour, relative to outside the harbour, whereas motions within the harbour at other period are suppressed.

2.5.3 Forced Seiches

A forced seiche occurs when the forcing event is cyclic, but with a period different to the natural period of the system. This causes the water level to oscillate at periods that are closer to the period of the forcing than to the natural period of the system Sorensen [1978]). Naturally there is resistance to oscillation at these periods, so some work must be done to maintain a forced seiche.

2.5.4 Causes of Seiches

Seiches can be caused by many reasons, as barometric fluctuations, impacts of wind gusts on the water surface, heavy rain, earthquakes and long waves. Since this study focuses in long waves action, the other mechanism will not be evaluated here.

Low-frequency bound waves can drive harbour seiches at the group frequency without breaking; this has been shown theoretically (Bowers [1977], Wu and Liu [1990]) and in laboratory experiments (Bowers [1977]). Okihiro and Guza [1996] made extensive field observation to characterize seiches in three small harbours with similar surfaces areas (about 1 [km_2]), water depths (from 5 to 12[m]) and swell climates. They related the changes of the seiche energy to the variations of the swell energy level, swell frequency, tidal stage and to meteorological changes, their results are summarized below.

2.5.4.1 Effects of Swell Energy

Okihiro and Guza [1996] correlated the seiche energy and the swell energy in three small ports and found a weak correlation in the lowest frequency band (0.0005-0.002[Hz]). In the midfrequency band (0.002-0.01[Hz]) the seiche energy was highly correlated with the swell energy. In the high-frequency band (0.01-0.03[Hz]) the correlation was high for two harbours and low for the last one. They also found that very energetic swell can excite detectable energy in the lowest frequency band, where the grave mode of the harbour is located.

2.5.4.2 Effects of Swell Frequency

Infragravity energy levels at the same offshore site with similar swell energy can vary by more than a factor 10 for the low and high frequency. The authors found a stronger dependence on swell frequency band (0.03 – 0.125 [Hz] in frequency and 8 – 30 [sec] in period) in the midfrequency seiche band. This variation is associated with the sensitivity of infragravity wave generation to the swell frequency (Okihiro et al. [1992]).

2.5.4.3 Effects of tides

In the port with the biggest tidal range, the infragravity waves in the highest frequency sub band were 5 to 10 times more energetic at high tide than at low tide both inside and offshore of the harbour. They also found higher correlations between swell energy and seiche energy when the records were separated by tidal stage. This research will not treat this phenomenon; tidal effects and other motions with long periods can be avoided selecting the correct time series length.

2.5.4.4 Effects of wave direction

Okihiro, Guza and Seymour [1993], described the excitation of seiches observed in a small harbour, compared them with a model and concluded that the amplifications are only weakly sensitive to the direction of low-frequency waves at the ocean. Van der Molen, Weiler and Ligteringen [2003] compared numerical models with physical test of long period wave forces on a moored ship and concluded that it is not required to give the wave direction for the determination of forces in long waves at the location of the ship.

2.6 Wave forces and ship motions due wave action

Consider a seaway with irregular waves of which the energy distribution over the wave frequencies is known. These waves are input to a system that possesses linear characteristics. The output of the system is the motion of the floating structure. This motion has an irregular behavior, just as the seaway that causes the motion. The block diagram of this principle is given in Figure 2.8.

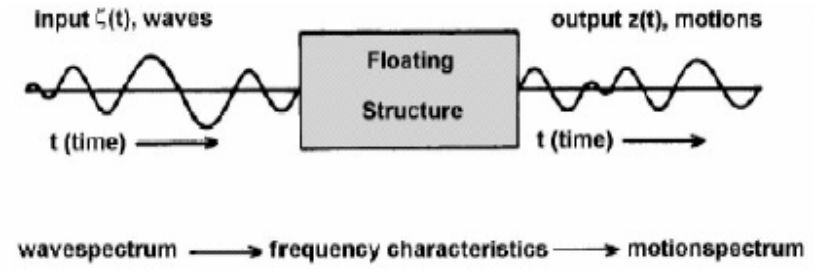

Figure 2.8 Relation between Motions and Waves (from Journée, J.M.J. and Pinkster, J.A [2001])

A mathematical model of the motions in a seaway can be obtained by making use of a superposition of these components at each of a range of frequencies; motions in the so-called frequency domain are considered.

In many cases, the ship motions have mainly a linear behavior. Because of the linear theory, the resulting motions in irregular waves can be obtained by adding together results from regular waves of different amplitudes, frequencies and possibly propagation directions. With known wave energy spectra and the calculated frequency characteristics of the responses of the ship, the response spectra and the statistics of these responses can be found.

2.6.2 Loads Superposition

Since the system is linear, the resulting motion in waves can be seen as a superposition of the motion of the body in still water and the forces on the restrained body in waves (see Figure 2.9).

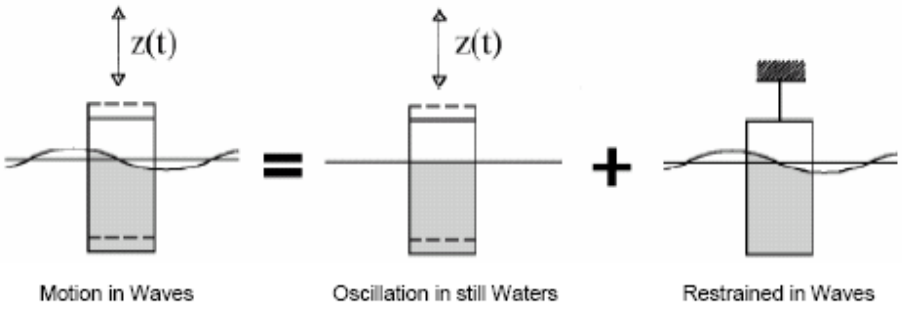

Figure 2.9 Load Superposition for floating bodies (from Journée, J.M.J. and Pinkster, J.A [2001])

Then, the Newton's second law for a floating body can be expressed as:

$$\frac{d}{dt}(\rho V z) = \rho V z = F_h + F_w \qquad (2.20)$$

Where:
ρ is the density of the water.
V is the volume of displacement of the body.
F_h are the so-called hydromechanical forces and moments induced by the harmonic oscillations of the rigid body, moving in the undisturbed surface of the fluid.
F_w are the so-called wave exciting forces and moments produced by waves coming in on the restrained body.

2.6.2.2 Hydromechanical Loads

A free decay test in still water is considered. After a vertical displacement upwards, the floating body (consider a cylinder) will be released and the motions can die out freely. The vertical motions of the cylinder are determined by the solid mass of the cylinder and the hydromechanical loads on the cylinder. After considering Newton's second law and Archimides law is easy to get:

$$(m + a)\, z + b\, z + c\, z = 0 \qquad (2.21)$$

Where:
m is the solid mass of the body.
a is the added hydrodynamic mass
b is the hydrodynamic damping coefficient
c is the restoring spring coefficient

The terms $a\ddot{z}$ and $b\dot{z}$ in equation (2.21), are caused by the hydrodynamic reaction as a result of the movement of the floating body with respect to the water. The water is assumed to be ideal and thus to behave as a potential flow.

The vertical oscillations of the cylinder will generate waves which propagate radially from it. Since these waves transport energy, they withdraw energy from the (free) body's oscillations; its motion will die out. This so-called wave damping is proportional to the velocity of the cylinder in a linear system. The coefficient *b* has the dimension of a mass per unit of time and is called the (wave or potential) damping coefficient. In an actual viscous fluid, friction also causes damping, vortices and separation phenomena. Generally, these viscous contributions to the damping are nonlinear, but they are usually small for most large floating structures; they are neglected here.

The other part of the hydromechanical reaction force $a\ddot{z}$ in equation (2.21) is proportional to the vertical acceleration of the cylinder in a linear system. This force is caused by accelerations that are given to the water particles near to the cylinder. This part of the force does not dissipate energy and manifests itself as a standing wave system near the cylinder. The coefficient *a* has the dimension of a mass and is called the hydrodynamic mass or added mass.

2.6.2.3 Wave Loads

Considering now, that waves are generated in a test basin for a new series of tests. The object is restrained so now the vertical wave load on the floating body (consider a cylinder) is measured. From the classic theory for waves and the linearized Bernoulli equation the expression for pressure distribution in the body is known, then the vertical force over the cylinder is:

$$F = \left(\rho g \xi_a e^{-kT} \cos(wt) + \rho g T \right) A \qquad (2.22)$$

Where:

ζ_a is the wave amplitude.
T is the draft
A is the vertical projection of the area

The harmonic part of this force is the regular harmonic wave force. More or less in the same way as with the hydromechanical loads, this wave force can also be expressed as a spring coefficient *c* times a reduced or effective wave elevation ζ^+. This wave force is called the Froude-Krilov force, which follows from an integration of the pressures on the body in the undisturbed wave.

Actually however, a part of the waves will be diffracted, requiring a correction of this Froude-Krilov force. Using the relative motion principle (also known as Korvin-Kroukovski's relative motion hypothesis), in which it is stated that with respect to the effect of the fluid velocity on the hull no difference can be made between the case of diffracted waves on a fixed hull and the case of the same hull oscillating in calm water; the diffraction force can be computed using the added mass and damping coefficients. The total wave force can be written as:

$$F_w = a\xi + b\xi + c\xi = F_a \cos(wt + \varepsilon_{F\zeta}) \qquad (2.23)$$

Where: F_a is the wave force amplitude.

2.7 Strip theory for Ships

Strip theory is a computational method by which the forces on and motions of a three dimensional floating body can be determined using results from two-dimensional potential theory.
Strip theory considers a ship to be made up of a finite number of transverse two-dimensional slices, which are rigidly connected to each other. Each of these slices will have a form that closely resembles the segment of the ship that it represents. Each slice is treated hydrodynamically as if it is a segment of an infinitely long floating cylinder; see Figure 2.10.

This means that all waves which are produced by the oscillating ship (hydromechanic loads) and the diffracted waves (wave loads) are assumed to travel perpendicular to the middle line plane, thus parallel to the *z-y* plane of the ship. This holds too that the strip theory supposes that the fore and aft side of the body does not produce waves in the *x* direction. For the zero forward speed case, interactions between the cross sections are ignored as well.

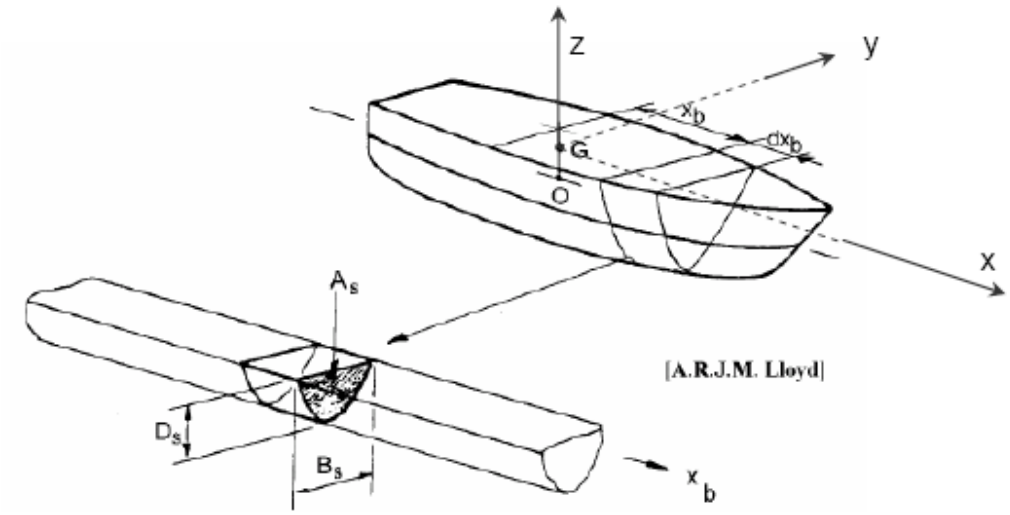

Figure 2.10 Strip Theory representation (from Journée, J.M.J. and Adegeest, L.J.M. [2003])

The followings assumptions are made:
- Any change in shape in a longitudinal direction is small with respect to changes in a transverse or vertical direction. This means that the floating body should be slender. In spite of this restriction, experiments have shown that strip theory can be applied successfully for floating bodies with a length to breadth ratio larger than three, at least from a practical point of view.

– The actual three-dimensional potential for heave, sway and roll is sufficiently approximated by the successive two-dimensional potentials for the various sections. In other words, the mutual interaction of sections is not accounted for. Moreover, because each section is supposed to be part of an infinitely long cylinder, the fluid flow is supposed to pass entirely underneath the body; fluid flow around the ends of the body is not taken into consideration. This assumption is violated especially near the vessel's ends.

Ogilvie has shown that for a body in forced oscillation the three-dimensional effects decrease at increasing frequencies: the second assumption is reasonably satisfied if the corresponding wave length is in the order of magnitude of the body's length or less.

– In hydrodynamic respect, pitching for any section is identical with local heaving at the same velocity and yawing is identical with local swaying at the same velocity.

The last because in two dimensions a body can perform only sway, heave and roll motions. The surge motion cannot be handled by the strip method and is calculated using some assumptions, as considering the body as a longitudinal strip.

2.8 Hydrodynamic Coefficients

In strip theory, the two-dimensional hydrodynamic sway, heave and roll coefficients can be calculated by several methods based on Ursell's Theory and Conformal Mapping. Ursell derived an analytical solution for solving the problem of calculating the hydrodynamic coefficients of an oscillating circular cylinder in the surface of a fluid, then using a conformal mapping the hull shape can be aproximated to the cylinder solution. Many authors have expanded the Ursell's solution to deep and shallow waters and considering different conformal maping, like Lewis method and close-fit method. The advantage of conformal mapping is that the velocity potential of the fluid around an arbitrarily shape of a cross section in a complex plane can be derived from the more convenient semicircular section in another complex plane. In this way, the hydrodynamic problems can be solved directly with the coefficients of the mapping function. See Figure 2.11.

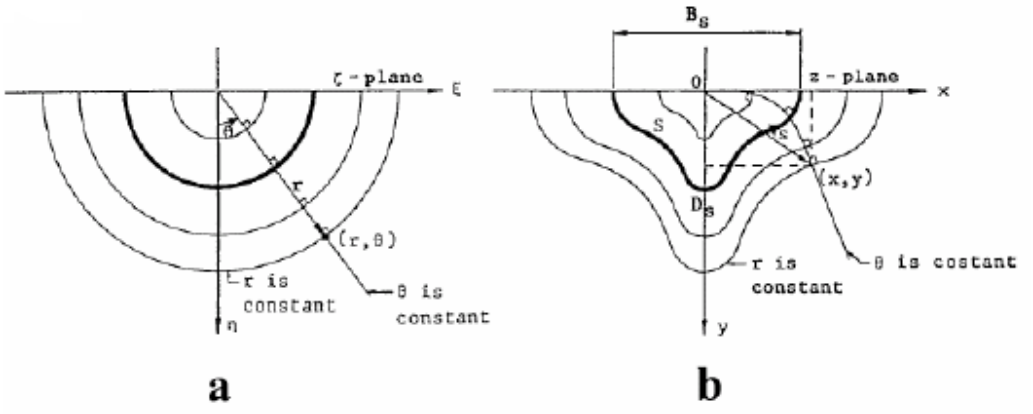

Figure 2.11 Mapping relation between two planes (from Journée, J.M.J. and Adegeest, L.J.M. [2003])

The 2-D potential pitch and yaw coefficients follow from the previous heave and sway coefficients and the lever, i.e., the distance of the cross section to the centre of gravity. For the surge motion an equivalent longitudinal cross section has been defined. For each frequency, the two-dimensional potential hydrodynamic sway coefficient of this equivalent cross section is translated to two-dimensional potential hydrodynamic surge coefficients, by an empirical method based on theoretical results of three-dimensional calculations. The 3-D coefficients follow from an integration of these 2-D coefficients over the ship's length.

2.9 Data Analysis

The data processing was mainly done with MatLab routines created specially for this or similar projects.

Chapter 3

Description and Analysis of Data

3.1 Introduction

This chapter gives a brief description of the study area and describes the different parameters needed to determine the input parameters as is explained in the next chapter. Main focus will be on the determination of the wave conditions and the analysis thereof, as these are considered to be crucial for the accurate modeling.

3.2 Study area

Saldanha Bay is situated some 100 km north of Cape Town in South Africa. It is the only deep water port for the west coast of South Africa.

Figure 3.1 Saldanha Bay location

Figure 3.2 shows the layout of the bay area. The total area of Saldanha Bay is around 9500 ha. The small bay contributes around 15 percent, the big bay around 45 percent with measures about 6 km by 13 km and the remainder is made up by the Langebaan lagoon, which is a tidal inlet that extends from the bay to around 20 kilometers to the south. The main bay is connected to deep water via a restricted entrance open to the WSW (West-Southwest).

A 2 km long solid causeway extends in a south-southwesterly direction into the main bay, leading to an ore loading jetty for large bulk carriers. This jetty in the main bay is about 1 km long and is founded on 16 m diameter caissons, such that the jetty is 60 to 65 % open (appendix A). Liquid and dry bulk carriers are frequently moored on this jetty. The tip of the jetty services liquid bulk carriers.

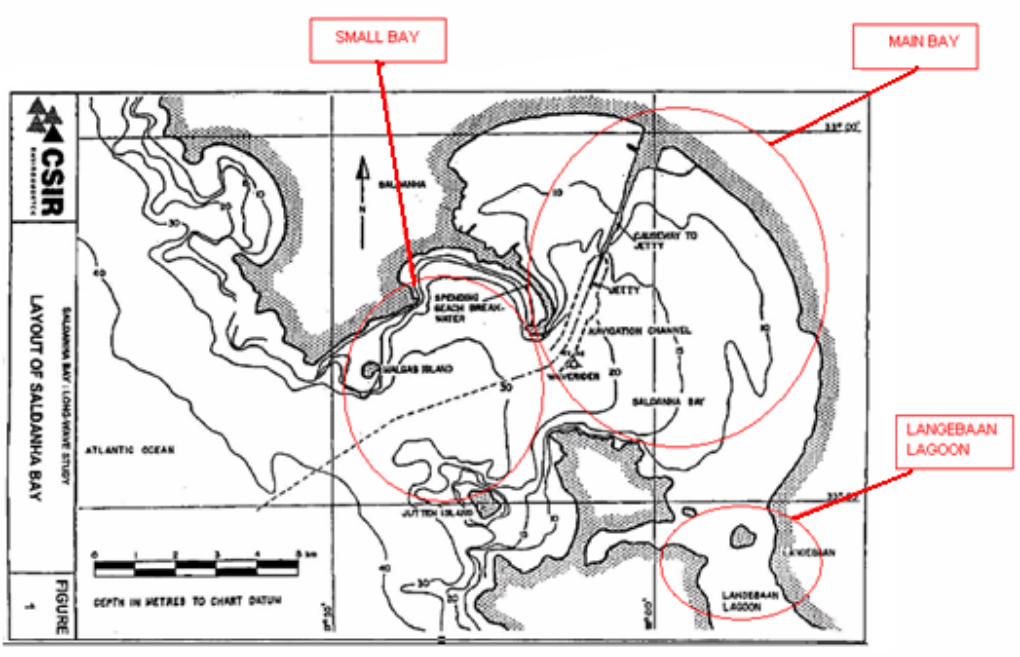

Figure 3.2 Saldanha Bay layout

3.3 Wave data

3.3.1 Description of measurements

There are three devices installed near Saldanha Bay for recording surface elevation and more information.

The first is a Valeport BTH700 Tide Recorder (27 m depth) for long wave recording. It is installed at the southernmost caisson of the jetty at -1.39 meter CD (appendix A). This instrument samples at 4Hz, but the water levels are averaged over three seconds. So the actual recording frequency is 0.33 Hz. Therefore like long waves have T > 30 s, at least 10 points will be got from each one what it's sufficient. The individual values are transmitted to a receiver at port control in 20-minute records. But for short waves with smaller periods between 2 – 5 s, this device is not accurate enough.

The second device is a Datawell Wave Rider buoy (24 m depth), which is located at the entrance of the main bay. This device samples the wave data at 0.5 seconds intervals. The data is stored at the same rate. This type of wave buoy is able to measure wave heights for wave periods ranging from 1.6 seconds to around 25 seconds, with a total accuracy of about three percent. Though, with the current sampling interval of 0.5 seconds, a wave with a period of 1.6 seconds cannot be measured accurately.

A Datawell directional Wave Rider device has been installed at Slangkop, which lies 120 km to the south of the entrance to Saldanha Bay. This may not be a reliable source for the wave height, but it can provide some information on the general wave direction during a specific storm as the distance from the Bay can be considered small in comparison with typical storm dimensions.

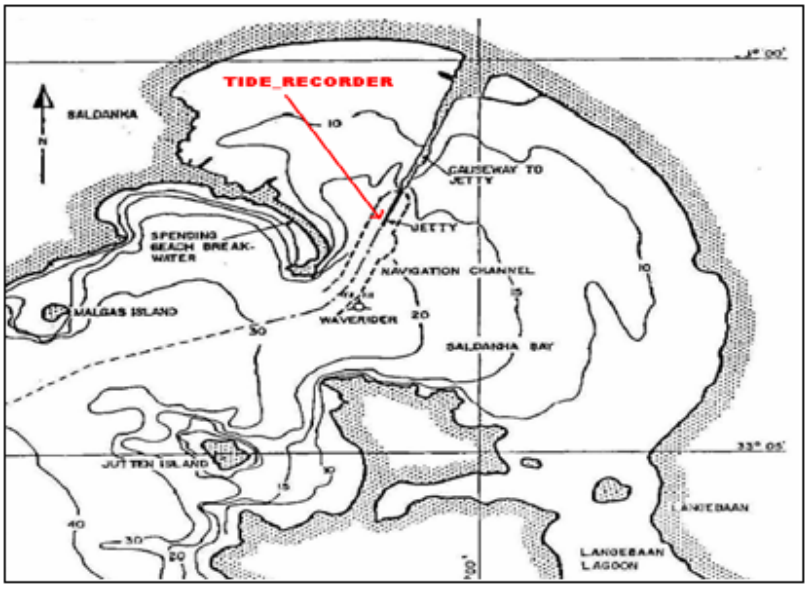

Figure 3.3 Devices location

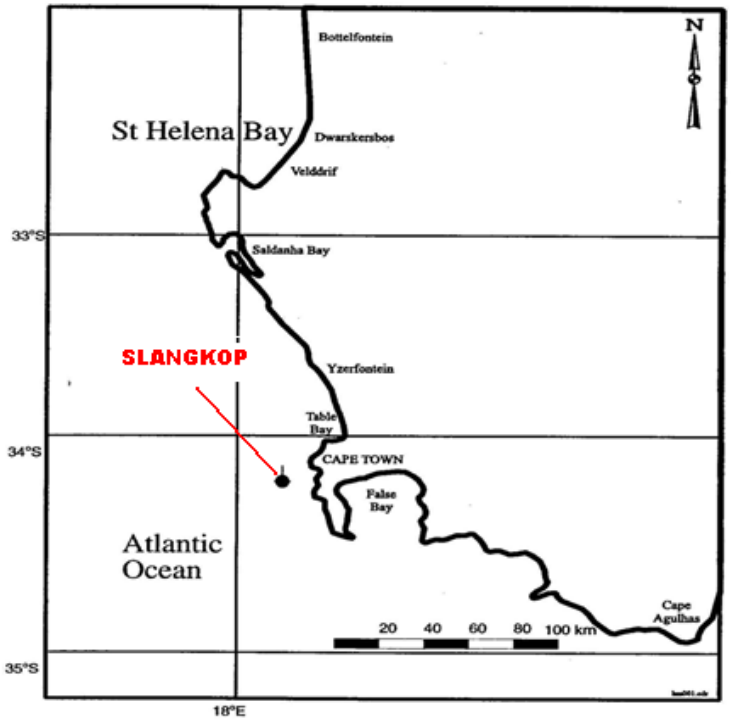

Figure 3.4 Devices location (Slangkop)

3.3.2 Selection of storms

Around two years of digitized wave records were available for further analysis. During this time period several storms passed the area. To select the storms to be modeled, first plots were made of the wave conditions over these two years. There were two storms that were significantly more severe than the average storm. As the long wave height usually increases at the same rate as the square of the H_s of the short waves, a storm with larger H_s may produce much more pronounced long waves. Beside these severe storms, two moderate storms were chosen from the records. These were actually the highest well-documented storms in these two years, next to the storms already selected. For this project four storms have been selected by significant wave height only. These are further described in section 3.2.4.

Storm	Date	Year	Day
1	July	2001	18, 19
2	September	2001	05, 06
3	May	2002	24, 25
4	June	2002	18, 19

Table 3.1 Overview of selected storms

3.3.3 Records to model

Required length

To determine the required record length, the long wave generated from the short waves at the Wave Rider was assumed to stay a bound wave until it reaches the shoreline near the Langebaan Lagoon. When the short wave energy has been dissipated on the shoreline, the long wave will travel back at the free wave celerity towards the jetty and will again reflect on the shoreline near the village of Saldanha. The long wave will decrease in height due to bed friction and reflection losses over time.
To determine the minimum record length needed for the computation, it is considered that a bound long wave traveling with the group velocity from offshore boundary until it reaches the Wave Rider will cover a distance of 10500 [m] approximately. After it reaches the Wave Rider, the wave will travel as a free long wave through the main bay about 6000 [m] till it reaches the coast. The fully reflection of the long wave on the coast will take twice the period of the wave. Finally after reflection, the free long waves will travel about 6000 [m] till the jetty. Then the time needed for the computation can be calculated as:

$$\text{time} = \frac{d1}{cg} + \frac{d2}{c} + 2T = \frac{d1}{n\ c0\ \tanh(kh)} + \frac{d2}{\sqrt{gd}} + 2T \qquad (3.1)$$

The group speed for 25 meters water depth will be approximately:

$$cg = 0.9\ \frac{9.81\ 16.5}{2\ \pi}\ 0.5 = 12.5\ m/s \qquad (3.2)$$

Distance traveled at this velocity is about 10500 meters, so it will take the wave roughly 840 seconds. From this point the waves will travel at approximately 10 meter per second.

$$c = \sqrt{gd} \; = 10 \; m/s \qquad (3.3)$$

It will take another 1200 seconds to reach the coast and come back to the jetty traveling as free long wave. A period of 150 [sec] for the long waves, seems suitable in average.

Thus considering this, the time needed is 39 minutes; say 40 minutes to reach a sort of equilibrium. So after 40 minutes the waves will have had enough time to reflect and reach the jetty as free long waves. It was decided to add time 20 minutes more because the 40 minutes, was just the time long waves, first as bound and after as free, required to reach the jetty after reflecting on the coast; then 60 minutes will be considered necessary to have some stationary situation.

To actually model 20 minutes of reliable conditions it is necessary to do a run of about 80 minutes length. For the runs for comparison with the measured data, runs of about 150 minutes will be made to get a good impression of the wave conditions with reflections in the bay. The period available for comparison will then be 90 minutes approximately.

Selection criteria

To select the records that are to be modeled from the storms that are selected some criteria have been devised. Some criteria are more important than others; significant wave height ($H_{s)}$ is the most important although the selection of stationary period conditions in the storm will be consider as well.

Starting conditions

For good starting conditions it is important to have a relatively undisturbed condition at the beginning of the model run. So during a high tide the tidal velocities are almost zero and can be easily modeled. Next to that it is necessary to have little grouping before the run starts as these groups will result in long waves that cause disturbances in the bay.

Hm0 the short wave height was an important parameter in the selection process. The significant short wave height is plotted for the Saldanha Bay Wave Rider. Frequency cut off for the determination of this parameter was set at 0.03 Hz. Data was gathered for only 1050 seconds of total 1200 seconds at 20 minute intervals.

Spectrum

A lot of information on the waves is contained within the wave spectrum. The wave spectrum has therefore been displayed at 30-minute intervals for 2 day storm periods.

Wave groupiness parameters k

Battjes and van Vledder (1984) proposed the use of a spectrum derived correlation parameter which gives a good indication of the wave group statistics. This parameter was used to determine if there were periods with increased wave grouping in the selected records. The parameter has been shown in the plots below, but no use was made of these parameters when selecting the wave records. This parameter is described in section 2.2.5 of this report.

Long wave action inside harbour
First tidal components were removed from the signal in Saldanha Bay. This was done using a linear detrending function.

Stationary pattern
Selected storms periods have to be approximately stationary to get real results which can be compared with the simulated ones. A “standard deviation – time” graph (see appendix A) was obtained for each storm to check that the standard deviation keeps constant during the selected periods.

3.3.4 Description of selected storms

Per storm a description is made of the storm parameters and possible explanations are given for interesting phenomena during that storm. Per storm a graph is shown, presenting wave data during the entire storm. The energy density spectrum is given for a detailed impression of the wave conditions in the selected period. Some characteristic parameters have been added to this plot as well. Finally a standard deviation - time graph of long waves for selected record, has been added to check the stationary pattern. The selected periods from the four storms are listed below. They will be named storm number 1 through number 4 throughout this part.

Storm 1: July 2001

This moderate storm had a significant wave height of 7.1 meters for the Slangkop Wave Rider. This was reduced, due to entrance restrictions in Saldanha Bay area to around 3.0 meters. This storm shows good visual correlation between long and short significant wave height (see figure 3.5). However around 18:00 on the first day of the storm the long wave height drops considerably, while the short wave height shows virtually no change at all. Several phenomena can explain this drop in wave height:

- The wave groupiness parameter k_f is considerably higher from around 12:00 to around 17:00 on the first day of the storm. This could mean increased long wave action inside the bay area.
- As direction is quite important for the wave vector pattern inside the bay area, this drop can also be explained by a slight change in direction. Due to storm distance the wave spreading can also change from Slangkop to Saldanha, but as no information was available on storm paths no further research was carried out.

The selected record (see table 3.2) shows a narrow banded spectrum (see figure 3.6) with several peaks. The record was selected when long wave height reached a maximum. Local wind wave generation is quite low at the location of the Wave Rider. The main contribution to the overall wave energy is composed of swell, with periods ranging from around 10 to around 16 seconds. Standard deviation keeps constant around 0.18 (figure 3.7).

Day	Start time	Stop time
18 07 2001	13:00	14:20

Table 3.2 Selected record storm 1

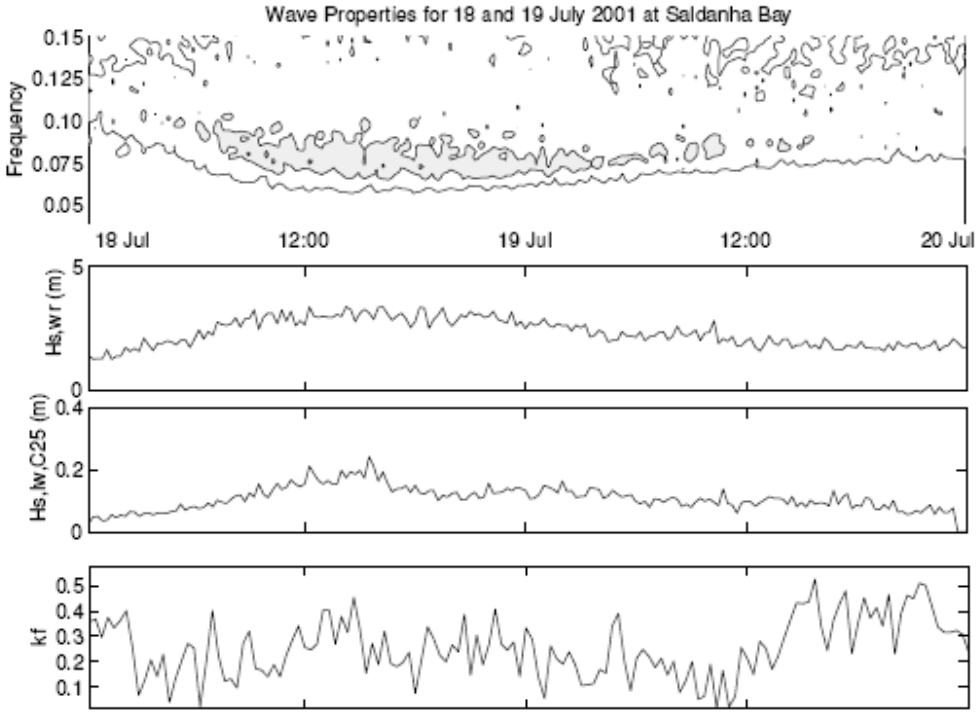

Figure 3.5: Selection criteria for 18 th & 19 th of July 2001. The upper plot shows the energy density in m^2/Hz. Next plots are the H_{m0} at the Wave Rider and at the jetty. The lower panel shows the groupiness parameter computed for the short waves.

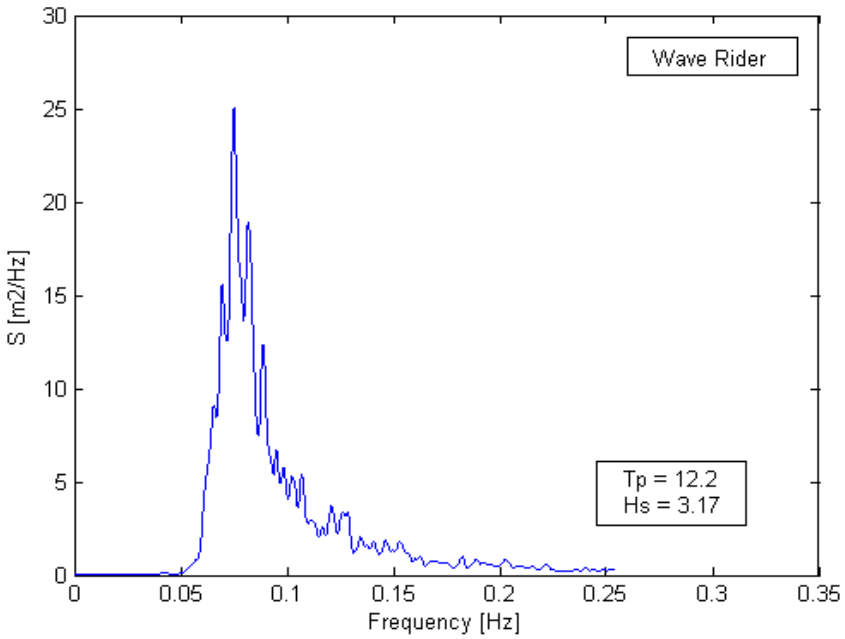

Figure 3.6: Spectrum of incident short waves for selected record on 18 th of July 2001 13:00 -14:20

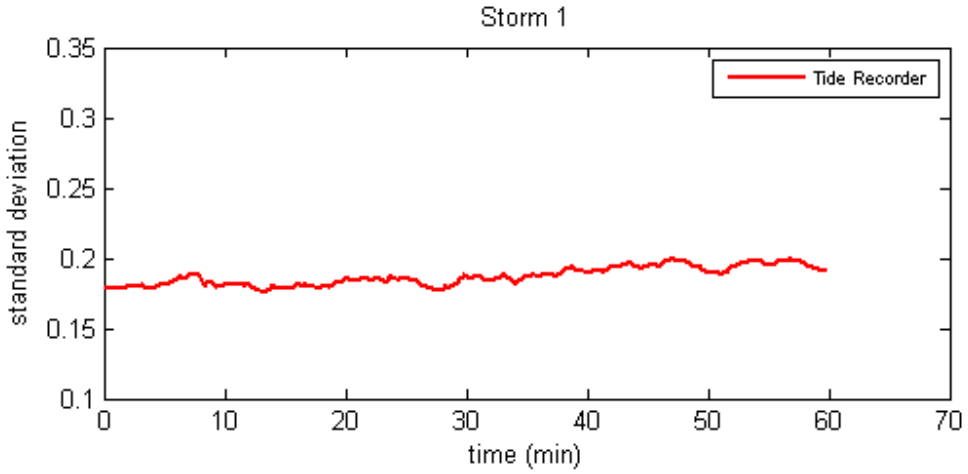

Figure 3.7: Standard deviation - time graph of long waves for selected record on 18 th of July 2001 13:00 -14:20

Storm 2: September 2001

This was the most severe storm for the area during the studied period. Significant short wave height at the Wave Rider reached around 5.1 meters during the peak of the storm (figure 3.8). This storm shows good correlation between long and short wave height as was observed for all other storms. The long wave height increases prior to the storm, while no notable increase for the significant short wave height was measured at the Wave Rider buoy. These fore-runners are hard to predict, so some properties of these waves will be further analyzed in section 3.4.2. Table 3.3 shows that the period in the beginning of the storm was chosen as long wave action before this period was not as severe as observed in the time after this period. The spectrum shows that most energy is concentrated around a peak period of around 17 seconds (figure 3.9). Wave periods for this storm are very high, which will influence long wave length considerably. During selected period long waves of around 0.4 meters in height were observed, which can be designated as severe long wave action (figure 3.8). This long wave is however not entirely composed of bound wave energy. A large contribution might be expected from reflections on the shoreline. Standard deviation keeps approximately constant for the period selected (figure 3.10).

Day	Start time	Stop time
05 09 2001	17:40	19:00

Table 3.3 Selected record storm 2

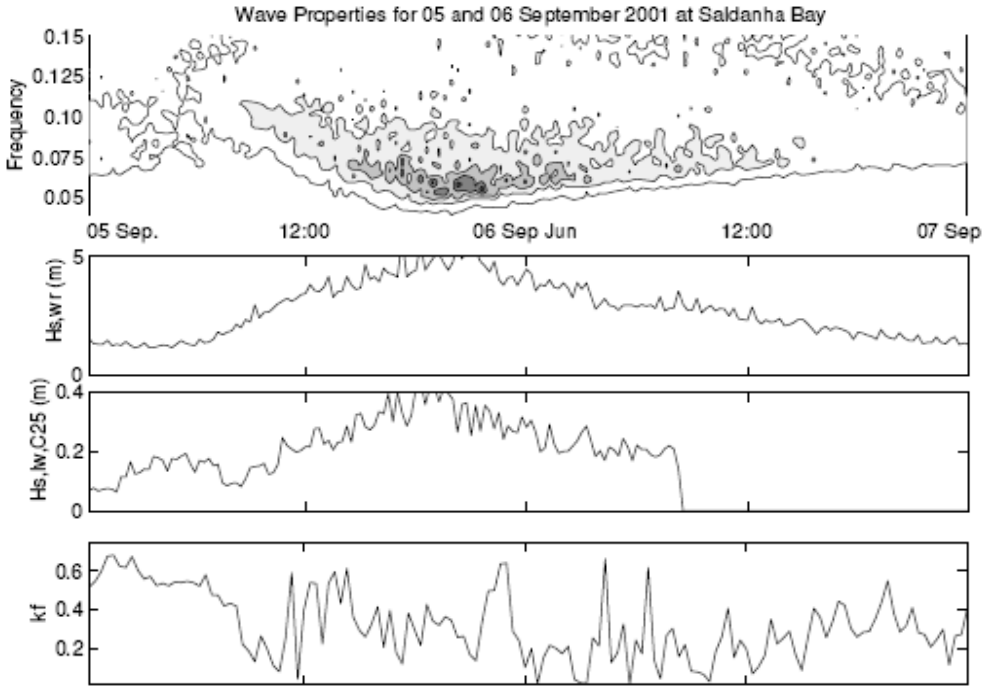

Figure 3.8: Selection criteria for 05 th & 06 th of September 2001. The upper plot shows the energy density in m^2/Hz. Next plots are the H_{m0} at the Waverider and at the jetty. The lower panel shows the groupiness parameter computed for the short waves.

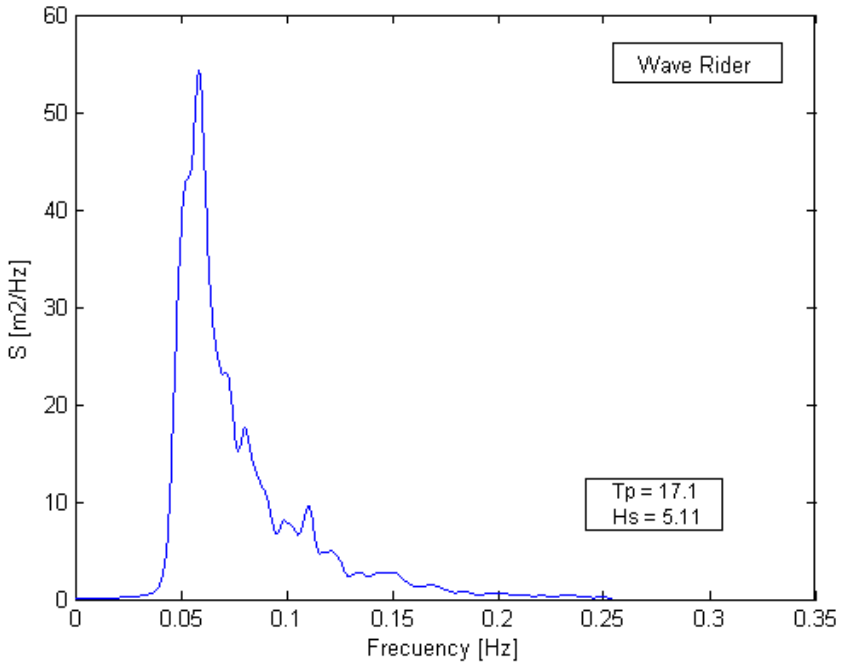

Figure 3.9: Spectrum of incident short waves for selected record on 05 th of September 2001 17:40 - 19:00

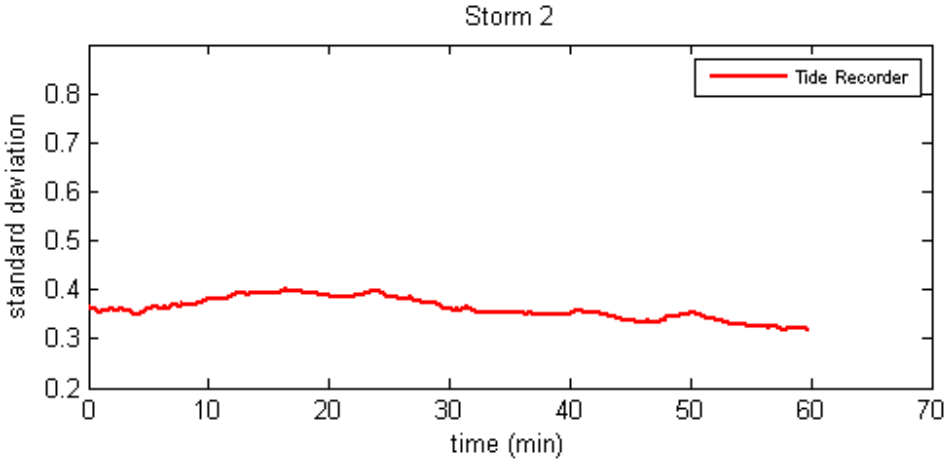

Figure 3.10: Standard deviation - time graph of long waves for selected record on 05 th of September 2001 17:40 - 19:00

Storm 3: May 2002

This storm is actually a three day storm (first day not shown here because was not so severe as the others). On the 25th a sudden increase in long and short wave height is observed (figure 3.11). Long wave height before peak of the storm is fairly constant at around 0.20 meter. Only a small peak can be observed, which cannot be explained by short wave height alone. Possible explanation for this is the increase in the narrowness in the spectrum (see increase k_f). The empty squares in the plot represent missing data or incomplete data files. As the groupiness parameter is calculated from the short wave spectrum no value is available for these periods. The selected record (see table 3.4) shows a narrow banded spectrum (see figure 3.12) with several peaks. Standard deviation keeps approximately constant for almost all the period (figure 3.13).

Day	Start time	Stop time
25 05 2002	5:20	6:40

Table 3.4 Selected record storm 3

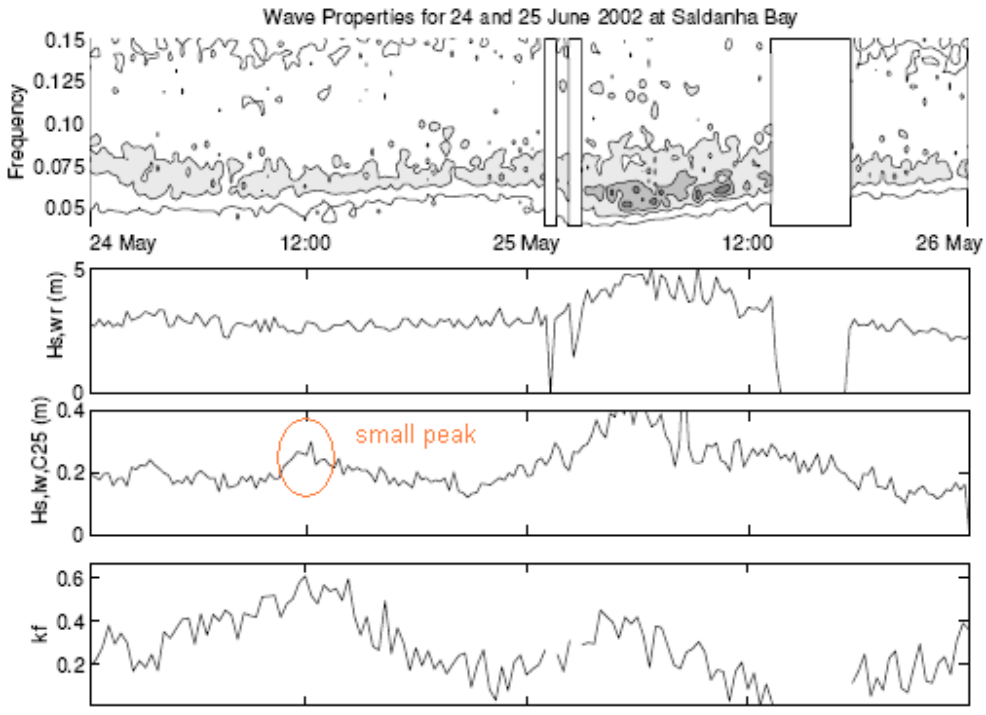

Figure 3.11: Selection criteria for 24 th & 25 th of May 2002. The upper plot shows the energy density in m2/Hz. Next plots are the Hm0 at the Waverider and at the jetty. The lower panel shows the groupiness parameter computed for the short waves.

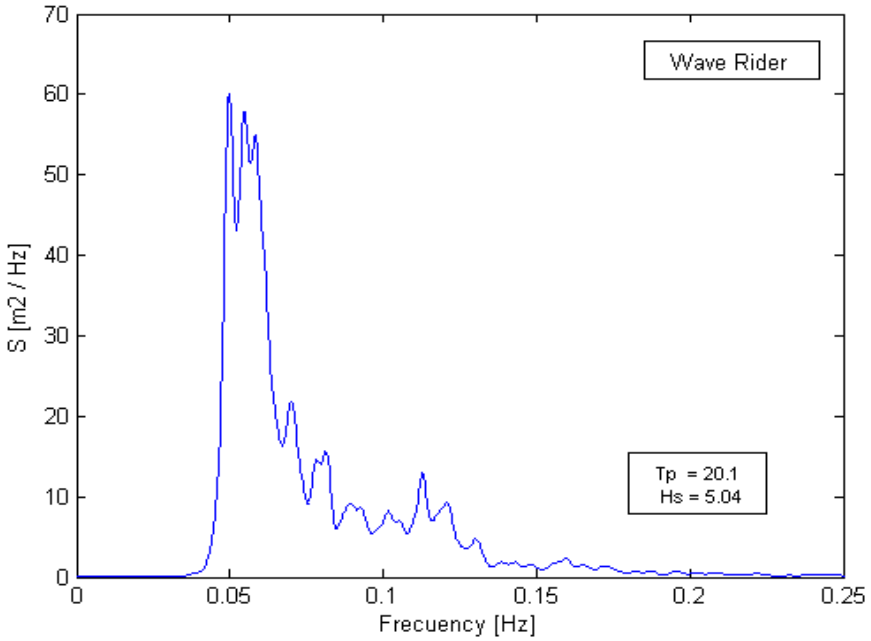

Figure 3.12: Spectrum of incident short waves for selected record on 25 th of May 2002 5:20 - 6:40

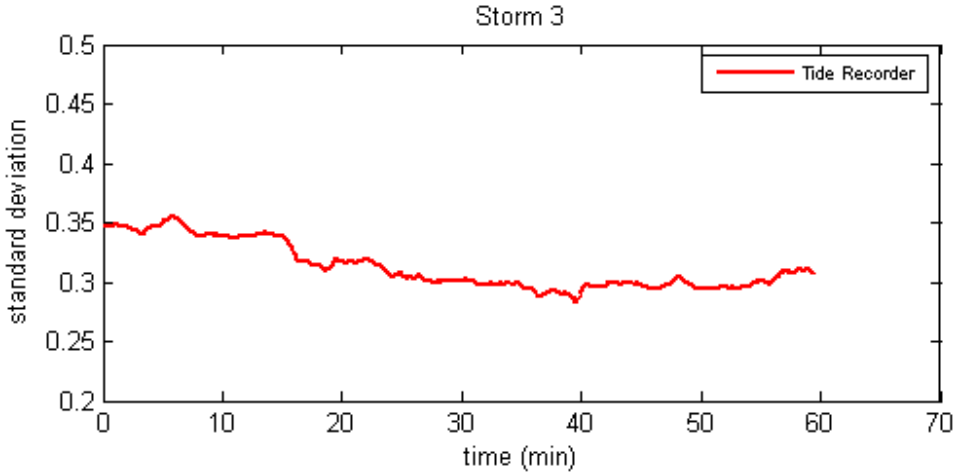

Figure 3.13: Standard deviation - time graph of long waves for selected record on 25 th of May 2002 5:20 - 6:40

Storm 4: June 2002

This storm has a very smooth increase in long wave height. The record with high long wave action was selected. Though significant short wave height is lower than observed during storm 2, the long wave action during the peak of this storm is almost equal in height (figure 3.14). The spectral shape could explain this high long wave height. The selected record (See table 3.5) shows a different concentration of energy at the peak frequency. As for the other storms, it can be considered that standard deviation is approximately constant (figure 3.16).

Day	Start time	Stop time
18 06 2002	22:00	23:20

Table 3.5 Selected record storm 4

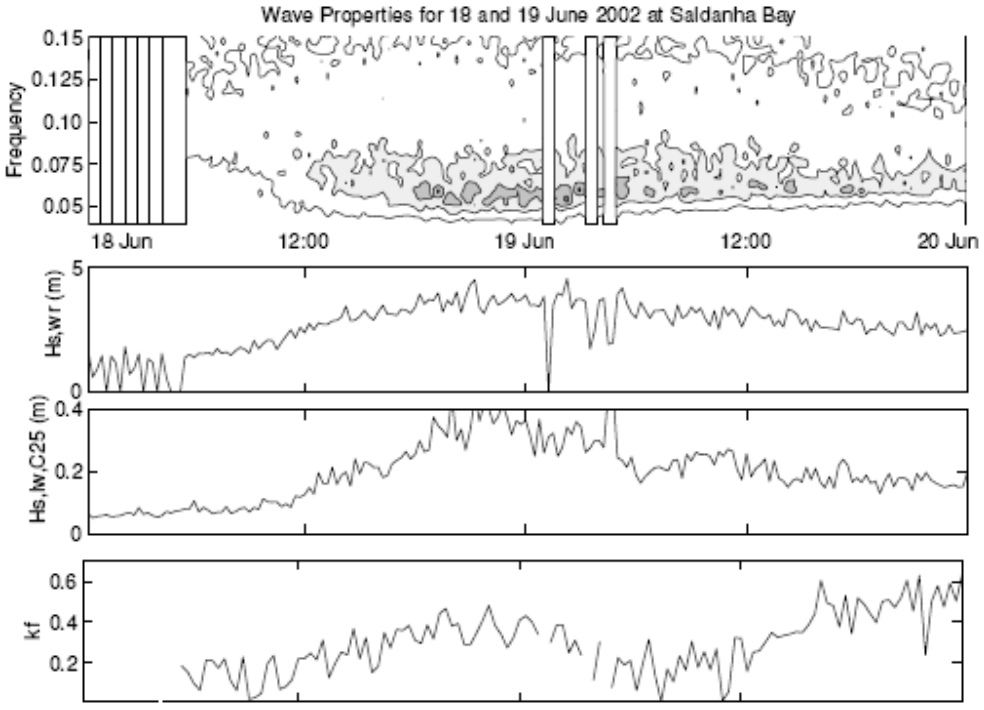

Figure 3.14: Selection criteria for 18 th & 19 th of June 2002. The upper plot shows the energy density in m^2/Hz. Next plots are the H_{m0} at the Waverider and at the jetty. The lower panel shows the groupiness parameter computed for the short waves. The sudden drop in significant wave height was caused by an interruption of the long wave recordings during this storm.

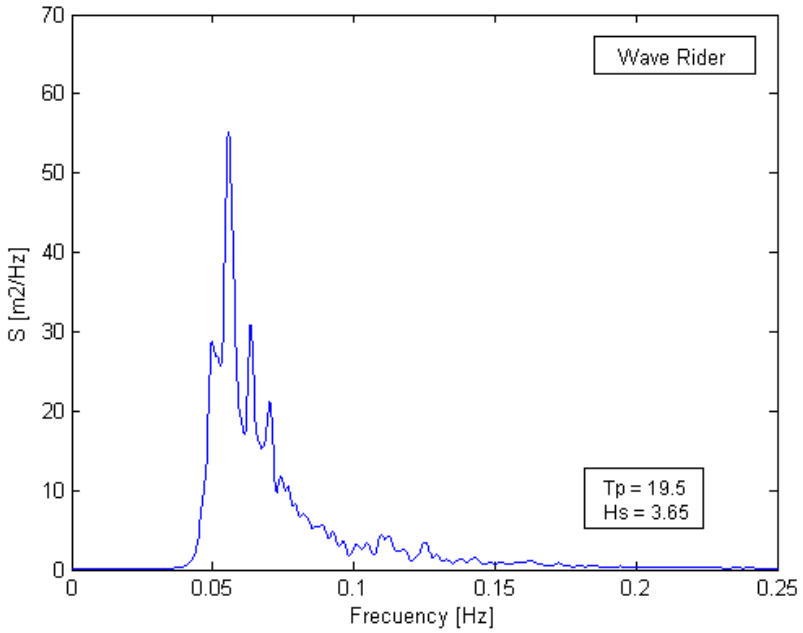

Figure 3.15: Spectrum of incident short waves for selected record on 18 th of June 2002 22:00 - 23:20

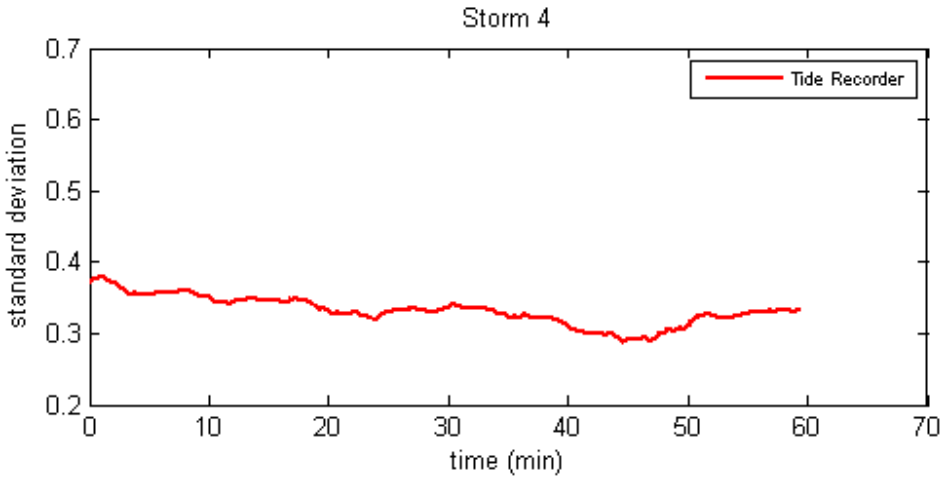

Figure 3.16: Standard deviation - time graph of long waves for selected record on 18 th of June 2002 22:00 - 23:20

3.2.5 Wave Direction

There is little data on the wave direction for the Saldanha Bay area. Since the Wave Rider buoy in Saldanha Bay is a non-directional Wave Rider, there is no information on direction for this specific location. Since the wave buoy is at the end of a “channel" with a somewhat restricted entrance, a good assumption can be made for the wave direction however. In the layout chart for the bay area (Figure 3.2) it can be seen that the two islands, the end of the breakwater and the northern top of the southern peninsula form a narrow gap. Therefore it is assumed that most energy comes from directions between 245 and 260 degrees in the nautical convention.
Some directional information was obtained from the Slangkop device located near Cape town (see Figure 3.4). Table 3.6 shows the observed mean incident wave direction and the observed wave spreading at the Slangkop Wave Rider.

Date	Year	Days	Mean direction (°)	Spread
July	2001	18, 19	265.28	14.77
September	2001	05, 06	252	15.68
May	2002	24, 25	224	18.35
June	2002	18, 19	237	15.67

Table 3.6 Wave directions at Slankop Wave Rider

3.4 Wave data analysis

3.4.1 Significant wave height correlation

As can be seen, from the plots of the storms shown above, a good correlation exists between the long and short wave height at any given time. Figure 3.15 shows the correlation between long and short wave height quite clearly. The black squares in this graph represent the data from the first part of the storm of September 2001, the earlier mentioned fore-runners. The long wave observations for these periods are thus less likely to be directly related to the incoming short wave. As can be observed the plotted points for storm 4 tend towards the upper part of the cloud, while points for storm 2 tend more to the lower part. Data for storm 1 is concentrated in the bottom left corner as energy levels were much lower. As a portion of the energy may be unbound, the wave height offshore is also quite important as it determines the wave height inside the basin to a great extent. If the wave direction is such that all short wave energy is transmitted into the basin, the correlation should tend to the line observed for storm 4. If the mean incident short wave direction is such that less energy is transmitted to the Wave Rider there will still be significant long wave action near the jetty as long wave diffraction will still cause waves to penetrate the basin.

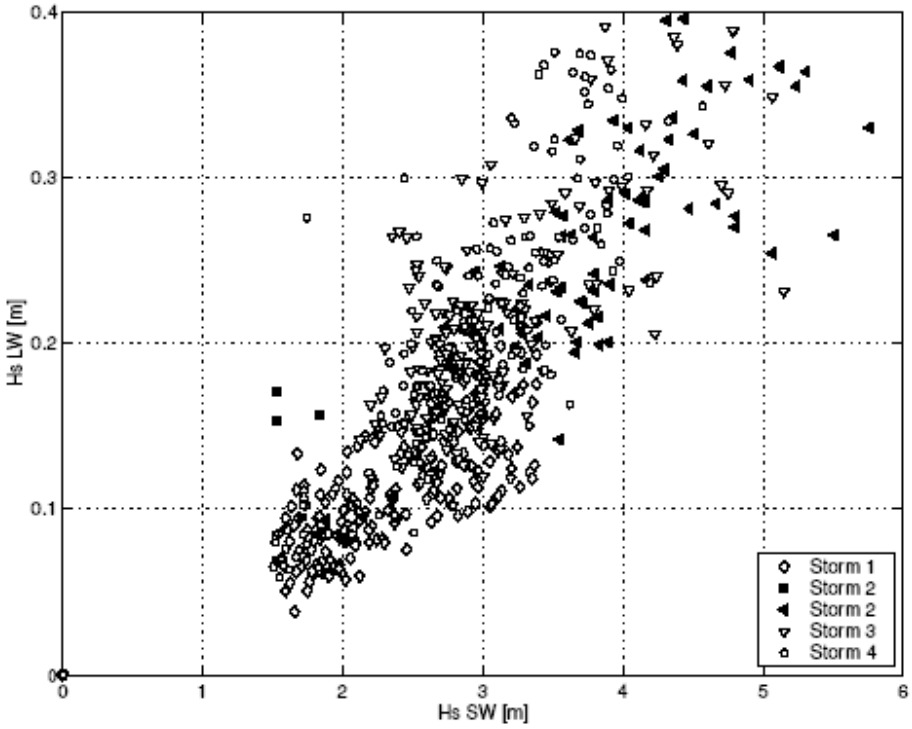

Figure 3.17: Observed significant long wave height plotted versus observed short wave height

3.3.2 Forerunners

Figure 3.18 shows the observed spectra during the first 12 hours of the 5th of September near the jetty. Though energy levels are quite low it can be observed quite clearly that energy levels are higher from around 2:00 to around 07:00. The significant shortwave height does not exceed 1 meter until 9:00 that day. This leads to the suspicion that these waves are probably not bound to the short carrier waves and arrive in advance of the storm (hence the name forerunners). Since they arrive in front of storms it is also highly probable that they are somehow generated by the following storm. Further research could point out whether they are generated inside the storm or somewhere during the travel to Saldanha Bay. This could be done quite easily as they travel faster than the bound waves. The time difference should point out where in time they would have originated. Assuming they originated from the same storm one could inspect storm paths for the point of origin.
While the peakedness parameter Kf shows an oscillating pattern for most periods, the parameter shows an increase for both forerunner events that could be somehow related to the observed long wave heights.

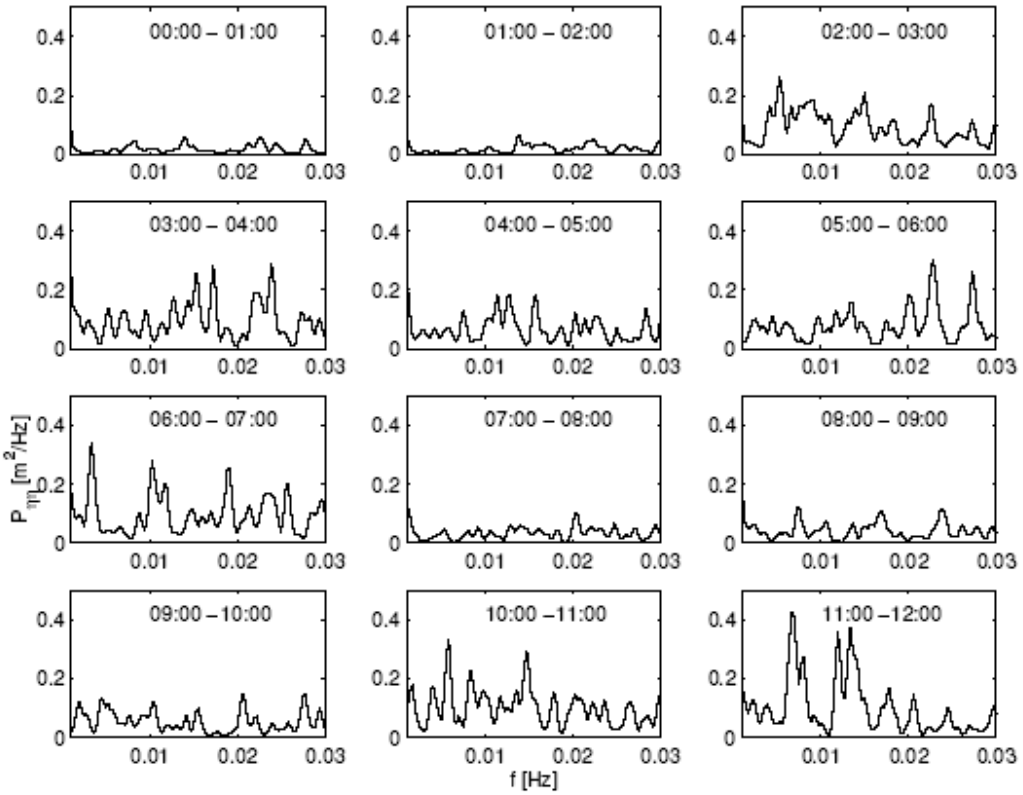

Figure 3.18: Observed spectra on th 5 th of September 2001 00:00 - 12:00

3.4 Bed material data

The Saldanha bay bottom consists mainly of sand as can be seen from tables 3.7 and 3.8. These samples were taken for a study on the effects of dredging in the bay on the environment. Since the effect of the friction generated by the bed material is expected to be low, no more research was done for better bed material data.

	Gravel ($\geq$ 2mm)	Sand (63 μ – 2 mm	Silt/ Clay ($\leq$ 63 micron)
Mean fraction	15.5	72.0	12.5

Table 3.7 Fractions of the bed material

Median grain size (D50 in mm)	
A	0.265
B	0.155
1-4	0.150
5-8	0.155

Table 3.8: Median grain size for different samples

3.5 Tidal conditions

Figure 3.19 shows the surface elevation relative to mean sea level for Saldanha Bay for the four storms selected. Tidal variations are small for storms 1 and 4. Tidal variations for storms 2 and 3 are higher than the other storms, but lower than 40 cm so we can consider not important for our study.

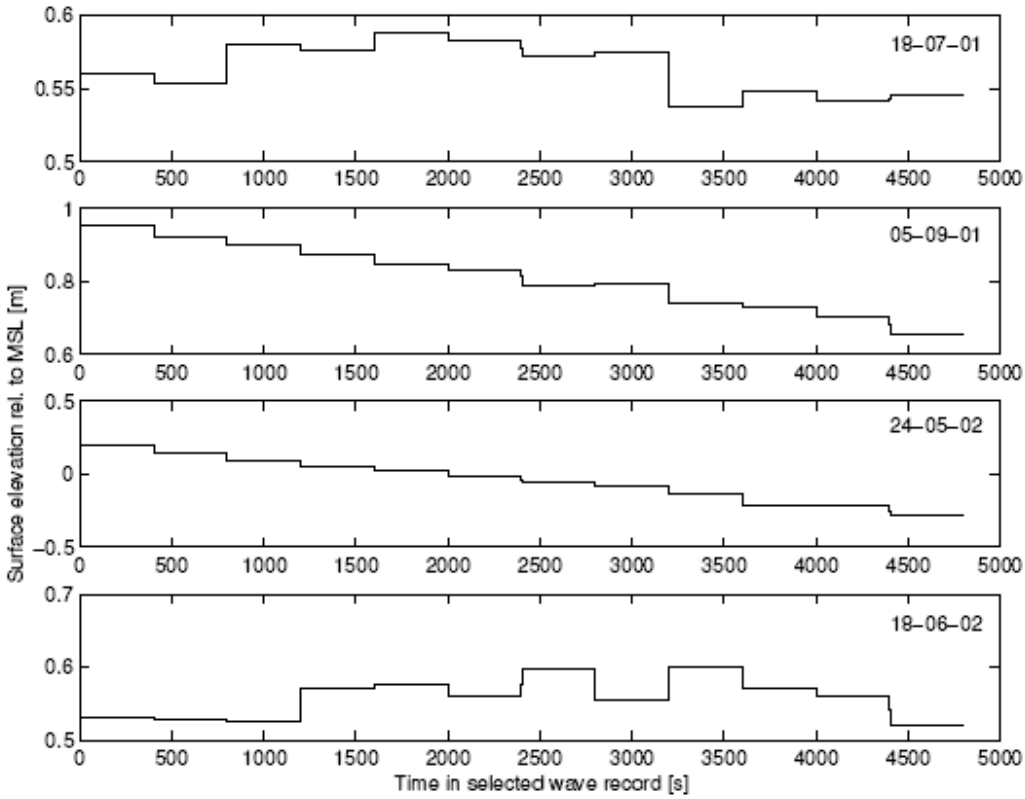

Figure 3.19: Tidal motions obtained from Tide Recorder.

Chapter 4

Numerical model description. Parameters

4.1 Chapter Overview

This chapter, in the first part, gives a general description of Delft 3D program: Swan module and the hydrodynamic model SURFBEAT are described with detail. Second part of the chapter describes all the steps required for the information processing from raw data to model input and it is organized following the same time line as the numerical method does.

4.2 Program description: Delft 3D

The Delft3D program suite is composed of a set of modules (components) each of which covers a certain range of aspects of a research or engineering problem. Each module can be executed independently or in combination with one or more other modules. The information exchange between modules is provided automatically by means of a so-called communication file; each module writes results required by another module to this communication file and reads from this file the information required from other modules. Other, module-specific, files contain results of a computation and are used for visualisation and animation of results.

For using Delft3D-FLOW and Delft3D-WAVE the following utilities are important:
- Delft-RGFGRID for generating curvilinear grids
- Delft-QUICKIN for preparing and manipulating grid oriented data, such as bathymetry or initial conditions for water levels, salinity or concentrations of constituents.
- Delft3D-TRIANA for performing off-line tidal analysis of time series generated by Delft3D-FLOW
- Delft-TIDE for performing tidal analysis on time-series of measured water levels or velocities
- Delft3D-NESTHD for generating (offline) boundary conditions from an overall model for a nested model
- Delft-GPP for visualisation and animation of simulation results

Delft3D-FLOW and Delft3D-WAVE are developed more in the followings sections while Delft-RGFGRID Delft-QUICKIN are well explained at appendix B.

4.3 Numerical model description

The numerical method applied in the research uses two different numerical models for the computation of the propagation of long waves in the harbor: Swan and Flow.

The infragravity wave model SURFBEAT calculates the propagation of bound waves and the free long waves generated as the short waves are dissipated by breaking. This model is also used for the calculation of long wave penetration and amplification due to harbor resonance.
The schematic calculation of the numerical model is summarized in Figure 4.1.

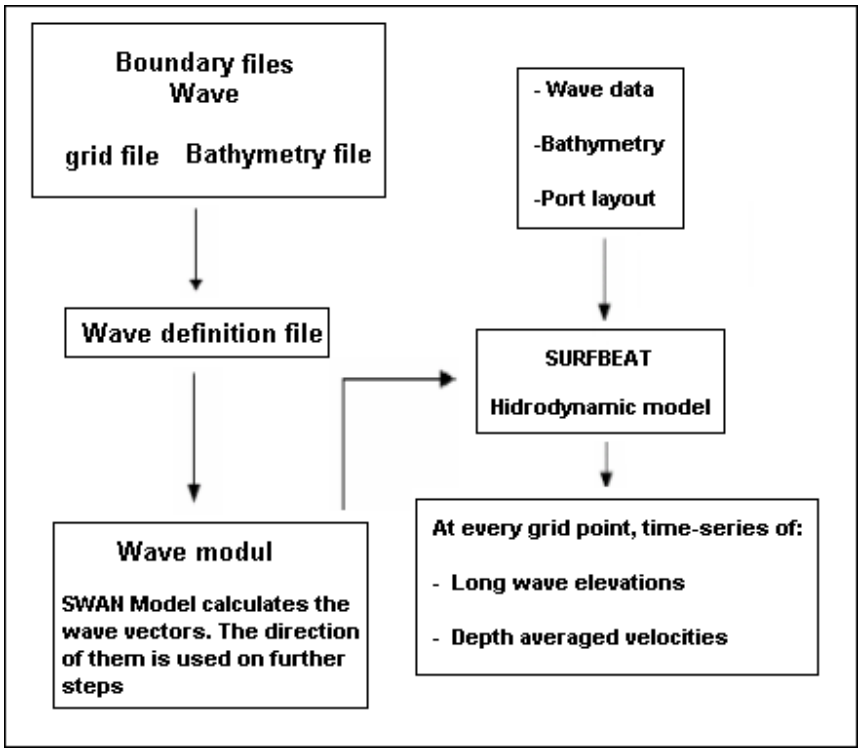

Figure 4.1Numerical model overview

The program operates in a different way than the other modules of Delft3D. It has an executable file “morssys file” (mdm file) that calls the input files and organize the Delft3D modules needed for the run, in this case WAVE and FLOW, furthermore permits to set up the time step of the running and its duration. The input file that command this operation is morf.<runid> and can be changed using a text editor or the program *tree.exe* from *D3D wizard*.

Figure 4.2 shows a schematic overview of the computational procedure of the program. First a brief calculation is done to set the dimensions of arrays in the com-file resulting from the grid, boundary and master definition file. The com or communications file is a file used by Delft 3D to communicate between the different modules. Main calculation input is stored for each calculation step on this file. The following SWAN calculation will calculate the wave vectors for the Swan grid structure according to its input file. Once the calculation is completed these vectors are transferred to the communications file. Surf Beat then calculates the short wave field energy envelope at the boundary location (wave components file) and the transportation throughout the computational domain (flow grid). Note that SWAN wave vector calculation is executed only once. In case of noticeable changes of water level, as high tidal level differences, is recommendable to execute more than one SWAN calculation, it is clear that the wave field can perform changes in these cases. In this specific case, it must be considered that the simulation completes a running of 2.5 hours only and then the tidal difference is minimum.

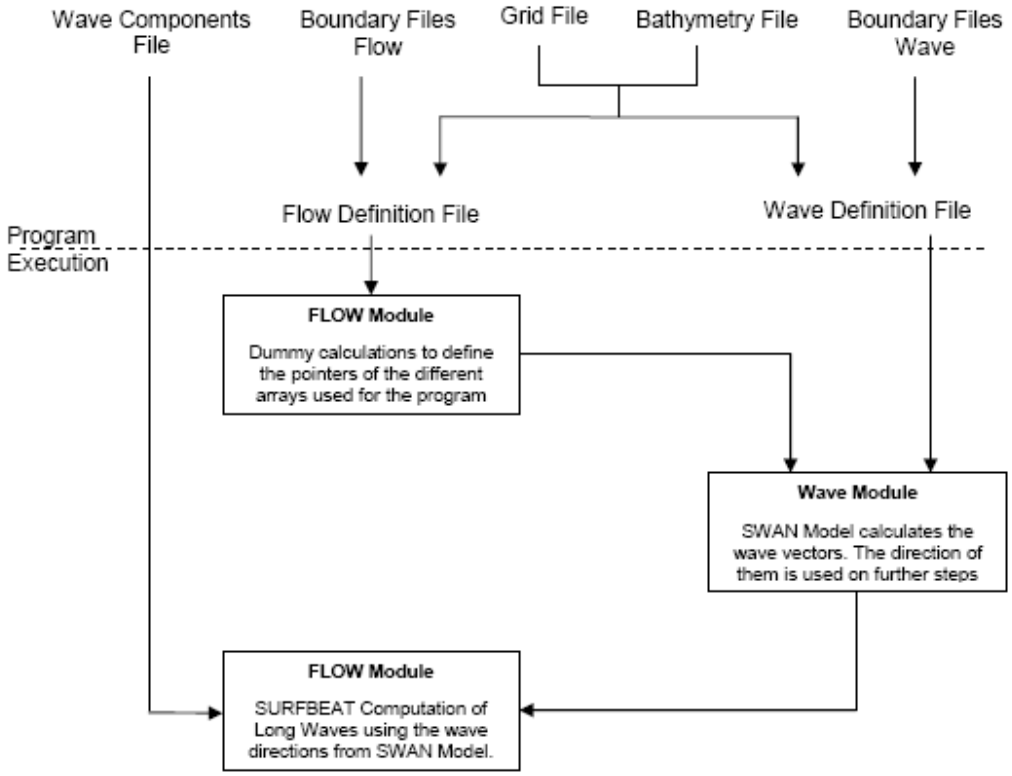

Figure 4.2 Schematic calculation overview

4.3.1 SWAN (Wave module)

SWAN (**S**imulating **WA**ves **N**earshore) wave model is a frequency-domain model. It is used for simulating the evolution of random, short-crested wind-generated waves.

The model is based on the discrete spectral action balance. The evolution of the wave spectrum is described by the spectral action balance equation, which, for Cartesian coordinates, is:

$$\frac{\partial}{\partial t}N + \frac{\partial}{\partial x}c_x N + \frac{\partial}{\partial y}c_y N + \frac{\partial}{\partial \sigma}c_\sigma N + \frac{\partial}{\partial \theta}c_\theta N = \frac{S}{\sigma} \qquad (4.1)$$

The first term on the left-hand side of (4.1) represents the local rate of change of action density in time, the second and the third term represent propagation of action in geographical space (with propagation velocities c_x and c_y in x and y space, respectively). The fourth term represents shifting of the relative frequency due to variation in depths and currents (with propagation velocity c_σ in σ space). The fifth term represents depth-induced and current-induced refraction (with propagation velocity c_θ in θ space). The expressions for these propagation speeds are taken from linear wave theory. The terms S at the right-hand side of the action balance equation is the source term in terms of energy density, representing the effects of generation (wind), dissipation, and non-linear wave-wave interactions.The physical phenomena accounted for in this equation are:

- rectilinear and refractive propagation
- wind growth
- bottom dissipation
- surf zone dissipation
- current dissipation
- diffraction

It is used exclusively for determination of the short wave vectors (representing the mean direction of propagation of the short waves) and group velocities. These are required for input in the Surf Beat module as they are used to determine the propagation direction of the bound long waves

This model is the successor of the stationary second-generation HISWA model. In this specific case, SWAN model has only some advantages compared to HISWA model.
The main differences between both models are:

- The wave computation in SWAN are unconditionally stable due to the fully implicit schemes that have been implemented and not limited to a directional sector of 180 º as in HISWA model.
- The computational grid in SWAN has not to be oriented in the mean wave direction, as in the HISWA model.
- SWAN can perform computations on a curvilinear grid, so the coupling between SWAN and FLOW is perfect.
- The main disadvantage is that the SWAN model is several times slower than the HISWA model, but in this type of simulation, this shortcoming is only of minor importance, because just the direction of propagation of the waves is needed and this is enough accurately calculated after two iterations. Besides, it must be taken into consideration that the SWAN computation time is marginal compared with the SURFBEAT computation time.

4.3.2 SURFBEAT

The wave model SURFBEAT is used for the calculation of the bound and free long wave action on time. SURFBEAT is an extension of the Delft3D program and allows the modeling of the effect of short-wave groups on long waves. This effect is caused by spatial variations in the radiation stresses and causes long waves to travel along with groups of short waves (called

carrier waves).The long waves attached to the groups of short waves are called bound waves. The groups of short waves and thus the long waves attached to these groups travel with the group velocity of the carrier waves.

Restrictions
The Delft3D program does not model the individual carrier waves; it does model the forcing caused by the short waves, the wave energy on the group scale that is proportional to the square of the short wave group envelope.
It can only be used in cases where the wave spectrum is narrow-banded both with respect to frequency and with respect to direction (appendix B).

Given these limitations it is possible to determine a dominant frequency (the peak frequency) and a dominant direction from the wave field information (mean direction). These two parameters are then used by to determine a directional field (Swan), which indicates the direction of propagation of the carrier waves; they provides in addition, the direction in which the short-wave energy propagates. This short-wave energy is a quantity that is modeled by Delft3D and it is directly determined from the short-wave components provided at the boundaries (wave components file). This short-wave energy is transported into the domain traveling with the group velocity (Swan), which is based on the peak frequency.
The mean wave direction field along which wave energy and roller energy, in case of breaking waves, are transported is not predicted by the SURFBEAT model, but is imported from SWAN using the usual coupling provided by the WAVE module.

In the following a summary of the wave and flow equations is presented.

Wave equations
The energy is calculated from wave components file at all open boundaries points. The following equation (short wave energy balance equation) (4.2) describes the propagation of this energy in the computational domain:

$$\frac{\partial E}{\partial t} + \frac{\partial \left(c_{gx} E \right)}{\partial x} + \frac{\partial \left(c_{gy} E \right)}{\partial y} = - D_w \qquad (4.2)$$

E represents the short wave energy.
C_g is the group velocity associated with the peak period of the waves and calculated with Swan.
X the distance in the cross-shore.
Y the distance alongshore.
Dw controls the wave energy dissipation due to wave breaking and is calculated using the formulation of Roelvink (4.3):

$$D_w = 2\alpha f_m \left[1 - \exp\left(-\left(\frac{E}{\gamma^2 \left(\rho g h / 8 \right)} \right)^{n/2} \right) \right] E \qquad (4.3)$$

f_m is the peak frequency, γ is a wave breaking parameter representing saturation, α is a short wave dissipation parameter, n a dissipation parameter corresponding to the randomness of the incident waves and h represents the total water depth (including setup and infragravity surface elevation.

Through the wave breaking process, the wave energy is reduced and transformed into roller energy, whose spatial variation generates forces on the water. These effects cannot be neglected in the generation of long waves. The program models the propagation of roller energy with the following roller energy balance equation (4.4):

$$\frac{\partial E_r}{\partial t} + \frac{\partial \left(2 c_{gx} E_r \right)}{\partial x} + \frac{\partial \left(2 c_{gy} E_r \right)}{\partial y} = D_w - D_r \qquad (4.4)$$

The roller energy dissipation is function of the roller energy (E_r):

$$D_r = 2\beta g \frac{E_r}{c} \qquad (4.5)$$

where C = 2 * C_g is the phase velocity.
The tunable parameters α, β, γ and n are explained in 4.4.2.

Flow equations

Once got the short and roller energy, the wave forcing components Fwx and Fwy are calculated using the equations given in 4.6. To calculate these wave forcing components the module calculates the radiation stresses (Sxx, Sxy, Syx and Syy) at the grid points. These can be calculated in turn from the energy calculated from the Fourier components of the short wave signal, the short wave vectors θb and the roller energy Er. The roller energy is a variable introduced to simulate the process of breaking waves.

$$F_{wx} = -\frac{1}{\rho \mathrm{h}}\left(\frac{\partial S_{xx}}{\partial x} + \frac{\partial \mathrm{S_{xy}}}{\partial \mathrm{y}}\right) \text{ and } F_{wy} = -\frac{1}{\rho \mathrm{h}}\left(\frac{\partial S_{yx}}{\partial x} + \frac{\partial \mathrm{S_{yy}}}{\partial \mathrm{y}}\right) \qquad (4.6)$$

$$S_{xx} = \left(n - \frac{1}{2} + n\cos^2(\theta_b)\right)E + 2\cos^2(\theta_b)E_r \qquad (4.7)$$

$$S_{xy} = S_{yx} = \cos(\theta_b)\sin(\theta_b)\left(nE + 2E_r\right) \qquad (4.8)$$

$$S_{yy} = \left(n - \frac{1}{2} + n\sin^2(\theta_b)\right)E + 2\sin^2(\theta_b)E_r \qquad (4.9)$$

The short-wave averaged, depth-averaged velocity field is computed with non linear shallow equations. Surfbeat solves the shallow water equations with a wave induced forcing as described in equations (4.10, 4.11 and 4.12).Here u and v are velocities in respectively the x and y direction, C is the smoothness parameter according to Chezy and ξ is the surface elevation.

$$\frac{\partial \zeta}{\partial t} + \frac{\partial}{\partial \mathrm{x}}\left(\left(h + \zeta\right)u\right) + \frac{\partial}{\partial y}\left(\left(h + \zeta\right)v\right) = 0 \qquad (4.10)$$

$$\frac{\partial u}{\partial t} + \mathrm{u}\frac{\partial u}{\partial \mathrm{x}} + \mathrm{v}\frac{\partial u}{\partial y} + \mathrm{g}\frac{\partial \zeta}{\partial x} - fv = F_{wx} - \mathrm{Cu}\sqrt{\mathrm{u}^2 + v^2} \qquad (4.11)$$

$$\frac{\partial v}{\partial t} + \mathrm{u}\frac{\partial v}{\partial \mathrm{x}} + \mathrm{v}\frac{\partial v}{\partial y} + \mathrm{g}\frac{\partial \zeta}{\partial y} + fu = F_{wy} - \mathrm{Cv}\sqrt{\mathrm{u}^2 + v^2} \qquad (4.12)$$

4.4 Description of Parameters

4.4.1 Swan

Significant Wave Height and Wave Period
Wave height and period Peak period were obtained from the wave data. Wave heights used were obtained from the Saldanha Bay Wave Rider calculated spectrums with the expression (4.13). Wave heights at the seaward boundary were iteratively calculated using the mean direction, spreading and peak period as constants. The offshore Hs, was increased until the wave height at the Wave Rider location was the same as the observed value for that particular storm. For most storms, this meant almost doubling of the significant wave height. Peak period was assumed not to change, which is probably of some influence to the results; this one was calculated from the Wave Rider spectrum using the expression (4.14).Table 4.1 contains the summary with the calculations performed.

$$H_{m0} = 4\sqrt{m_0} \qquad m_i = \int_0^{\infty} w^i E \; dw \tag{4.13}$$

$$Tp = \frac{1}{fp} \tag{4.14}$$

Width Energy Distribution and Mean Direction
The directional standard deviation can be computed in degrees or using the parameter *ms*, since the directional distribution of incident energy has been supposed to be described by the relation:

$$D(\theta) = \cos^{ms}(\theta) \tag{4.15}$$

.
The SWAN model considers the mean wave direction.
Directional information from the Slangkop Wave rider was used to obtain directional information. These parameters were not changed as they are near deep water conditions. The Slangkop Wave Rider is situated at a location with 78 meters water depth. As the seaward boundary is located at nearly the same depth the directional information is probably the most suitable and the only information regarding direction. The spreading parameter and mean wave directions used for all storms are shown in table 4.1.

Parameter	storm1	storm2	storm 3	storm4
Hmo Wave Rider [m]	3.17	5.11	5.04	3.65
Hmo Boundary [m]	5.6	8	9.6	6
Wave direction [°]	265.3	252	224	237
Wave spreading ms [-]	14.77	15.68	18.35	15.67
Peak period [s]	12.2	17.1	20.1	19.5

Table 4.1 Measured waves characteristics

Peakedness parameter (γ)
JONSWAP spectrum was used for the simulations with Swan as input at the sea boundary. Values for the peakedness parameter and Jonswap spectrums for each storm are shown in appendix C.
The peakedness parameter was iteratively calculated for each storm using the peak period (table 4.1) and spectrum peak energy from the Wave Rider as constants (see 3.3.4). First, Jonswap spectrum was calculated using a value of peakedness parameter of 3.3 and peak period constant value from the Wave Rider spectrum. Then, Jonswap and Wave Rider spectrum m_0 values were known; so dividing Jonswap spectrum energy values for Jc (equation 4.16) we got Jonswap spectrum m_0 value to be the same as Wave Rider spectrum m_0. Finally we had just to change peakedness parameter (γ) value till Jonswap spectrum energy peak was the same as Wave Rider energy peak. In this way, we get that Jonswap spectrum has the same m0 and peak energy values than Wave Rider spectrum.

$$Jc = \frac{\text{m0 Jonswap}}{\text{m0 Wave Rider}} \qquad (4.16)$$

Other parameters
All other parameters were set as default, they are:
- Water density: 1020 [kg/m3]
- Depth induced breaking: gamma = 0.73

  Note that this depth induced breaking parameter is different from the one used for the Surfbeat computation. In this case, the main output from Swan, are the wave directions and the value of the SWAN gamma parameter does not affect the Surfbeat computations.

Bottom friction
SWAN incorporates several bottom friction options. The default is the semi-empirical expression from the JONSWAP results by Hasselmann et al [1973]. The recommended friction coefficients are 0.067 for wind wave conditions, and 0.038 for swell. The value for swell was selected.

4.4.2 Surf Beat

Bed friction
Bed friction is probably quite important for Saldanha Bay as the propagation distances of the waves inside the modeled area are large.
SURFBEAT uses several friction formulations; in this case, for conversion of the Nikuradse roughness to the Chezy smoothness factor the White-Colebrook formulation, as stated in equation (4.17), is used by the Surf Beat module.

$$C = 18^{10} \log\left(\frac{12\,h}{K_s}\right) \qquad (4.17)$$

The bottom friction is an important parameter and an equivalent geometrical roughness of 0.2 [m] was used in almost all the computations, which is the default value the manual recommends in case of lack of data. This value will be analyzed in the calibration procedure.

Wave component file
The Surf Beat module needs the wave field energy at each open boundary point for each time step. This energy envelope is calculated from Fourier components. In appendix C, we describe the structure of the file ' wavecmp' (wave component file) needed to get the Fourier components of the incoming short and long wave signals.
The file contains the discretization of an amplitude spectrum, the phase angle of the wave signal and its direction considering the spreading angle; these values are presented in an equidistant frequency grid. Amplitude and frequency information are obtained from an energy spectrum at flow boundary calculated from swan runs.

Split frequency
As SURBEAT calculates both the bound waves, carried by the group of short waves, and the free waves, it is necessary to input the split frequency that will make the difference between short and

long waves. The split frequency was selected using the energy spectra from figure 4.3. As can be seen for smaller frequencies than 0.03 we do not have energy as the Wave Rider just record short wave data.

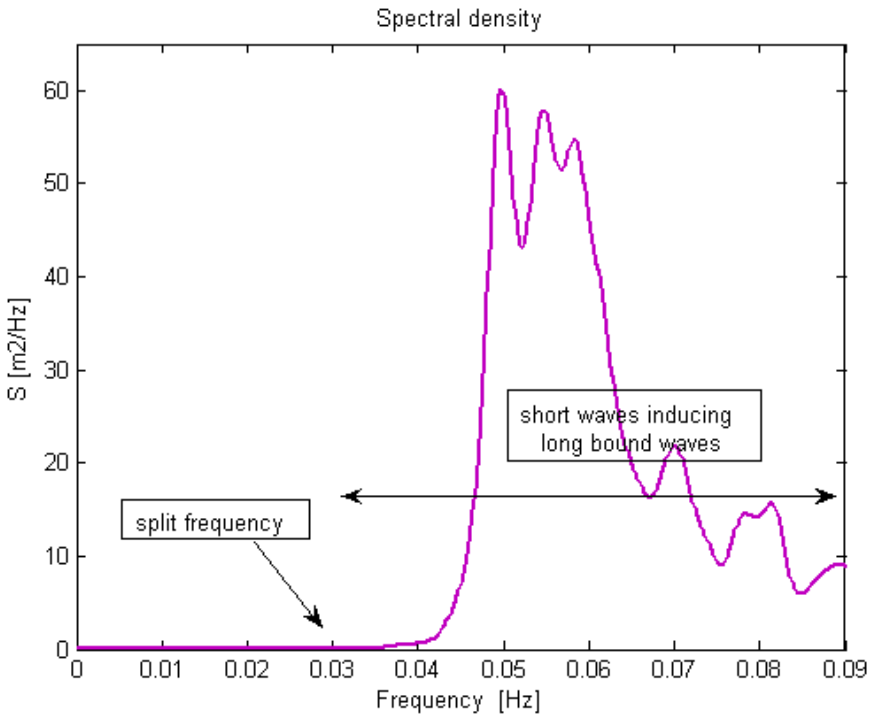

Figure 4.3 Wave Rider energy spectrum: storm 3

In this case has selected 0.03 [Hz] as split frequency, which is concordant with the value of 30 [sec] proposed by Hiraishi et al[1997] as minimum period for the long waves in Tomakomai Port [Numerical model of long waves in harbors - Patricio Monárdez Santander, July 2004].

Bathymetry and layout

Boundary location The boundary location is situated at some 3.5 Km offshore. The local water depth at this location is 68 meters on average.

Computational grid it is very important to define the right cell size; a rough grid, can make us lose information about the higher frequencies [0.02-0.03 Hz], less information as more rough is the computational grid (appendix C).
The final computational grid shown in figure 4.4 features a grid composed of some 214.000 active grid cells. This rather large amount of cells will take little over 12 hours to compute, depending on numerical issues. Grid size is on average some 30 meters. The Langebaan lagoon, stretching out some 20 kilometers down south, was not modeled as it was assumed that the long wave would dissipate to a large extent due to the shallow water depth. Grid size would have to be almost doubled for the modeling of this lagoon.
The jetty servicing the liquid bulk carriers consists of some circular caissons. Considering the open type of the structure it was decided not to model this part of the mooring facilities as long waves probably travel virtually undisturbed through this part of the jetty.

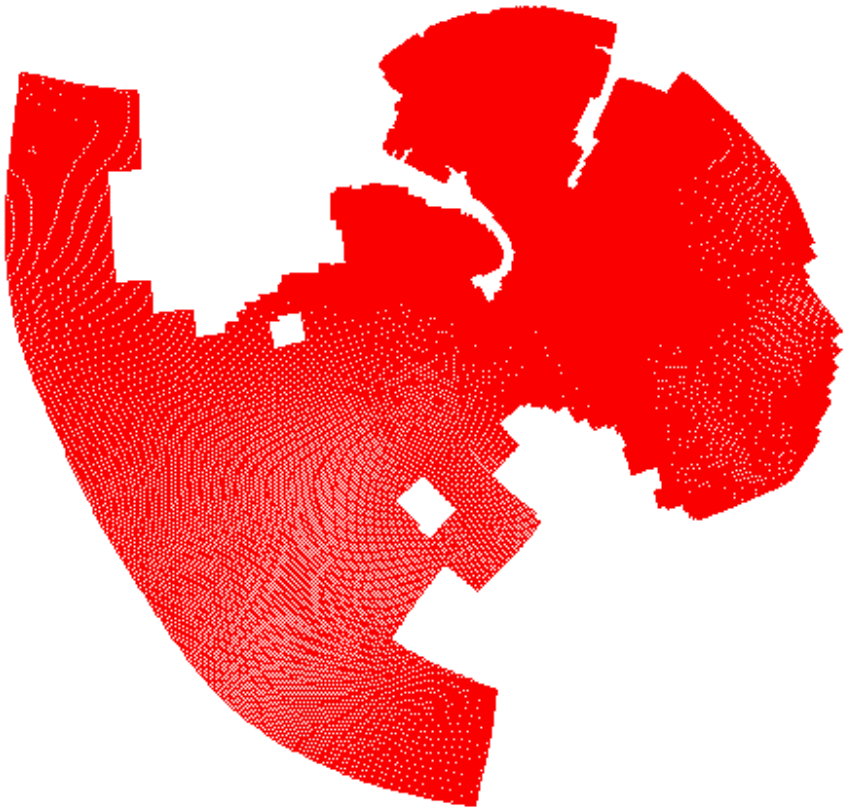

Figure 4.4 Final computational grid (flow) for Saldanha Bay area

Bathymetry The bathymetry is specified on the computational grid shown above. The water depths were computed using samples of the water depth for the area. The resolution of these

samples exceeded the grid resolution by far, which made the current bathymetry quite accurate. Figure 4.5 shows a map of the area with water depths at all grid points.

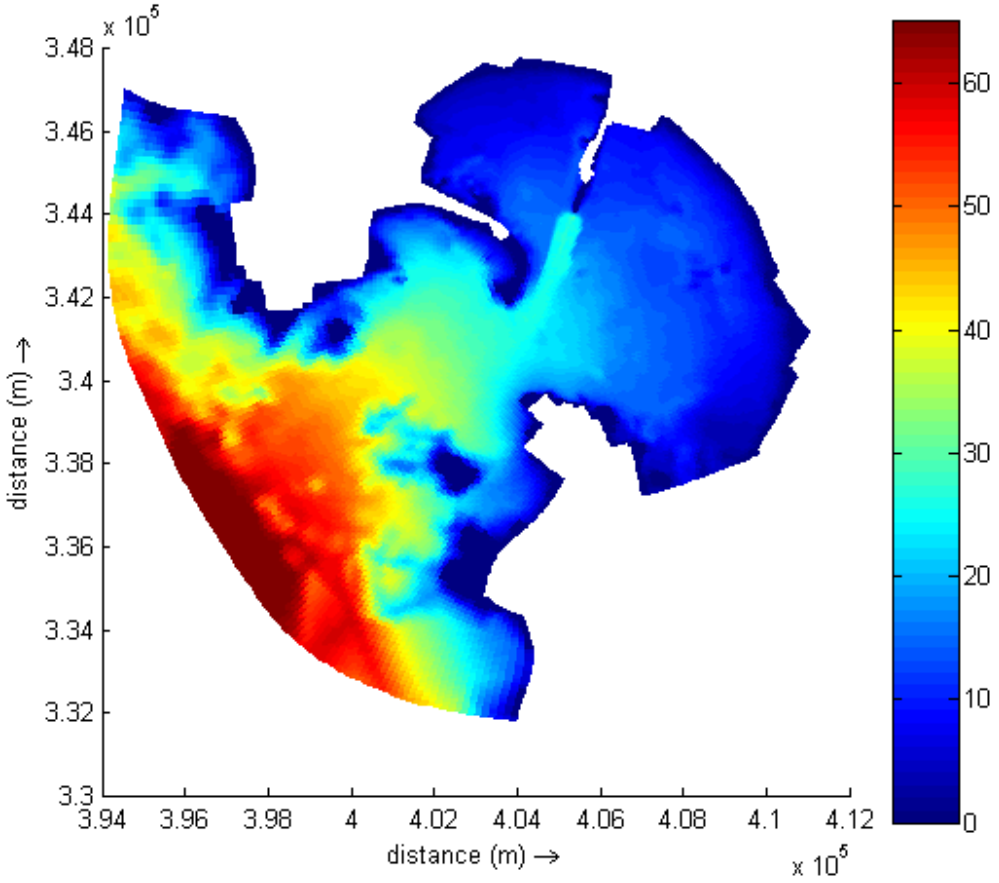

Figure 4.5 Bathymetry for Saldanha Bay area including the nearshore region

Short Wave dissipation

The parameters α, β, and *n* were set at first as the default parameters described by Roelvink [1993], although was not in this way for γ. In his work he reaches the conclusion that for certain constant values of those coefficients the dissipation formulation produces accurate results over a range of conditions with random waves. According his calibration, the values are:

$\alpha = 1.0$ $\beta = 0.1$ $\gamma = 0.55$ n = 10

The γ parameter is defined as the wave height to water depth ratio, which is related to the wave depth-breaking condition. The recommended value of *0.55* was obtained from several simulation cases with data obtained from one-dimensional laboratory using bichromatic waves and random waves over a shallow bed without reflection. An investigation carried out by Baquerizo and Losada [1999], showed that in front of a reflective structure, γ follows a two parametric Weibull distribution with one of the parameters depending on the wave reflection; values of γ from 0.2 to 0.9 were calculated. Van Gelder and Vrijling [1999] investigated the probability of a breaking wave in front of structure as a function of the γ parameter. According to their results, the probability of breaking starts at γ = 0.35, this value is lower than the one calculated for wave breaking over a shallow bed without reflection (γ = 0.55).
Losada [1999] proposed a relation between γ and the foreshore slope. A slope value of 0.035 corresponds to γ = 0.55; so like the slope in Saldanha Bay is smaller, was decided to use a value of γ = 0.45 for the first simulation (appendix C).

Tide
It was decided not to model tidal conditions for Saldanha Bay. The effect on the wave field is uncertain, though expected to be low. First tidal components were removed from the signal in Saldanha Bay.

Reflection coefficients
As it is hard to implement a frequency dependent boundary reflection coefficient for each structure in the bay it was decided to leave the boundary conditions as they are by default (fully reflection). Effects of this measure could be an overestimation of the reflections of the long waves and resulting higher energy levels than should be expected.

Chapter 5

Numerical model calibration, validation and sensitivity analysis

5.1 Chapter Overview

The calibration procedure is thoroughly explained in this chapter. The sensitivity analysis is carried out to perform a qualitative analysis of the program behavior. For the sensitivity analysis the wave data for storm 3 was used. The effects of changes in certain parameters are studied to analyze the behavior of the model. Finally validation of parameters was done with the other storms.

5.2 Calibration procedure

In general, a model calibration is needed to tune free parameters, such as the breaker index parameter (γ) and the friction coefficient. However, for this case, it was complicated by the fact that information about the boundary conditions was not known, for instance directional information of the short waves; only directional information from Slangkop was provided.
Because of the time required for the simulations, the calibration procedure was done for the third storm (May 2002). The third storm is one of the most severe storm; from the previous report it was seen that energy levels at different energy spectrums in calibration procedure were higher and more clear to check than for the other storms.
Although the 80 minutes length was selected for H_s criteria, finally we decided to select the last 50 minutes to get the long wave spectrum to compare with the simulated. As can be seen in figure 5.1 standard deviation keeps approximately constant between 30 and 80 minutes. So then the period between 5:50 and 6:40 was selected for calibration.

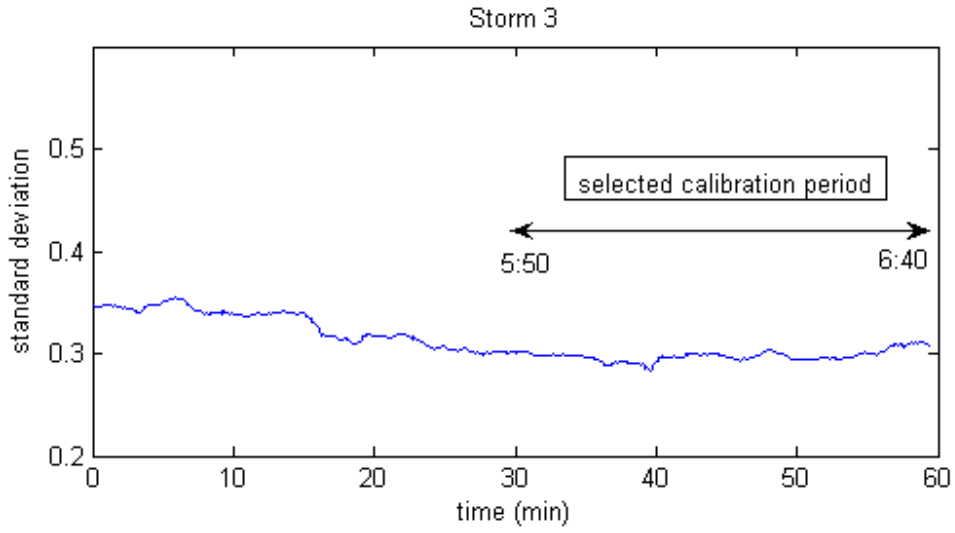

Figure 5.1 Standard deviation - time graph for the selected records on 25 th of May 2002 5:20 - 6:40

5.2.1 Storm 3: first run

A starting point is necessary: directional information from Slangkop, peak period from Wave Rider and significant wave height from the previous calibration procedure with Swan (see 4.4.1) were selected for the first run (table 4.1). The main direction for short waves was assumed as 224 nautical degrees. The standard deviation for short waves was assumed about 10 degrees (ms = 18.35). For the short wave dissipation a value γ = 0.45 was selected and value of 0.2 [m] for bed friction (see 4.4.2).
For the first run a time length of 150 min was selected (see 3.3.3.); after 60 minutes, it can be considered that some stationary situation is established. Then we have 90 minutes data to get the energy spectrum at Tide Recorder location.
In this point before analyzing the results, a study of the time period influence was carried out for the first simulation.

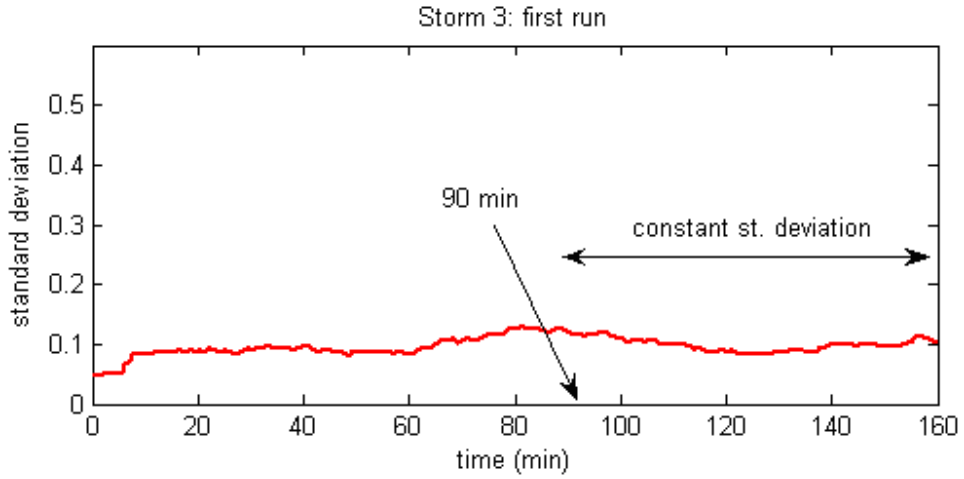

Figure 5.2 First run: standard deviation for period 0-180 minutes

Figure 5.2 represents the standard deviation for the first simulation: for the period between 60 and 150 minutes we have a bump in the graph (60 - 90 minutes) that causes a variation of the standard deviation. However after 90 minutes, the standard deviation keeps approximately constant.

Two spectrums corresponding a different periods were calculated (figure 5.3).The energy for the peak frequency for the period 60-150 minutes of the simulation is higher than the one for the period of 90-150 minutes. We can consider that stationarity has not reached yet.

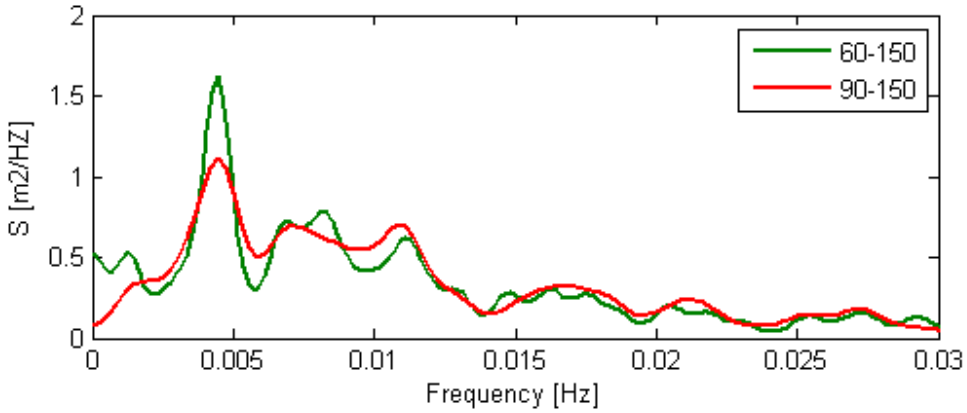

Figure 5.3 First run: energy spectrums for periods 60-150 and 90-150 minutes

A longer run of 3 hours for the first simulation was done to check what happened with the energy spectrum if we chose another longer period. Figure 5.4 shows the results for 90-150 and 90-180 periods. As can be seen, both spectrums are quite similar; so then we can consider for this and next simulations that the stationary situation is established at 90 minutes. A 3 hours simulation takes more time so for the next runs of the calibration procedure was decided to continue with 2.5 hours (150minutes) getting then 60 minutes of simulated data for comparison with the measured ones.

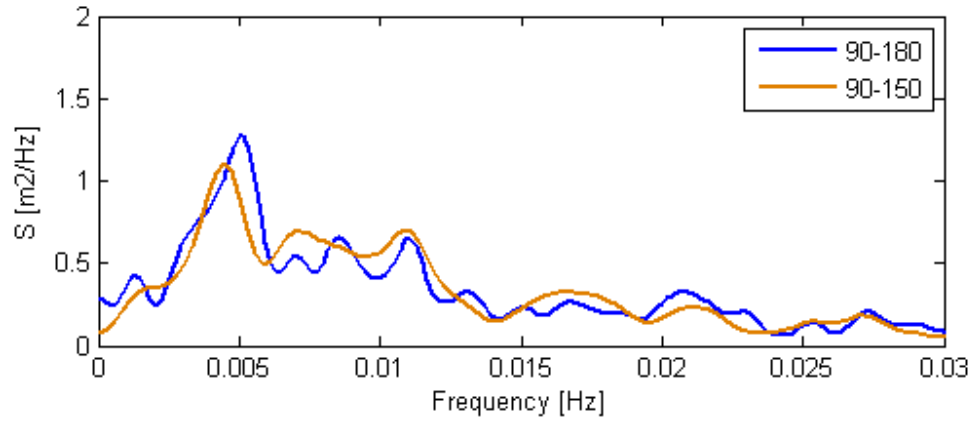

Figure 5.4 First run: energy spectrums for periods 90-150 and 90-180 minutes

Calibration criteria

The H_s for the long waves at the Tide Recorder can be used for the calibration purposes. In addition, the spectral shape of the long wave energy content is used (equation 5.3), which is supposed to match qualitatively with the measured one. From the measured and simulated data at Tide Recorder, H_s was calculated for long waves components using the relation (4.14).

Tide Recorder	H_s [m]
measured	0.406
simulated	0.405
error [%]	0.25
skill	0.81

Table 5.1 Tide Recorder: storm 3 first run

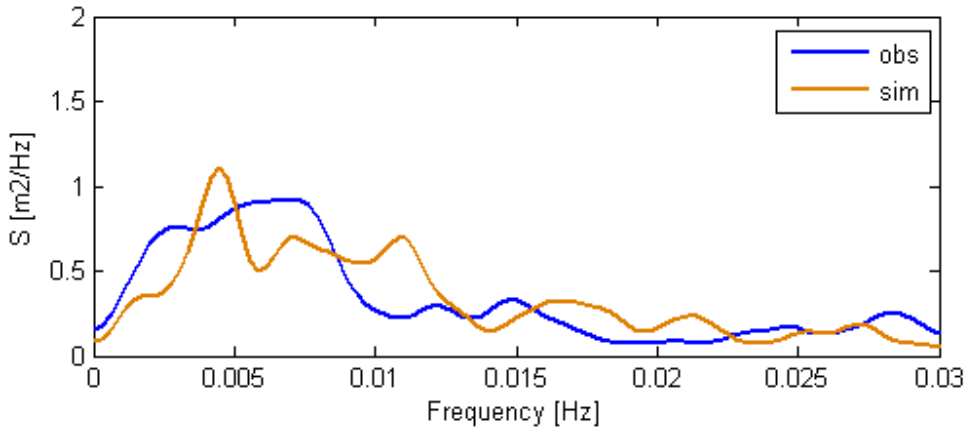

Figure 5.5 Storm 3 first run: observed and simulated spectrums at Tide recorder location

In spite of high skill value, figure 5.5 shows a few differences for the simulated and observed spectrums. For the frequencies 0.0045 and 0.011 [Hz] simulated spectrum has two peaks higher than energy in observed, while around frequencies between 0.0055 - 0.008 [Hz] the energy in observed spectrum is higher than simulated. In general, simulated spectrum has more peaks than observed that is more flat. However the error in H_s for the long waves is 0.25 % (table 5.1).We will try to reduce these differences between both spectrums. Then some parameters as main direction, directional spreading, breaker index parameter and the friction formulation will be calibrated. Once selected the mean short wave direction and directional spreading, breaker index parameter and bed friction will be able to be tuned.

5.2.2 Parameters sensitivity analysis

The effects of changes in certain parameters are studied to analyze the behavior of the model. Finally, based on this analysis, definitive parameters will be chosen for the final simulation.

Table 5.2 shows the different simulations used in the analysis.

Simulation	Direction	D. spreading	Breaker I.parameter	Friction
1	**224**	10	0.45	0.2
2	**215**	10	0.45	0.2
3	**235**	10	0.45	0.2
4	224	**8**	0.45	0.2
5	224	**10**	0.45	0.2
6	224	**16**	0.45	0.2
7	224	**20**	0.45	0.2
8	224	10	**0.4**	0.2
9	224	10	**0.45**	0.2
10	224	10	**0.5**	0.2
11	224	10	**0.55**	0.2
12	224	20	0.5	**1**
13	224	20	0.5	**0.5**
14	224	20	0.5	**0.2**
15	224	20	0.5	**0.05**

Table 5.2 Sensitivity analysis simulations

For friction coefficient analysis, other values different from the first simulation for breaker index parameter and directional spreading were used; it was done because during calibration analysis, simulations with the first values were not run and the only runs available were with these other values.

5.2.2.1 Mean Direction

Two simulations more were done for the main direction calibration; one with 10 degrees more (235°) and another one with 10 degrees less (215°) than the measured to compare with the first run (224°).

In the table 5.3, we can see that the H_s value for 224 ° is the one with the lowest error.
For the spectrum shape, the 224° run shows the best agreement with the measured (figure 5.6); peak frequency [0.0045 Hz] is in the peak energy interval for the measured spectrum. The peak at 0.011 Hz does not appear in the measured spectrum; this problem will be studied later.

For the other directions, 215 and 235 degrees, the peak frequencies 0.009 and 0.0105 respectively (peak energy), are out from the peak energy interval for the measured spectrum [0.003 - 0.008 (Hz)]. However the energy for frequencies [0.005 - 0.01 Hz] for 235 degrees is higher than for 215 degrees, being of the same order of 224 ° simulated energy for [0.005 - 0.008 Hz].

Comparing simulated spectrums, it is clear that the sensitivity to the mean direction is large. The shape of simulated spectrums is completely different above all for the low frequencies.

Directional Spreading (standard deviation)	Mean short direction (nautical degrees)					
	215		224		235	
	H_s [m]	Error [%]	H_s [m]	Error [%]	H_s [m]	Error [%]
ms = 18.35 (10.03 °)	0.35	13.79	0.405	0.25	0.381	6.16

Table 5.3 H_s calculated for the Tide Recorder. Measured value H_s = 0.406 [m].
Directional spreading = 10°

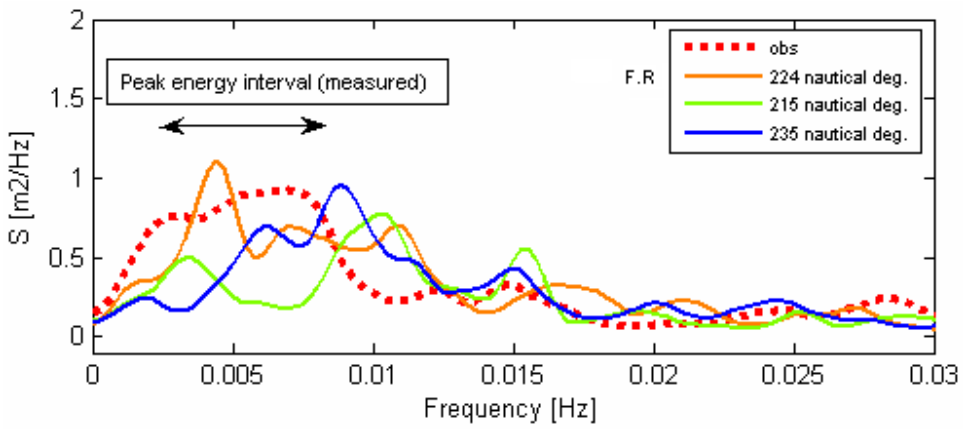

Figure 5.6 Mean direction spectrum comparison
Directional spreading = 10°

5.2.2.2 Directional spreading

Some simulations were run with different directional spreading: 5, 8, 10, 12, 16 and 20°.

Directional Spreading (standard deviation)	Main short direction (º) 224		
	$H_{s\ [m]}$	Error [%]	skill
5 º	0.388	4.43	0.76
8 º	0.406	0	0.72
ms = 18.35 (10.03 º)	0.405	0.25	0.81
12 º	0.407	0.25	0.81
16 º	0.389	4.19	0.82
20 º	0.364	10.34	0.79

Table 5.4 H_s calculated for the Tide Recorder. Measured value H_s = 0.406 [m].
Mean direction = 224 °

As can be seen in table 5.4, results are not what we hoped. We hoped to have smaller wave height values as higher was the directional spreading but the results do not agree with this. For higher values than 10°, the energy decreases more as higher is the value of directional spreading; however for smaller values of standard deviation, the energy increases or decreases depending on the value selected. We suppose this random behavior is consequence of Saldanha bay restricted entrance; in the main bay we have some obstacles like islands, breakwater..., so the effects on the results will be different depending on the interaction of directional spreading-direction with this restricted entrance.

Although skill values are quite good for all the values, we can see some differences between measured and simulated spectrums that we will try to reduce.

For 5 and 8 ° the spectral shape is quite similar; just the energy for 8 ° spectrum is higher for some frequencies. For 0.0044 Hz both spectrums have an energy peak higher than the value measured for that frequency; we have the same situation for 0.011 Hz frequency. However for the frequencies between [0.005-0.009] the simulated energy is much smaller than measured (figure 5.7).
Simulation with 10 ° gets to increase the energy in the frequencies interval [0.005-0.009 Hz] while the energy value for 0.011 Hz keeps constant (figure 5.7). The peak for 0.0044 Hz decreases a little bit, but is still far from the measured one; however, the H_s is similar to the measured, with an error very small. The shape for 12 ° is practically the same as 10 ° simulated spectrum.

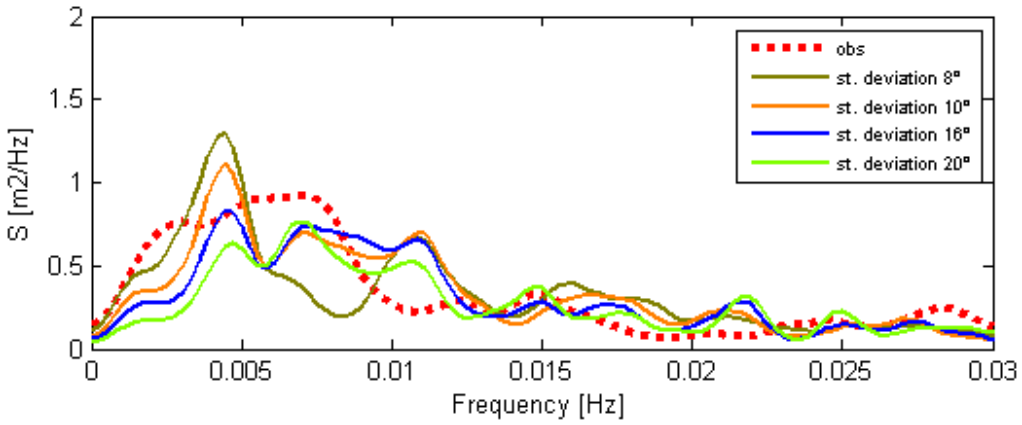

Figure 5.7 Directional spreading comparison
Mean direction = 224°

If we go on increasing the value of directional spreading (16° and 20°), the peak value of 0.0044Hz, continues decreasing while the energy for [0.05-0.009 Hz] frequencies keeps approximately constant, decreasing a little bit for 0.011 Hz.
As can be seen in figure 5.7 the model is sensitive to the directional spreading. The most sensitive are the lowest frequencies [0 - 0.013 Hz], above all the peak frequency around 0.0044Hz.

5.2.2.3 Breaker index parameter (γ)

As happened with the directional spreading, variation of the spectral energy is higher for the low frequencies [0-0.013 Hz] than for the others. The only difference is that the model is very sensitive for the frequencies around 0.011 Hz while for the directional spreading the energy at this frequency kept approximately constant.
If we increase the value of breaker index parameter (0.5 and 0.55) the energy for all the frequencies increases, much more for the low frequencies [0-0.013Hz] (special mention for the peaks at 0.0044 and 0.011 Hz). If we decrease gamma parameter (0.4) the effect is the opposite: energy drops for all the frequencies although higher for the low frequencies (appendix D).

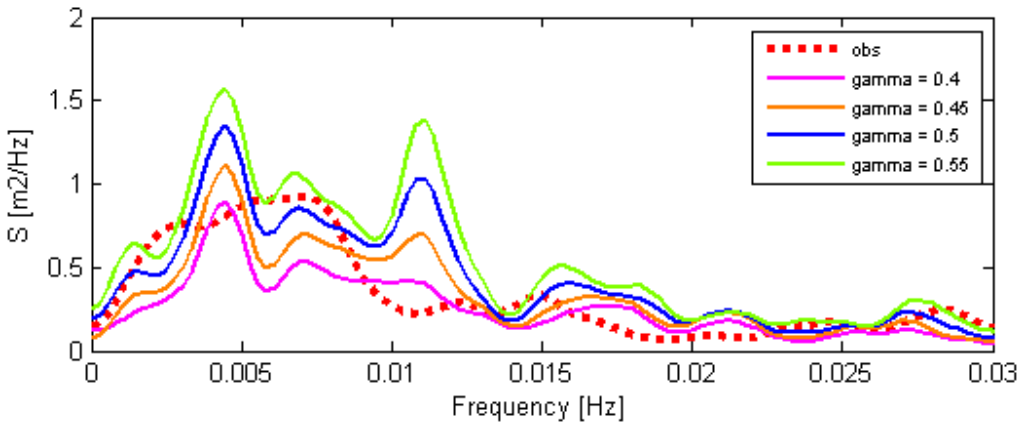

Figure 5.8 Breaker index parameter comparison

5.2.2.4 Friction coefficient

Friction coefficient is the last parameter to analyze. A value of 0.2 [m] was chosen for the previous simulations. This value is the default value the manual recommends in case of lack of data. Some simulations with different value for the friction were run to study its influence; unlike the other parameters, the sensitivity of the model to the friction is smaller; as is we hope, as higher is the friction coefficient as smaller is the spectral energy because we have more dissipation of energy in the bay; but these differences in spectral energy for the different values of friction are smaller than we got for breaker index parameter and affect in the same way the energy of the whole spectrum. So we can conclude that the model is not very sensitive to the friction as we stated in 3.4 (bed material data).

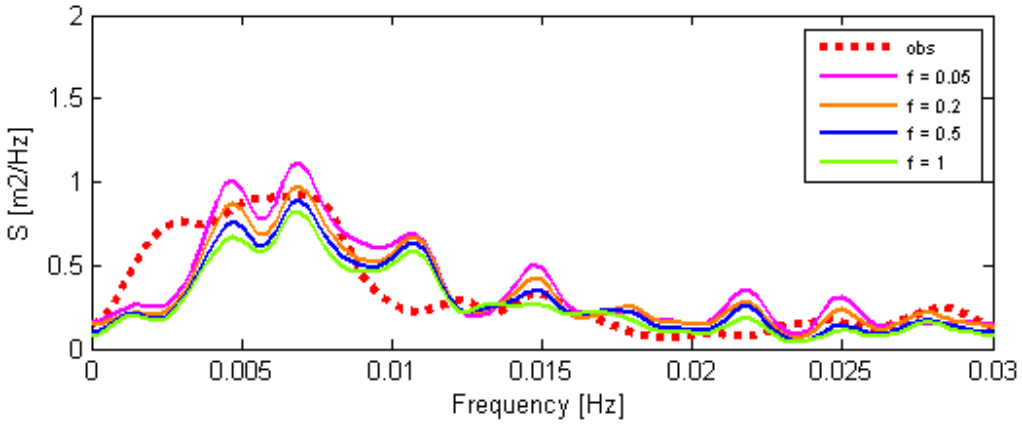

Figure 5.9 Friction coefficient comparison

5.2.3 Resonance

Long wave action inside the port due to resonance was analyzed to find out if the peaks at 0.0044, 0.007 and 0.0108 Hz for the simulated spectrum were caused for resonance inside the bay. It was decided to calculate natural modes of resonance for Saldanha bay port area (figure 5.10).
As we know, we chose default boundary conditions for reflection coefficients (fully reflection); effects of this measure could be an overestimation of the reflections of the long waves and resulting higher energy levels than should be expected.

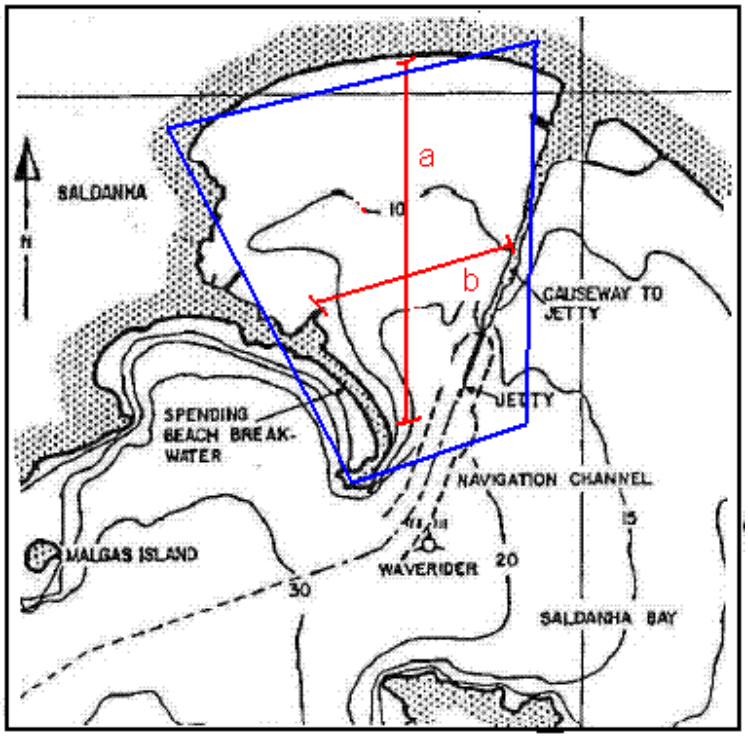

Figure 5.10 Saldanha Bay: resonance study area

Although Saldanha Bay harbor is not a closed basin, harbors or parts of harbors can behave much like closed basins under some conditions.
A harbor basin generally has several modes of oscillation with corresponding natural resonant frequencies (or periods) and harmonics. The natural frequencies of the port were calculated using the most simple and wide known method: Merian's method (Raichlen, [1966]), which applies the expression (5.1):

$$T = \frac{2}{\sqrt{gh}}\left[\left(\frac{n}{a}\right)^2 + \left(\frac{m}{b}\right)^2\right]^{-1/2} \qquad (5.1)$$

This formula gives the natural period of the basin in terms of its lengths (*a*, *b*) and depth (*h*) for some modes of oscillation. It is valid for rectangular basin which has significant width as well as length. We can approximate Saldanha Bay as a rectangular basin with significant width.

Parameter	Value
a [m]	4193
b [m]	2790
h [m]	8

Table 5.5 Resonance parameters values for Saldanha Bay

Table 5.6 shows a summary of the modes of oscillation for Saldanha Bay.

Merian method	Natural period 1 [s]	Natural period 2 [s]	Natural period 3 [s]
	262.2	131.1	87.4
f [Hz]	0.0038	0.0076	0.0114

Table 5.6 Natural frequencies values for Saldanha Bay using Merian method

The values for the natural frequencies were calculated (table 5.6). If we see the figure 5.11, it is very easy to check that the natural modes fit in with the peak frequency values (energy peaks) for the third storm (.0044, 0.007 and 0.0108 Hz).It is possible to suppose that the energy at these frequencies for the simulations is higher than they would have to be, due to the effect of the resonance as in the simulations, Surfbeat considers fully reflection at the boundaries what it is a simplified assumption of the reality.

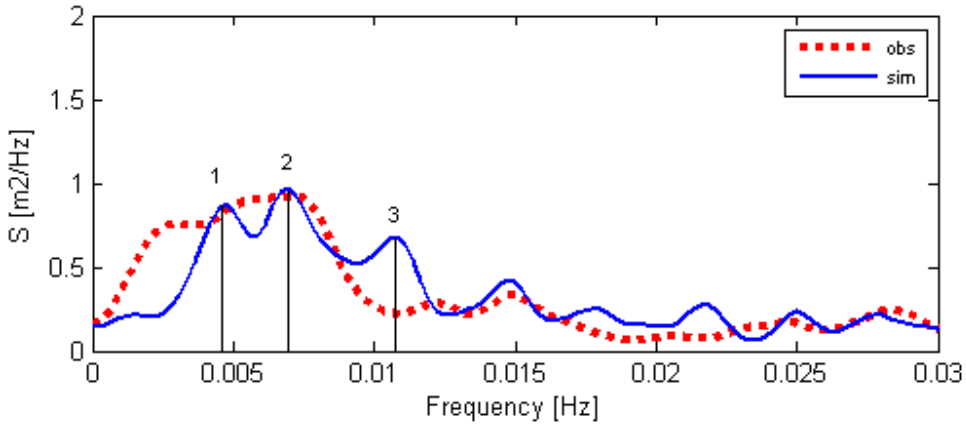

Figure 5.11 Natural frequencies for Saldanha Bay: storm 3 calibrated simulation.

5.2.4 Calibration conclusion

The values for the different parameters selected from the calibration of the third storm are represented in table 5.7.

Parameter	value
Main direction [º]	224
Directional spreading [º]	20
Breaking index parameter [-]	0.5
Friction coefficient [m]	0.2

Table 5.7 calibrated parameters for storm 3

Value from Slangkop was selected for the mean direction while for the directional spreading a value of 20º was used instead of the measured of 10º. Explanation of this decision is given in validation section. For the other parameters, a value of 0.5 was chosen for breaker index parameter, in between the calculated with Losada's relation (see 4.4.2) and the default one of Roelvink, and a value of 0.2 [m] for bed friction (default value in case of lack of data).

The parameters were calibrated such that the model results at Tide Recorder matched optimally by minimizing the error equation (5.2) and maximizing the skill equation (5.3).

$$Error = \frac{Hs_{sim} - Hs_{meas}}{Hs_{meas}} 100 \qquad (5.2)$$

where Hs_{sim} is the simulated significant wave height and Hs_{meas} is the measured significant wave height, both for long waves at Tide Recorder.

$$\text{skill} = 1 - \frac{\sum_{1}^{N} (y_i - x_i)^2}{\sum_{1}^{N} (x_i)^2} \qquad (5.3)$$

where y_i are the model results and x_i are the observations of spectral energies at Tide Recorder.

Table 5.8 shows the simulated significant wave height for the chosen parameters values and the comparison with the measured data:
- Error: give us an idea of the difference between the simulated and measured significant wave height.
- Skill: give us an idea of the difference between simulated and measured spectral shape.

Tide Recorder	H_s [m]
measured	0.406
simulated	0.406
error [%]	0
skill	0.85

Table 5.8 Analysis results of storm 3 calibration

As we can check in figure 5.12, the simulated spectral shape is accurate enough. We only have some differences with the measured spectrum:
1. Peak energy at 0.011 Hz that is common for all the simulations run. We can consider it related to resonance effects.
2. Small energy level for the frequencies between 0-0.004 Hz (it will be studied in validation section).

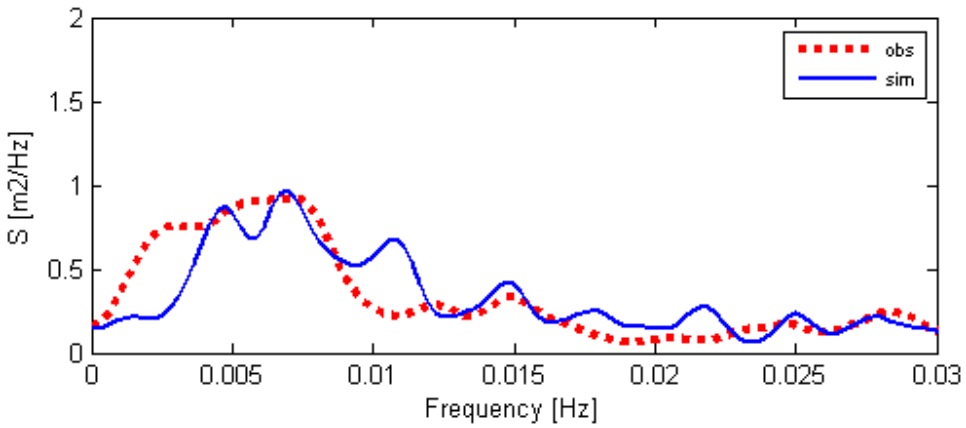

Figure 5.12 Calibrated simulation for storm 3

Like shows table 5.8, results for the definitive storm 3 simulation are quite accurate, both significant wave height and spectral shape. The value of the simulated significant wave height is the same as the measured. The spectral shape for both spectrums (simulated and measured) has a few differences as we mentioned. Skill parameter was used to study these differences; a value of 0.85 was obtained for the final simulation what is a good value. We can consider the calibrated parameter values like good values.

5.3. Validation

5.3.1 Study of the other storms

The conclusions from the study of the third storm were used in the study of the other storms to make sure that the parameters chosen were correct.
The H_s results for the storms 1 and 2 are far from the measured (table 5.9); however the agreement in the spectral shape between the measured and all the storms, is quite good as we can check in table 5.9 and figures 5.13, 5.14 and 5.15; values of skill parameter are over 0.5 for all the storms, being around 0.8 for three of the four storms (storm 2, 3 and 4).

Storm	$H_{s\ obs}$ [m]	$H_{s\ sim}$ [m]	Error [%]	Skill
1	0.199	0.136	31.66	0.62
2	0.443	0.346	21.90	0.79
3	0.406	0.406	0.00	0.85
4	0.357	0.349	2.24	0.81

Table 5.9 H_s, error and skill values for all storms (γ = 0.5 and f = 0.2 [m])

For the storm 1, the energy level for the simulation is lower than measured for almost all the frequencies. Moreover, the simulated H_s for this storm, is much smaller than measured. This storm has the lowest skill value as well although higher than 0.5.

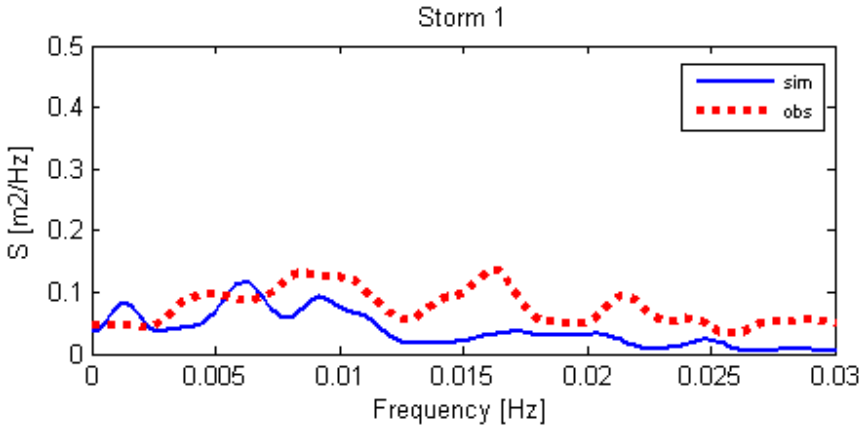

Figure 5.13 Storm 1 simulation (γ = 0.5 and f = 0.2 [m])

Energy values for storm 2 are smaller for almost all the frequencies as well, like happened with storm 1, but the differences between the measured and simulated values are not so high as for storm1 except for the lowest frequencies [0-0.006 Hz]; these low frequencies are for sure the reason of the high significant wave height error. So except for the low frequencies, the spectral shape matches with the measured.

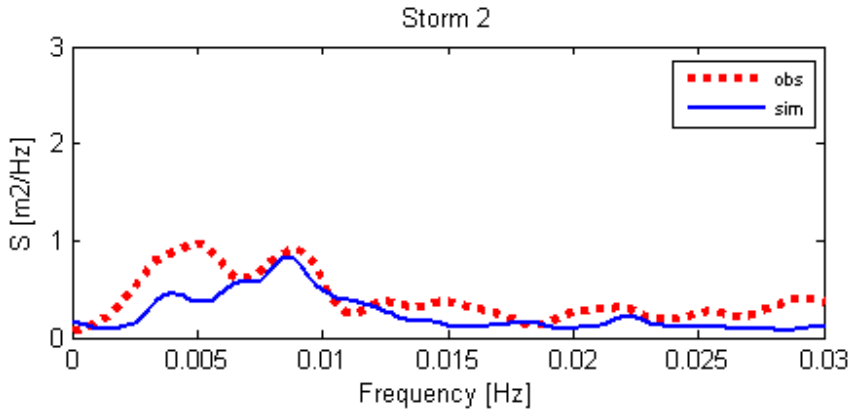

Figure 5.14 Storm 2 simulation (γ = 0.5 and f = 0.2 [m])

Storm 4 shows the best agreement with the measured data of all the storms used for the validation. Significant wave height and spectral shape are quite similar to the measured as proves the values of error and skill in table 5.9.

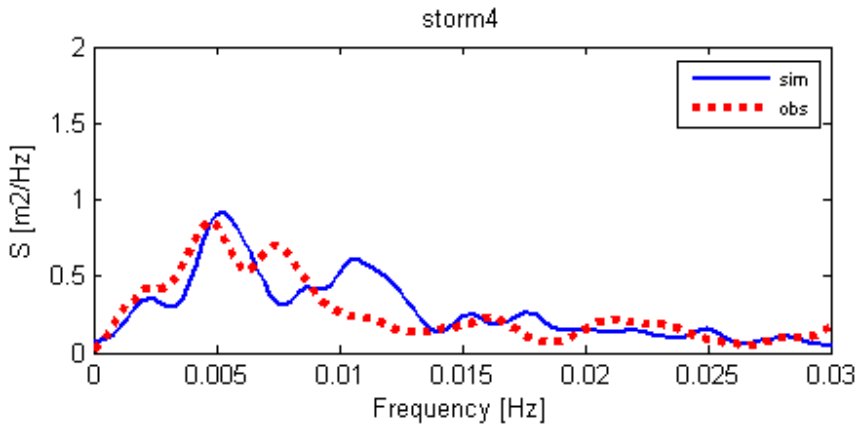

Figure 5.15 Storm 4 simulation (γ = 0.5 and f = 0.2 [m])

5.3.2 Directional spreading discussion

Directional spreading data from Slangkop was used in all the storms except for storm 3. For this storm, it was 10º but after calibration procedure we decided to use a value of 20º for the final simulation.

As can be seen in figures 5.16 and 5.17, significant wave height is higher at the small bay for storm 3 than for storm 2; then dissipation will be higher for storm 3, above all on the left side at the gap between the island and the breakwater where the differences for significant wave height between both storms are the highest. If we remember, storm 3 has a direction of 224º (figure 5.16) then more southern than the other storms. It causes that the waves can not enter so direct into the main bay, finding first some obstacles like the islands or breakwater; all these obstacles make increase the amount of wave breaking, reflections, refractions...etc, in the area. This increase in all this process in turn will do to increase the chaos in the area and then the directional spreading in the entrance of the main bay. So it is possible that the directional spreading at the entrance of the main bay is higher that at the boundary. On the other hand, storm 2 direction, 252º, makes that the waves get into the main bay more direct so they do not have so much interaction with the obstacles as what happened with storm 3. This less interaction with the different obstacles means that the amount of refraction, reflection....in the small bay decreases therefore the directional spreading in this area will not be so much different as at the boundary.

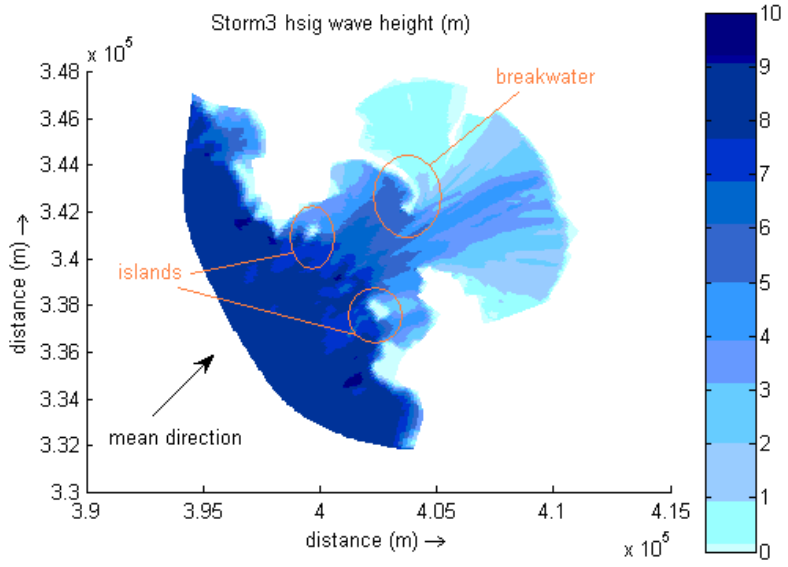

Figure 5.16 Significant wave height for storm3: γ = 0.5, D.spreding. = 20° and M.direction =224°

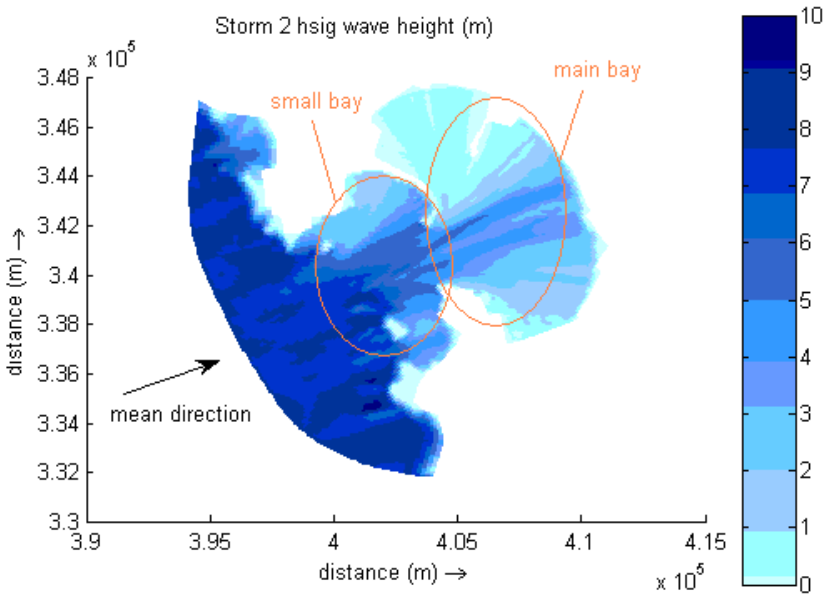

Figure 5.17 Significant wave height for storm2: γ = 0.5, D.spreding. = 10° and M.direction =252°

Depending on the value of directional spreading, Surfbeat generates different wave groups, more as higher is the directional spreading. These wave groups travel according to the mean direction calculated by swan so the direction for all the waves of a group is the same. Then with Surfbeat we do not have so much variability of the wave directions as in the reality. If we have less direction variability at the boundary, this can cause that the processes of refraction, reflection...etc in the small bay are smaller than are in the reality. Then the directional spreading at small bay will be lower than real.

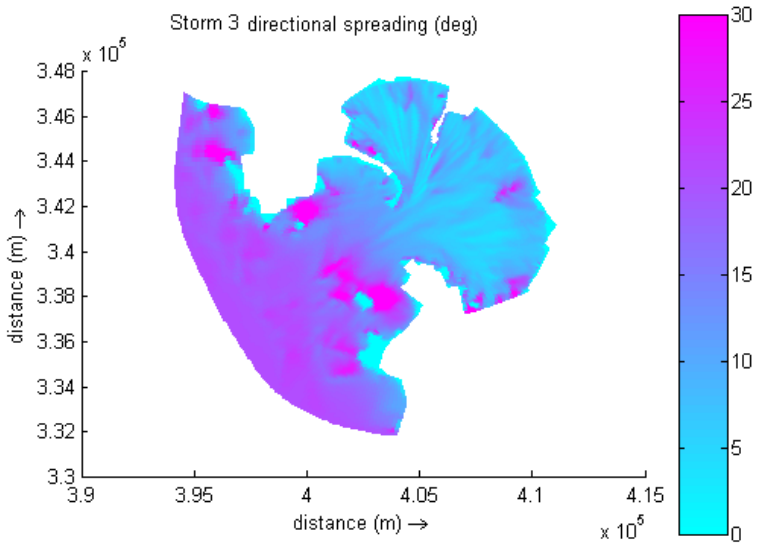

Figure 5.18 D. spreading for storm 3: γ = 0.5, D.spreding. = 20° and M.direction =224°

As we can see in figures 5.18, the directional spreading at the entrance of the main bay is lower that at the boundary for surfbeat simulation; then if the processes of refraction, reflection, wave breaking...etc, increase the directional spreading at the small bay in the reality, surfbeat can not model it.

A way to increase with Surfbeat the directional spreading at the small bay is increasing the directional spreading at the boundary. In this artificial way we get more direction variability at the boundary and then a higher directional spreading in the small bay.

5.3.3 Free long waves

For the lowest frequencies [0-0.007 Hz], the energy measured for the most severe storms (2 and 3) was still higher than simulated at Tide Recorder. Simulated energy spectrum was obtained for storms 2 and 3 at the Bay entrance (figure 5.19). For both storms, measured spectral energy at Tide Recorder location is higher than simulated spectrum at Bay entrance for the low frequencies (Figures 5.20 and 5.21). Some possibilities can explain this situation:

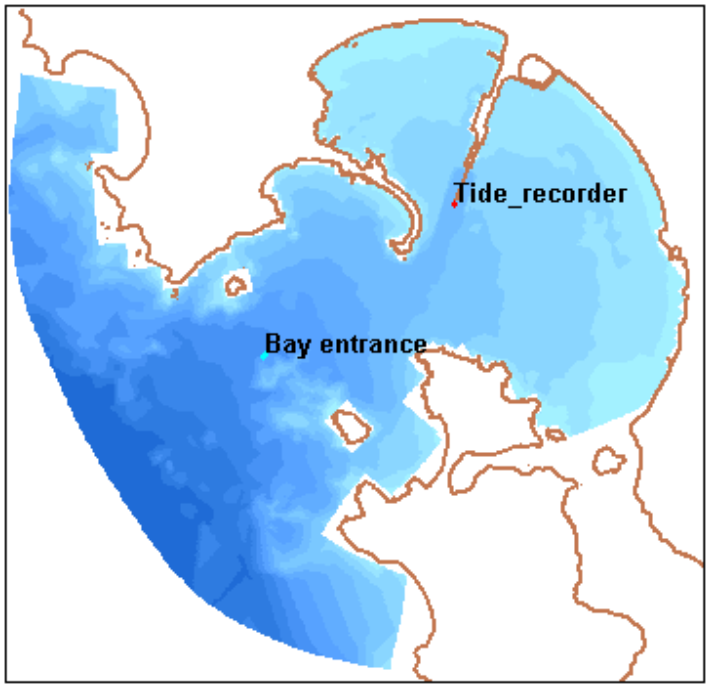

Figure 5.19 Bay entrance point location

We have only chosen 50 minutes to get the measured spectrum; then for frequencies so small (f < 0.005 Hz) we will have a few waves. There is a possibility that chosen data correspond only a period of high waves so it does not include smaller waves. This can cause an overestimation of measured energy for these frequencies. Choosing longer measured series, we could check if the measured energy decreases because of supposed inclusion of all kind of heights. If this happens, it will not be necessary to include long free waves. If it does not work, may be the data chosen are right and the absence of energy for the low frequencies is due to not inclusion of free long waves at the boundaries.

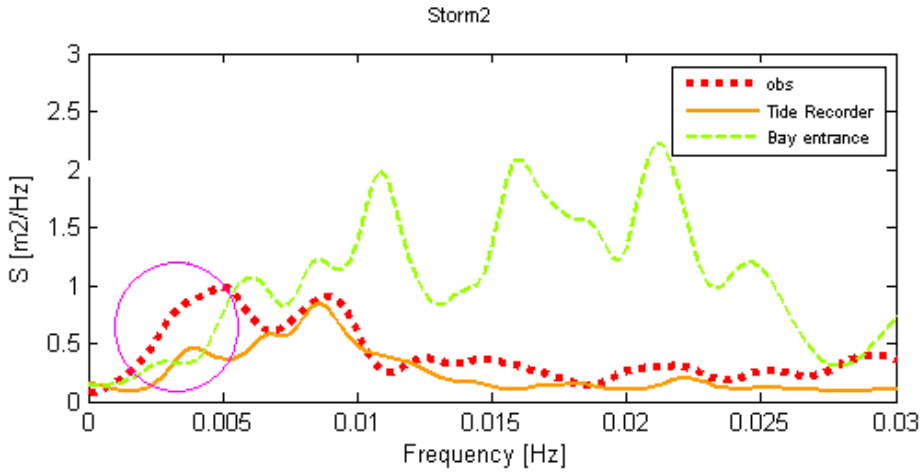

Figure 5.20 Bay entrance spectrum: storm 2

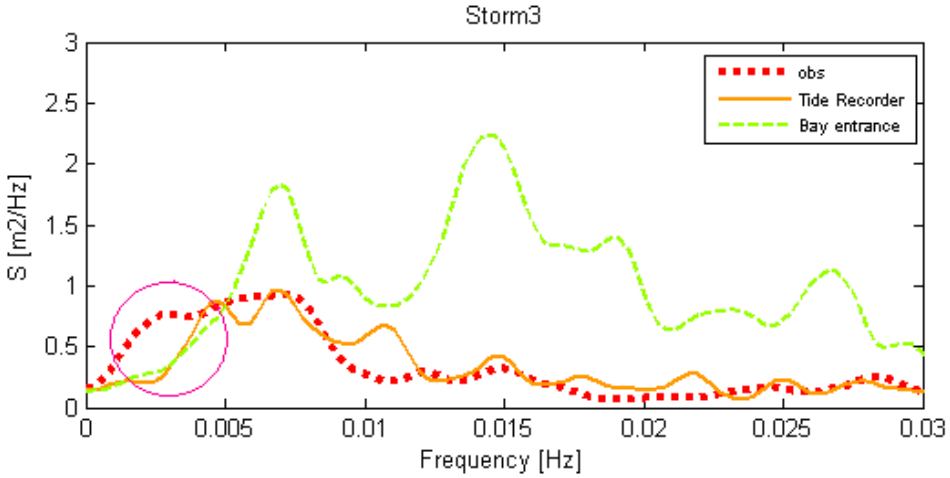

Figure 5.21 Bay entrance spectrum: storm 3

We decided to analyzed longer measured series for storms 2 and 3. Figures 5.22 and 5.23 show the results; for 50 and 180 minutes series, spectral energy is quite similar for the low frequencies. We can conclude that this lack of energy for the low frequencies in simulated spectrums is caused for not inclusion of free long waves at the boundaries.

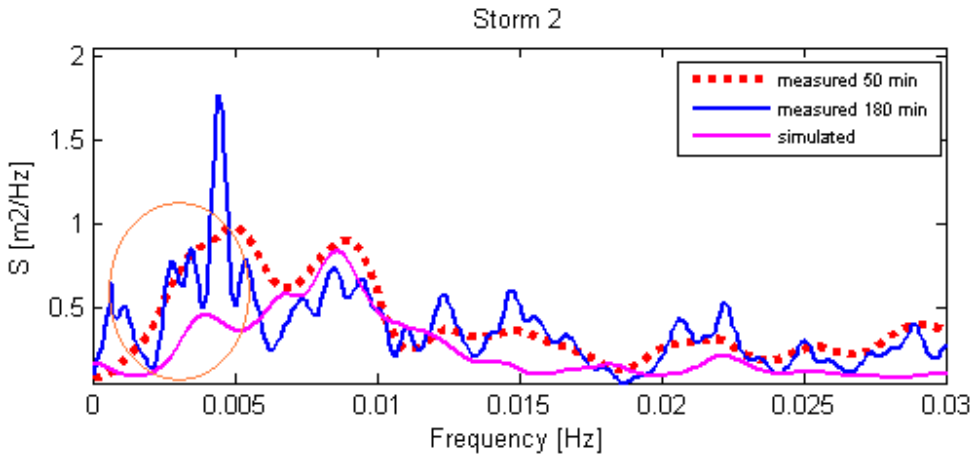

Figure 5.22 Measured series comparison: storm 2

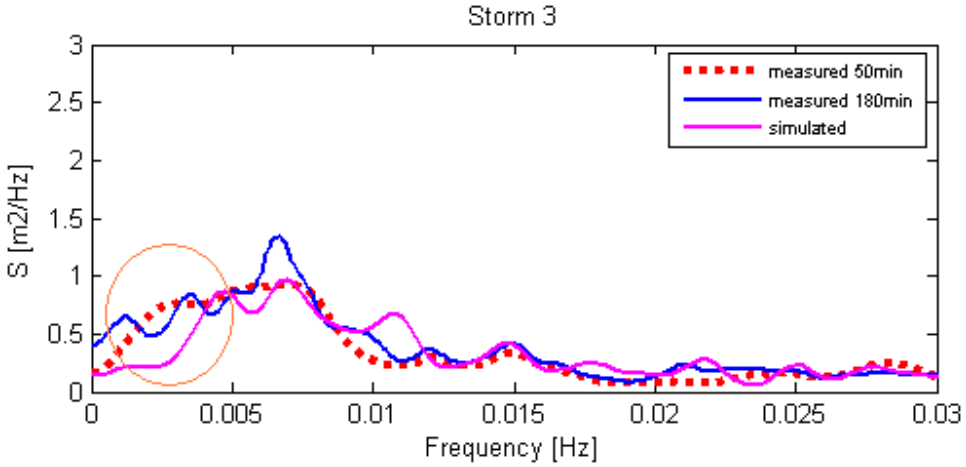

Figure 5.23 Measured series comparison: storm 3

Like we do not have any data about free waves and the results are accurate enough, was decided not to carry out any analysis with free waves.

5.3.4 Validation conclusion

Chosen parameters from the calibration procedure, work good enough for almost all storms. Only storm 1 shows not really good agreement, but it is not a severe storm. Spectral shapes show a good agreement as can we check at table 5.9 for the skill values and at the different figures of 5.3.1. We will continue the analysis with the calibrated values (table 5.7) for breaking index parameter and friction coefficient.

Chapter 6

Surfbeat simulations: new buoy location

6.1 Chapter overview

Once calibrated and validated the hydrodynamic model, different runs were done to study the best location for a new buoy. First, variables data used and points (locations) studied in the analysis are described. After that, a detailed analysis for the new buoy location is carried out for each area: East and West (figure 6.3).

6.2 Variables and points selected

Ship motions can be classified as: surge, sway, yaw, heave, roll and pitch (figures 6.1 and 6.2).
For Saldanha Bay study, only surge motion was analyzed. Ore jetty is located inside the bay, not exposed to the open sea, so most incoming short and long waves have a direction quiet parallel to the jetty. Natural periods of ship's motions in surge are very close to these parallel long period waves, causing the presence of resonance. If resonance is present, the cargo operations in ore jetty are severely affected.
Resonance in sway is not excited because there is not much wave action in the ore jetty, in perpendicular direction and the natural periods for sway are smaller than the long wave periods in the area.

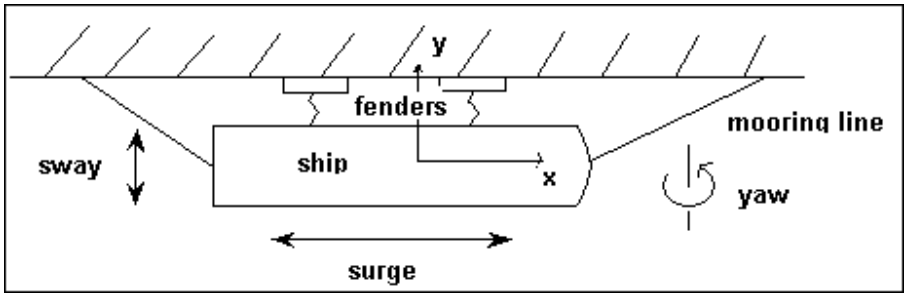

Figure 6.1 Ship motions. Floor plan

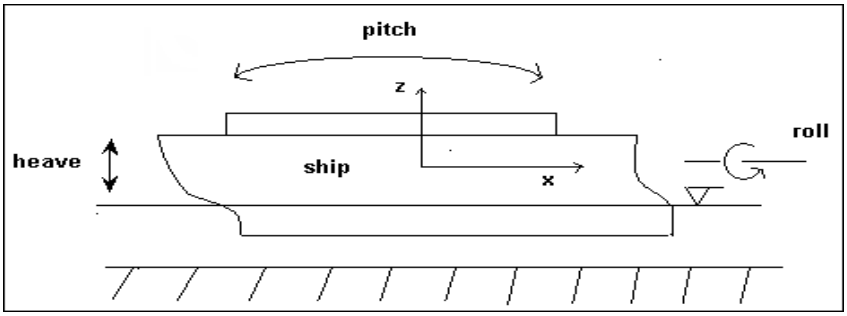

Figure 6.2 Ship motions. Elevation

For the location of the buoy, we are interested in points with high water level variation to get good measurements of water levels, so points located as near as possible to antinodes. As near we are from nodes as lower will be the variation of WL, so we will not have so good WL measurements. Then, we will look for points with high water level energy and small for the velocities, as nearer node location we are, smaller velocity gradient will be have.
The variables chosen for the study of the new buoy location were water level and discharge in the direction parallel to the jetty. Like we have different depth for the different points, it was decided to analyze the discharge q = v * h instead of the velocity. Although we will be studying the discharge, we will call this variable velocity to make clear, which is the real variable we are interested in; so from now to the end of this chapter and in the next chapter (chapter 7), when we are talking about velocity, we will be referring to the discharge.
This study was carried out for both sides of the jetty: West and East areas. Figure 6.3 shows the points selected in both areas for the analysis. We just selected some points spread in the areas of interest (appendix E).

For the analysis of new buoy, and new jetty location (chapter 7), storm 3 data and simulations were used as is one of the most severe storms that passed the area, and was the storm with which we carried out the calibration procedure.

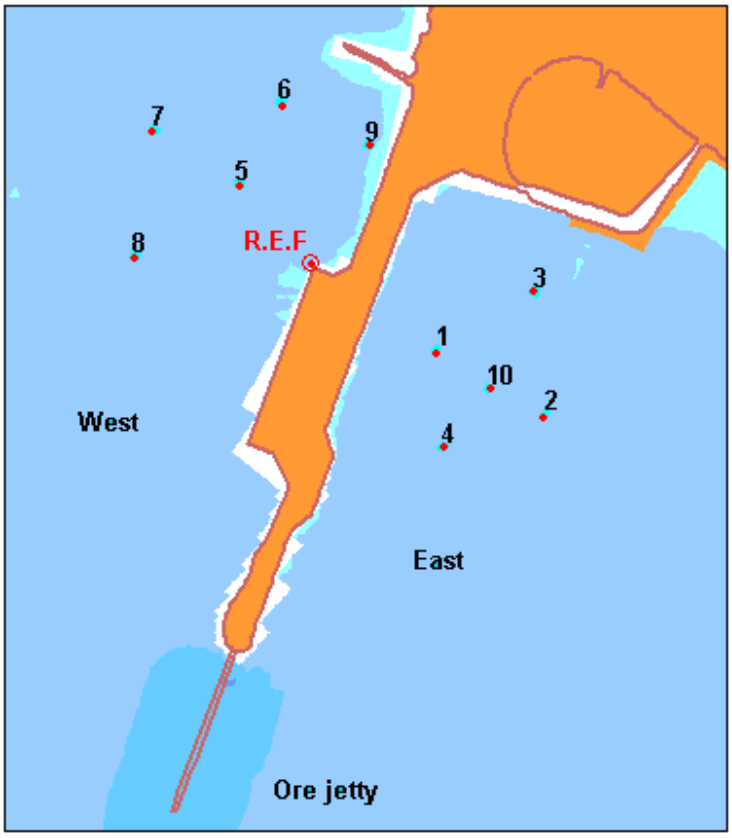

Figure 6.3 New buoy location. Selected points: East and West areas

6.3 East and West area analysis

Long waves with direction parallel to the jetty are the main cause of mooring problems; but not all the long wave periods can excite the natural periods of ship's motions in surge. The natural periods for the ships moored in the jetty varies between 70 - 150 seconds depending on the ship. So, just the energy values in this interval for water levels and velocities spectrums will be analyzed in the study.

The variables calculated from the variables selected in a previous step and analyzed in the study are:

- m0-bias: spectral area contained in the interval of study (70 - 150 seconds)
- spectral shape: we are looking for high spectral energies for water levels and small for the velocity.

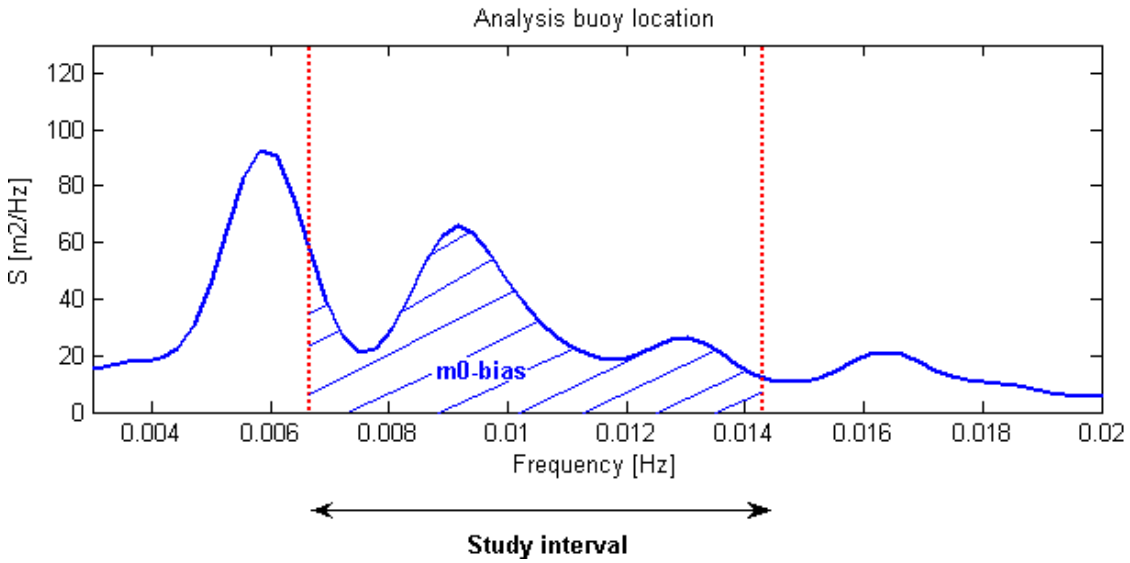

Figure 6.4 Analysis buoy location. Study interval

6.3.1 East Jetty Area

Table 6.1 shows different results for the points selected in east area. For each variable, first shows significant wave height for water level (Hs) and total spectral area for velocity (m0), and selected interval spectral area (m0-bias) in the second column.

	WL		Velocity	
	Hs (m)	m0-bias (m2/s)	m0 (m4/s2)	m0-bias (m4/s2)
1	0.483	0.0036	1.72	0.308
2	0.562	0.0076	1.24	0.459
3	0.552	0.0053	1.83	0.648
4	0.562	0.0061	1.14	0.34
10	0.496	0.0047	1.36	0.126

Table 6.1 Analysis buoy location. East area results

Points 2 and 3 have high value of m0-bias for velocities; if we check the spectrum (figure 6.6), we can see like for point 2 we have a high peak around 0.009 Hz (small energy for WL at 0.009Hz, near node) and for point 3 the energy for interval low frequencies is very high.
Point 1 has really small energy for water level and point 10 shows one of the smallest values of m0-bias for water level and has a peak around 0.009 Hz for velocity spectrum.
Point 4 has one of the highest values of m0-bias for water level and the value of m0-bias for the velocities is close to the smallest ones; moreover if we check figures 6.5 and 6.6, water level spectrum for point 4 has high energy values and the spectrum for velocities is quite flat, above all for the lowest frequencies of the interval.
We decided that point 4 is a good location in east area for a new buoy.

Next we give the coordinate of selected point and a point of reference in the jetty:

Point	X (m)	Y (m)
4	406304	345007
R.E.F	405714	345821

Table 6.2 Analysis buoy location. East area: coordinates selected and R.E.F points

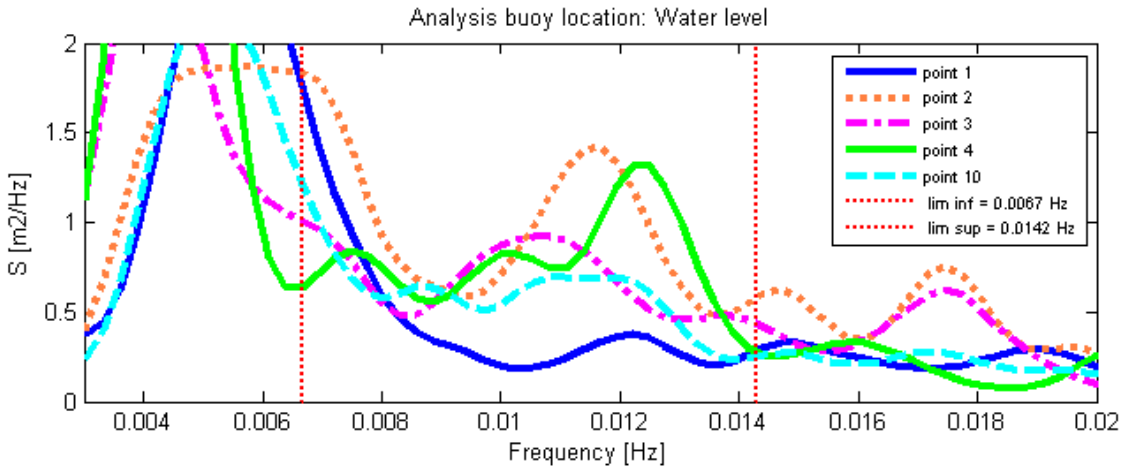

Figure 6.5 Analysis buoy location. East area: WL spectrums

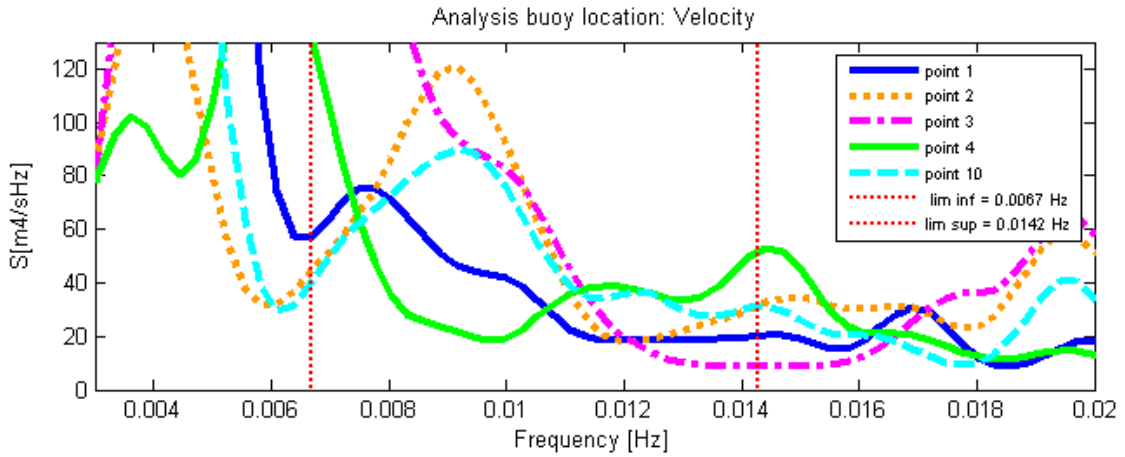

Figure 6.6 Analysis buoy location. East area: velocity spectrums

Next figures, 6.7 and 6.8, show the spectrums of the selected point for water level and velocity.

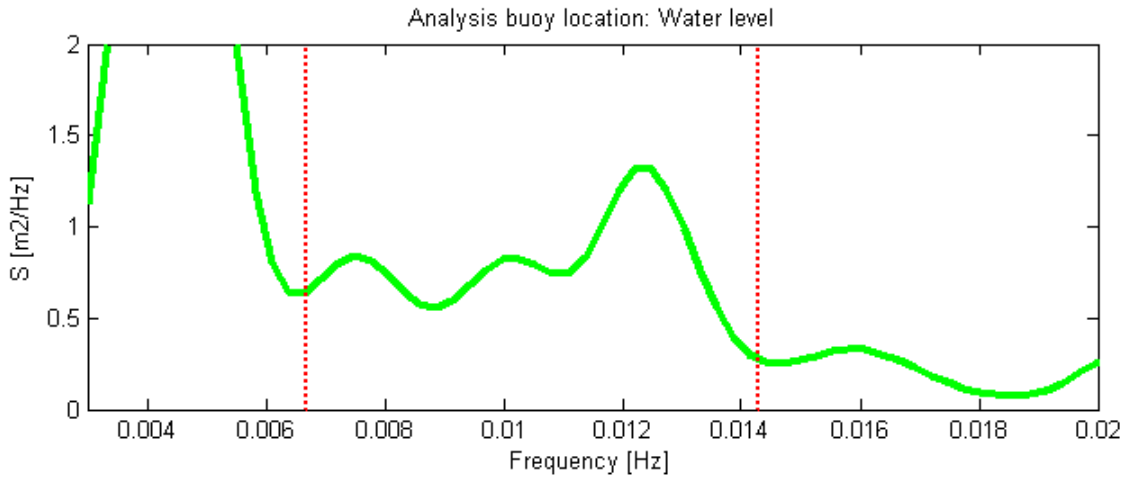

Figure 6.7 Analysis buoy location. East area: Selected point WL spectrum

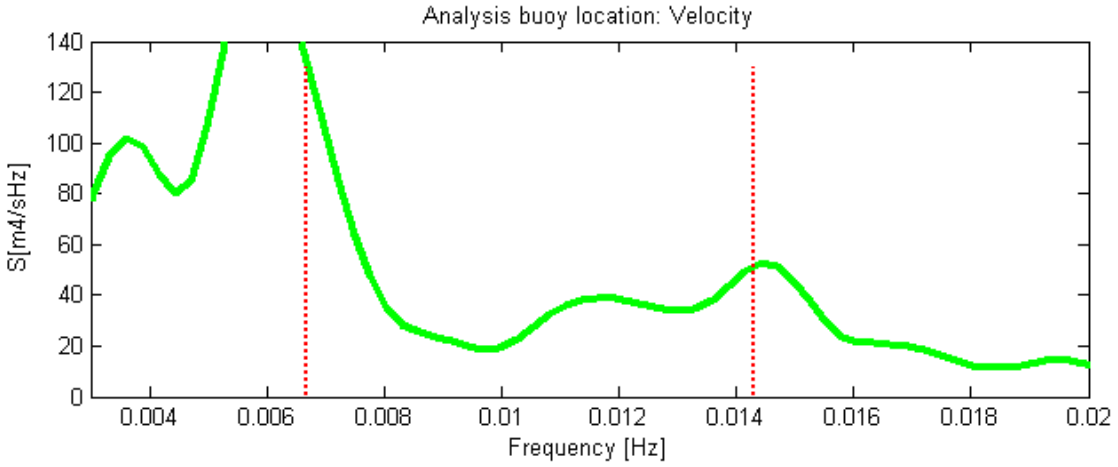

Figure 6.8 Analysis buoy location. East area: Selected point velocity spectrum

6.3.2 West Jetty Area

Table 6.3 shows different results for the points selected in west area. As we can see values in general are smaller than for east area as we are in a more closed and protected area.
Points 7 and 9 have high values for water level m0-bias, but have high values for the velocity m0 bias as well. Point 9 has high energies for velocity spectrum at the lowest frequencies of the interval. Point 7 has a high peak around 0.009 Hz for velocities (figures 6.9 and 6.10).
Point 6 is the opposite case, has small m0-bias value for velocity and small value for water level as well.
For point 8 we have an intermediate value for water level m0-bias but a high one for velocities. Like point 7, has a high peak at 0.009 Hz for velocity spectrum (figure 6.10).
The last one, point 5, has a small m0-bias for velocity and quite high value for water level.
Point 5 is the best among the points we selected in this area. Although for the shape for both spectrums, WL and velocity, is possible to say that this point is an intermediate location between node and antinode for most frequencies. If we check figures 6.11 and 6.12, we can see like the shape for both spectrums is quite parallel, the peaks in water level spectrum fit in with the peaks for velocity spectrums, and the same for the valleys. So, we decided to analyze area around point 5 to select a better point.

	WL		Velocity	
	Hs (m)	m0-bias (m2/s)	m0 (m4/s2)	m0-bias (m4/s2)
5	0.366	0.0032	0.403	0.125
6	0.291	0.0016	0.432	0.109
7	0.339	0.003	0.564	0.227
8	0.34	0.0024	0.624	0.262
9	0.426	0.0052	1.015	0.357

Table 6.3 Analysis buoy location. West area results

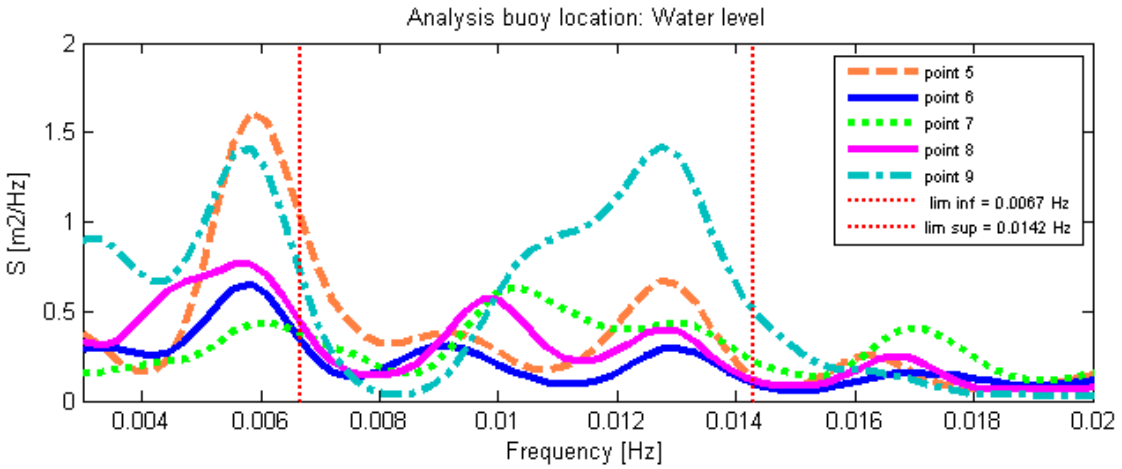

Figure 6.9 Analysis buoy location. West area: WL spectrums

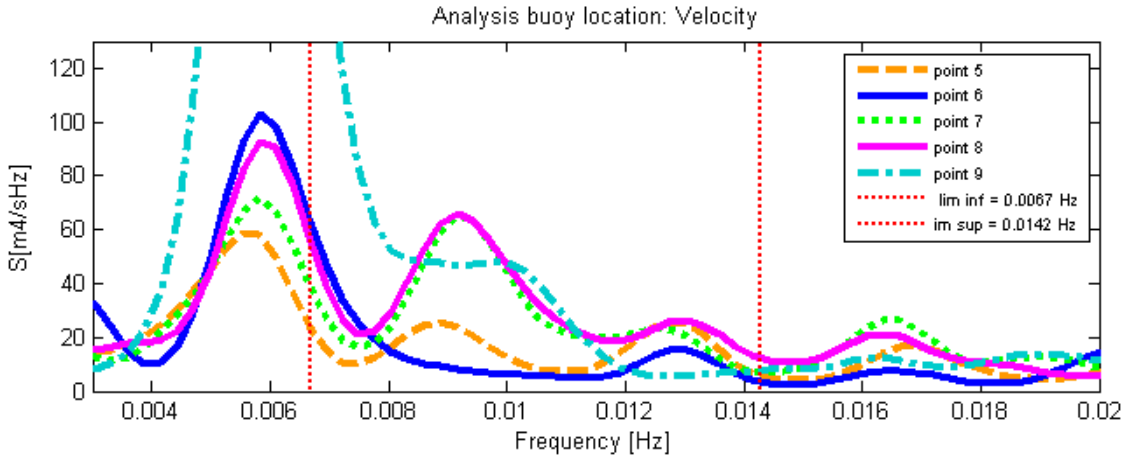

Figure 6.10 Analysis buoy location. West area: velocity spectrums

6.3.2.1 Analysis point 5 area

Figure 6.11 shows the points selected for point 5 area analysis (appendix E).

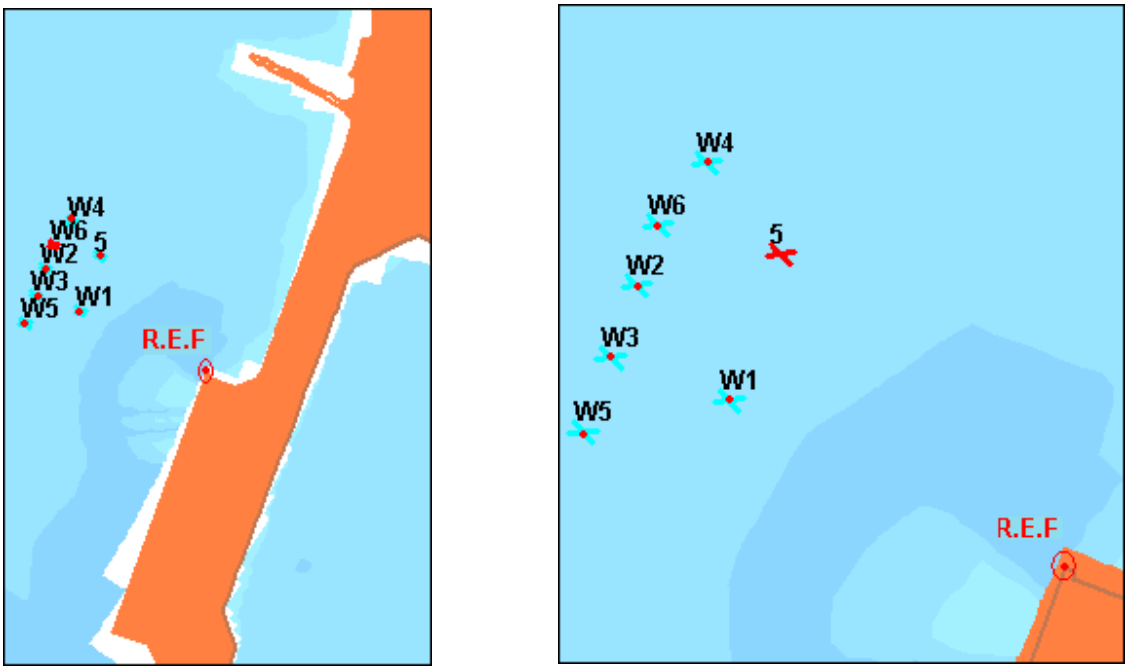

Figure 6.11 New buoy location. Selected points: point 5 area

Table 6.4 shows different results for the points in point 5 area. Points W4 and W5 have smaller m0-bias value for water level than point 5 and higher for velocity; For points W1 and W6 we only get to improve the results for one of the variables (WL for W1 and velocity for W6), while for the other one is worse than in point 5. It is clear that the points that have the best results for both variables (WL and velocity) are W2 and W3. Between points W2 and W3, W2 has the best values for WL and velocity m0-bias (table 6.4); WL spectrums are quite similar for both points except for the highest frequencies in the interval, where W2 has more energy than W3 (figures 6.12 and 6.13). For velocity spectrums, energies for W2 are smaller than for W3 almost in all the interval frequencies. Moreover, velocity spectrum for point W2 is quite flat.

Point W2 seems to be the best election among all the points studied in point 5 area; spectral shape and m0-bias value for WL are similar to point 5 ones, while for velocity, m0-bias value for point W2 is smaller than for point 5 and its spectrum more flat (no peaks).

	WL		Velocity	
	Hs (m)	m0-bias (m2/s)	m0 (m4/s2)	m0-bias (m4/s2)
5	0.366	0.0032	0.403	0.125
W1	0.372	0.0023	0.368	0.138
W2	**0.375**	**0.003**	**0.371**	**0.105**
W3	0.389	0.0027	0.359	0.121
W4	0.335	0.0022	0.482	0.16
W5	0.358	0.0021	0.46	0.147
W6	0.356	0.0027	0.392	0.106

Table 6.4 Analysis buoy location. Point 5 area results

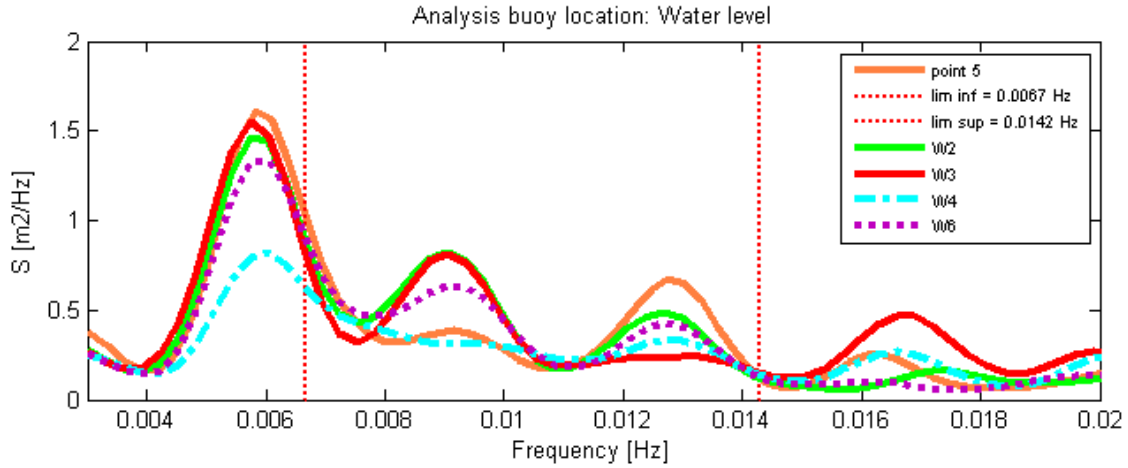

Figure 6.12 Analysis buoy location. Point 5 area: WL spectrums

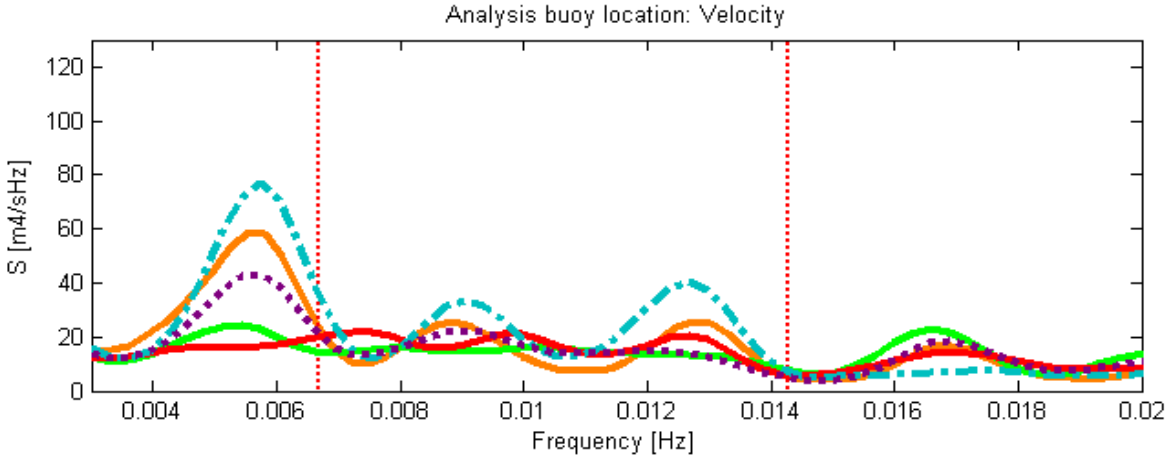

Figure 6.13 Analysis buoy location. Point 5 area: velocity spectrums

We can recommend point W2 like location for a new buoy in west area. Next we give the coordinate of selected point and a point of reference in the jetty:

Point	X(m)	Y(m)
W2	405200	346165
R.E.F	405714	345821

Table 6.5 Analysis buoy location. Point 5 area: coordinates selected and R.E.F points

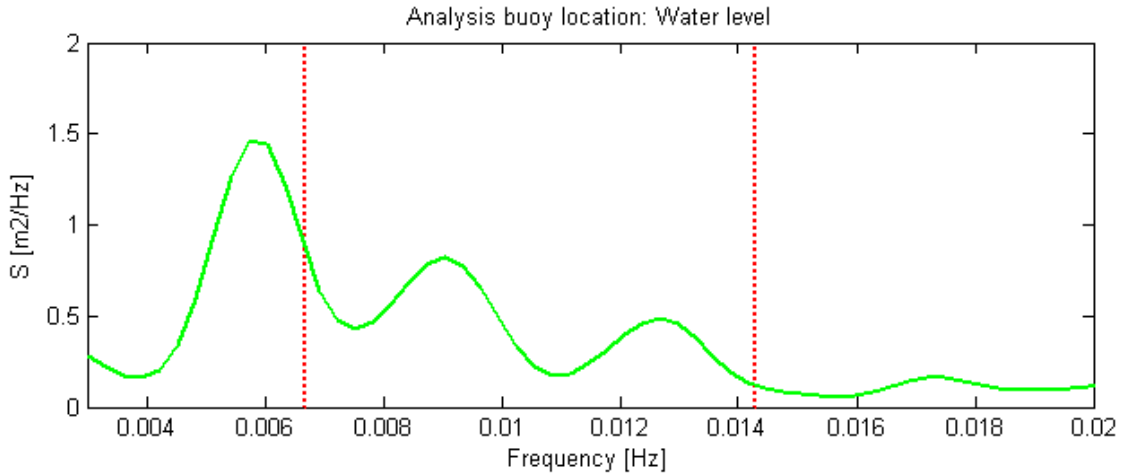

Figure 6.14 Analysis buoy location. Point 5 area: point W2 WL spectrum

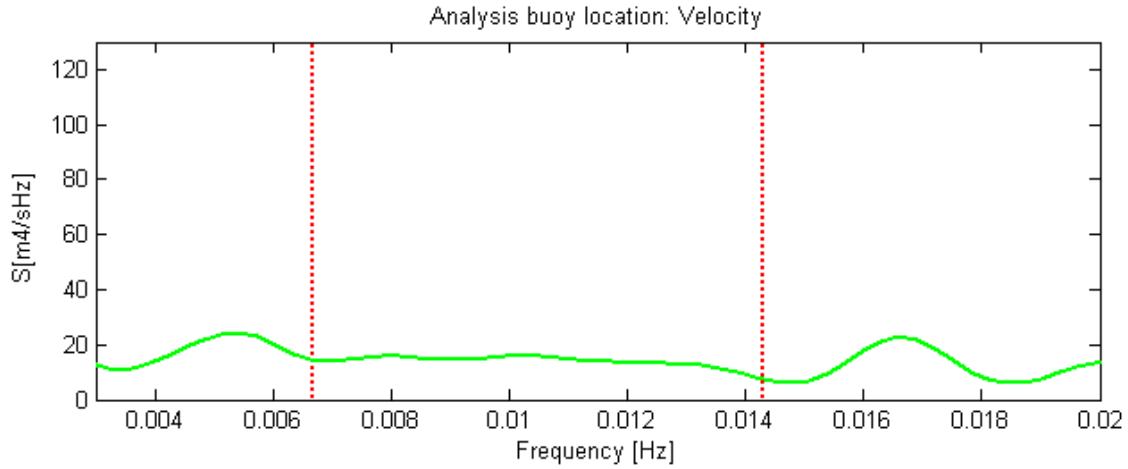

Figure 6.15 Analysis buoy location. Point 5 area: point W2 velocity spectrum

6.4 Comparison results

Figures 6.16 and 6.17 show WL and velocity results for Tide Recorder and points selected for a new buoy location at each area.

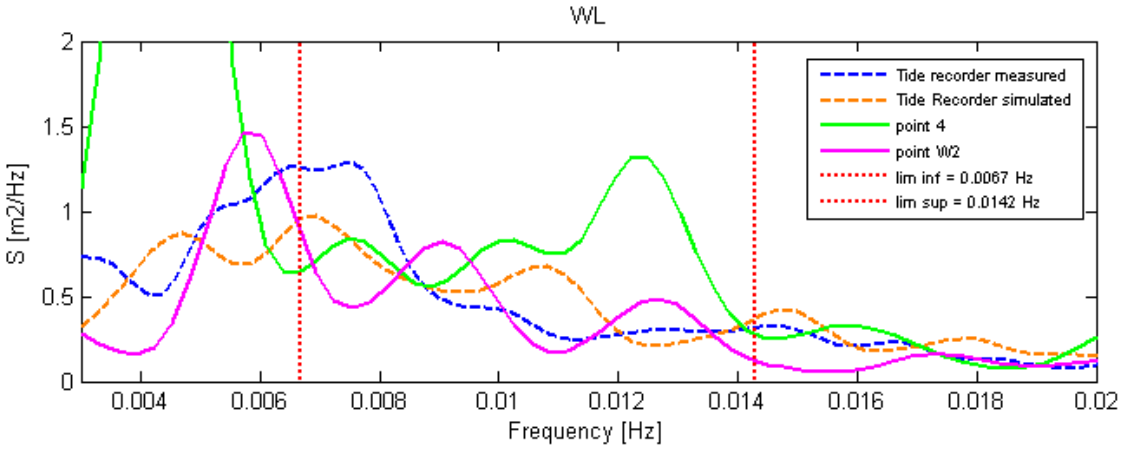

Figure 6.16 Analysis buoy location. Tide Recorder and points 4 and W2 WL spectrums

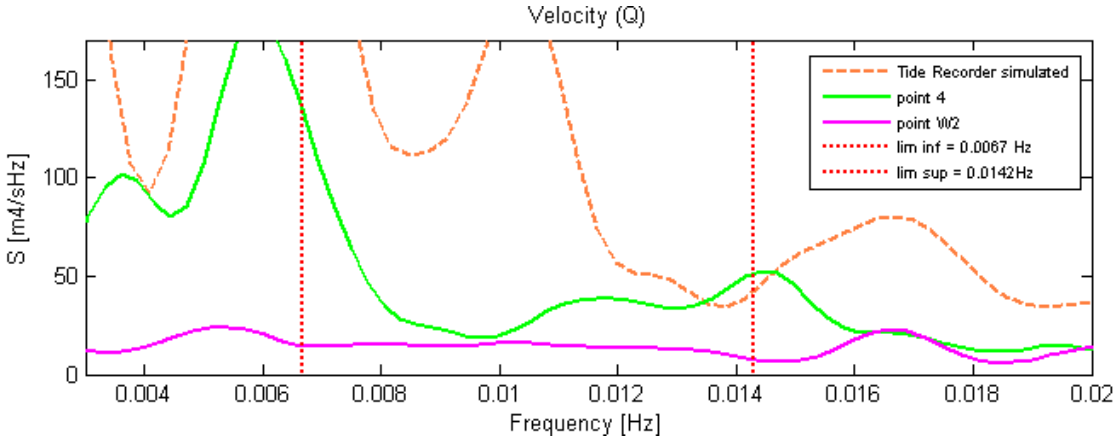

Figure 6.17 Analysis buoy location. Tide Recorder and points 4 and W2 velocity spectrums

Chapter 7

Surfbeat simulations: new jetty location

7.1 Chapter overview

Chapter7, different runs were done to study the best location for a new jetty. First, variables data used and points (locations) studied in the analysis are described. Once selected all variables and study points, a detailed analysis for the new jetty location is carried out. East and West areas centre the first part of analysis; two different analysis were done: actual layout without channels and second one with the inclusion of channels. Finally a comparison of both areas is included.
Last part is an analysis of the area 3 (figure 7.3) and a general conclusions for all the areas.

7.2 Areas, points and variables selected

Long waves cause problems (motions) to moored ship at the ore jetty; because of these motions, moored ships at the jetty experience conditions of resonance during the occurrence of these long waves. Then, actual location (Ore jetty) does not seem the best location for the ships.

For the analysis, storm 3 data and simulations were used (see 6.2).
First, rough study of the whole main bay was done; a movie of the bay was obtained to check the distribution of energy in the bay. Most of the time, the energy in the main bay is higher than for the ore jetty area (figure 7.2); moreover, in the south-east area of the main bay, there are some environmental restrictions to build a new jetty. So, it was decided to centre the study in the jetty-causeway area and small bay (figure 7.1).

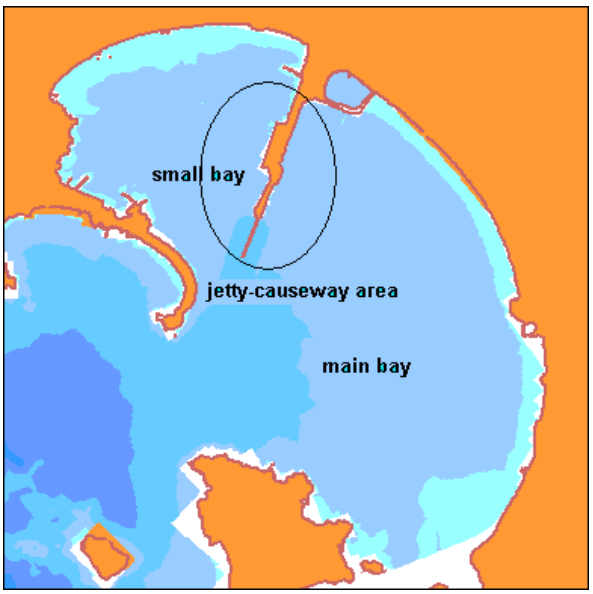

Figure 7.1 New jetty location. Main and jetty-causeway area

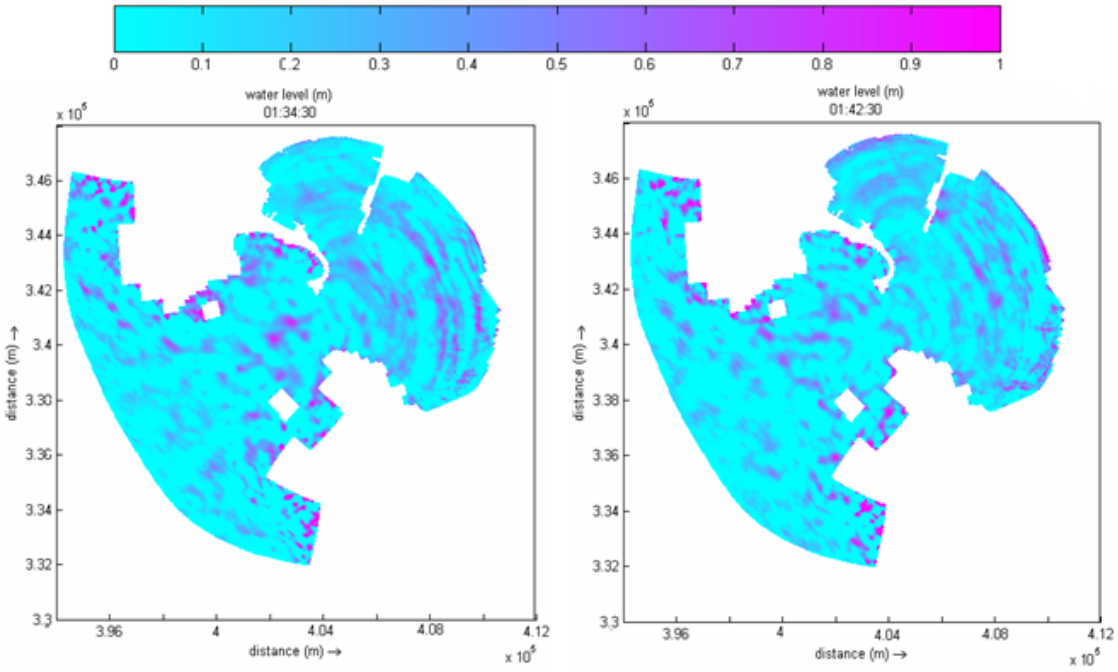

Figure 7.2 Water level maps for different moments of the movie

Figure 7.3 shows the areas selected for the study of a new jetty location. Main study was carried out in East and West areas; for area 3, just a brief analysis was done.

Figure 7.3 New jetty location. Selected areas

Figure 7.4 shows the points selected in each area for the analysis (appendix E). At East and West areas, these points were located opposite the wider area at the causeway and about 80 m from this one. For area 3, studied points were selected at distances around 250 and 850 m from the coastline.

Figure 7.4 New jetty location. Selected points

We know that there are some problems with ship motions at the ore jetty area because of the amount of wave energy in it, so we will try to choose an area with smaller spectral energy for both, WL and velocities, than ore jetty area. In the new studied areas, we must avoid points located near nodes for new ships location; as near we are from nodes as higher is the velocity gradient and therefore higher will be the forces on ships and ship motions. Near the nodes, with the highest velocity gradients, we will have high horizontal velocities and small variation of water level. Therefore, we will look for a point with high water level energy and small for velocities in each area for the new jetty location.
For this study, like in chapter 6, water levels and discharge in the direction parallel to the jetty were selected as variables for the study. The reason for selecting discharge instead of velocity is the same as explained in chapter 6 (see 6.2). Although we will be studying the discharge, we will call this variable velocity (see 6.2).

Like in chapter 6, the interval of study, will include all the periods between 70 and 150 seconds (see 6.3).

7.3 West and East area analysis

The analysis of these areas is based on the comparison of results between ore jetty area and East-West areas. Like we said before, we know that there are some problems at the ore jetty area, so we are looking for areas with smaller energy for WL and velocities.

As we can see in figure 7.4, three points were selected at ore jetty area: a, b and c.
For WL, spectral shapes and m0-bias values are quite similar for the three points (figure 7.5 and table 7.1); for velocities there are some differences although not important at the study interval (figure 7.6). Then, for the comparison analysis, we decided to choose point b. Point a is closer to the tip of the jetty than b, and point c is closer to the computational boundary. Point b is in an intermediate position at ore jetty and probably closer to the location at which the ships are moored now; so we think point b is the best option to compare with the other areas.

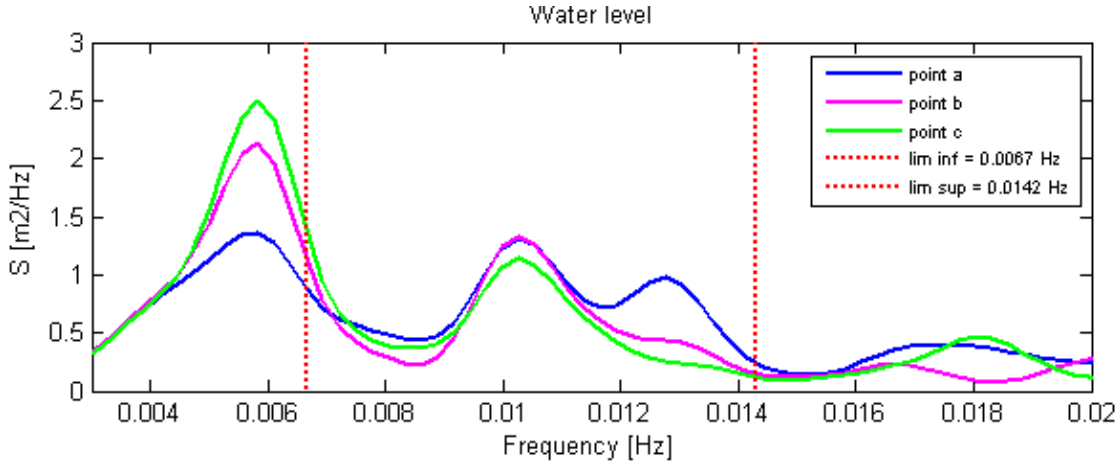

Figure 7.5 Ore jetty area. WL spectrum

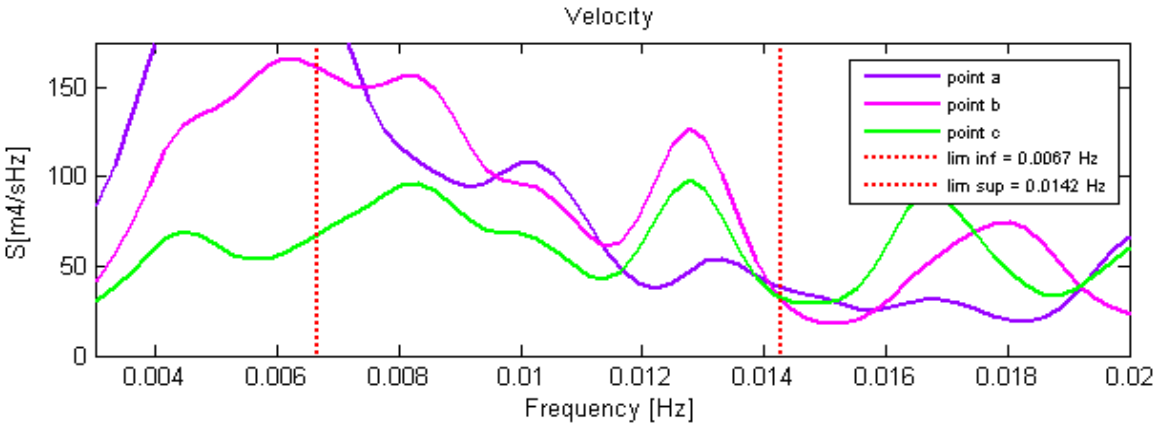

Figure 7.6 Ore jetty area. Velocity spectrum

	WL m0-bias	Velocity m0-bias
a	0.0061	0.736
b	0.0047	0.850
c	0.0045	0.678

Table 7.1 m0-bias values for WL and velocities at points of ore jetty area

The variables calculated from the variables selected in a previous step and analyzed in the study are:

- m0-bias: spectral area contained in the interval of study (70 - 150 seconds) (see 6.3). This parameter will be calculated for all the points in the new areas of study and compared with the value of b. Parameter used for comparison is m0 difference (equation 7.1).

$$m0difference = \left(\frac{m0.bias(b) - m0.bias(x)}{m0.bias(b)} \right) * 100 \qquad (7.1)$$

where x are the different points of study in the new areas.

We will choose the best point and area by minimizing the m0-bias and maximizing the m0difference (equation 7.1), for both WL and velocities.

First, an analysis of the actual layout was done for both areas; after that, a new analysis was done, but with a new layout: two channels, one at each side of the jetty-causeway, were included in the depth file.

7.3.1 Actual layout analysis: no channels

Results for actual layout are shown in table 7.2. First, WL results were analyzed for both areas, and after that the same for the velocities.

		WL		Velocity	
		m0-bias (m2)	m0 difference [%]	m0-bias (m4/s2)	m0 difference [%]
West area	g	0.0042	10.64	0.518	39.04
	h	0.0037	21.28	0.390	54.10
	i	0.0094	-100.00	0.139	83.64
East area	j	0.0118	-151.06	0.574	32.45
	k	0.0124	-163.83	0.495	41.74
	l	0.0134	-185.11	0.444	47.75
	m	0.0133	-182.98	0.474	44.22
	o	0.0092	-95.74	0.560	34.12
	p	0.0103	-119.15	0.802	5.61
	b	0.0047	-	0.850	-

Table 7.2 Actual layout analysis: no channels. Results for West and East area points: m0-bias and m0 difference

Water Levels

West area: for points g and h, the total energy in the interval is smaller than for point b but not much smaller as we can check for the values of m0-bias and m0 difference (Table 7.2). As we can see at figure 7.7, the energy levels for g and h are approximately the same as point b but with peaks in different frequencies. However, for point i, we have negative values for m0 difference. The energy in this point is higher in the interval than for point b (figure 7.7). This negative values is probably due to the small depth in that point, as while for points g and h we have about 13.5 m, for point i we only have 3.5 m. So we think only g and h are representative of this area; we will check the behavior of i in the case with channels, to know if it is similar to the behavior in the other two points. Excluding point i, we can conclude that the energies in west area for WL are a little bit smaller than at ore jetty area.

East area: in general for all the points we have a higher energy levels than for point b like we can see in table 7.2 (all the values for m0 difference are very negative) and figure 7.8. We can appreciate a high difference, above all for the lower frequencies in the interval.

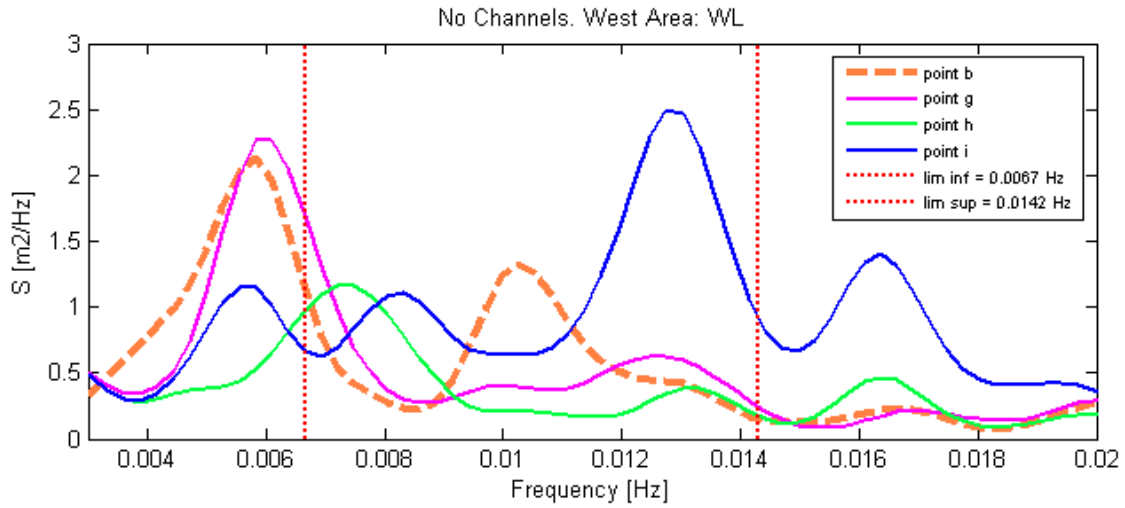

Figure 7.7 Actual layout analysis: no channels. WL spectrums for West area points

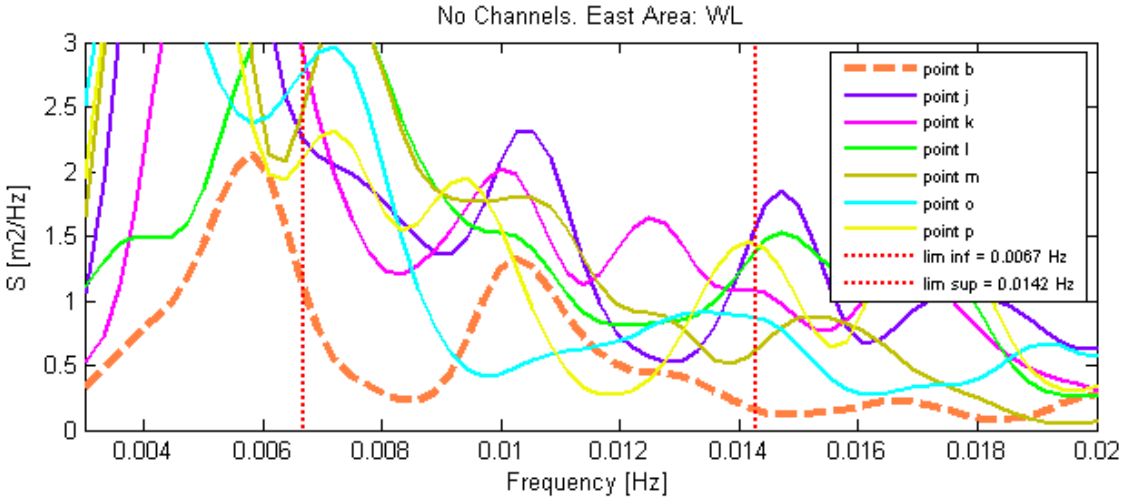

Figure 7.8 Actual layout analysis: no channels. WL spectrums for East area points

Velocities

Remember that we are analyzing the discharge when we talk about velocity (see 6.2).

West area: The m0 difference values are positive for the three points of the west area (table 7.2); it is clear that the spectral energies for points g, h and i are below point b spectral energies for all the frequencies in the interval of study (figure 7.9). This difference is higher for the lower frequencies [0.0067 - 0.011] Hz. We can say that west area has a better behavior in velocities than point b.

East area: Like in west area, values of m0 difference are positive for all the points as well (table 7.2). Then in almost all the points, the spectral energy is smaller than for point b (figure 7.10), although for the frequencies [0.009 - 0.011] Hz the energies of the studied points and b are quite close. Only in point p, the spectral energy is higher than point b energy in some frequencies. This is the reason to have so small values for m0 difference in point p.

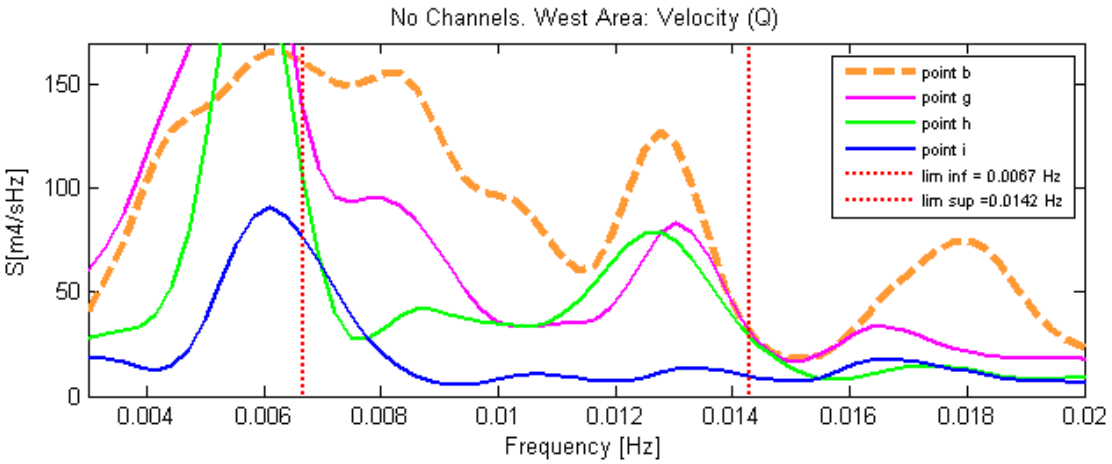

Figure 7.9 Actual layout analysis: no channels. Velocity spectrums for West area points

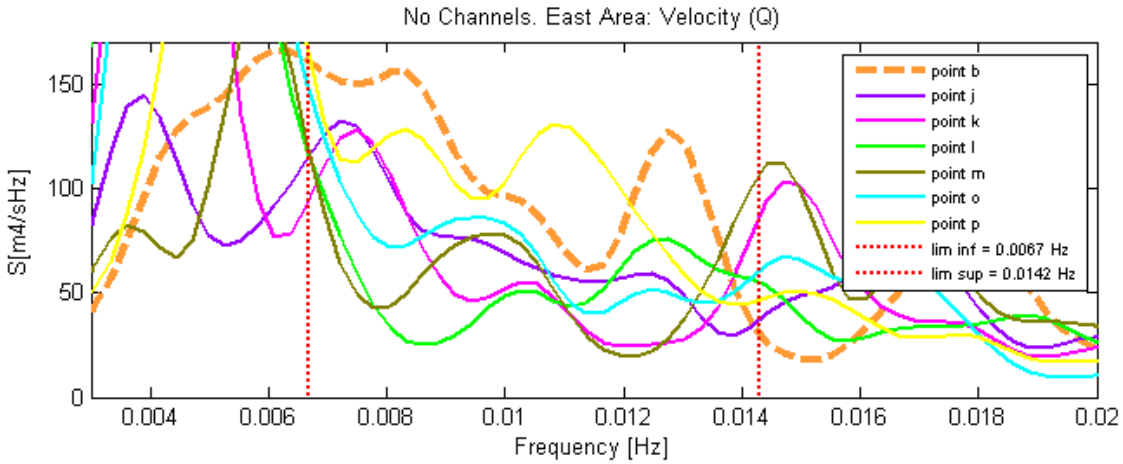

Figure 7.10 Actual layout analysis: no channels. Velocity spectrums for East area points

7.3.2 New layout analysis: channels

After the study of the West and East areas with the actual layout, was decided to do a study with the corresponding channel for each area to simulate the future situation: a channel is required in each area to let the entry and traffic of the ships.

Simulation run for the analysis was done with both channels. In the real situation, we will only have one of the channels depending on which one is the best area, but because of the presence of the causeway in between, the interaction between the channels it is hoped to be negligible.

Depth at ore jetty area is around 24 m, so it was decided to do both channels with a depth a bit smaller than this one but deep enough for the ships traffic: so we chose a constant depth of 20 m for both channels.

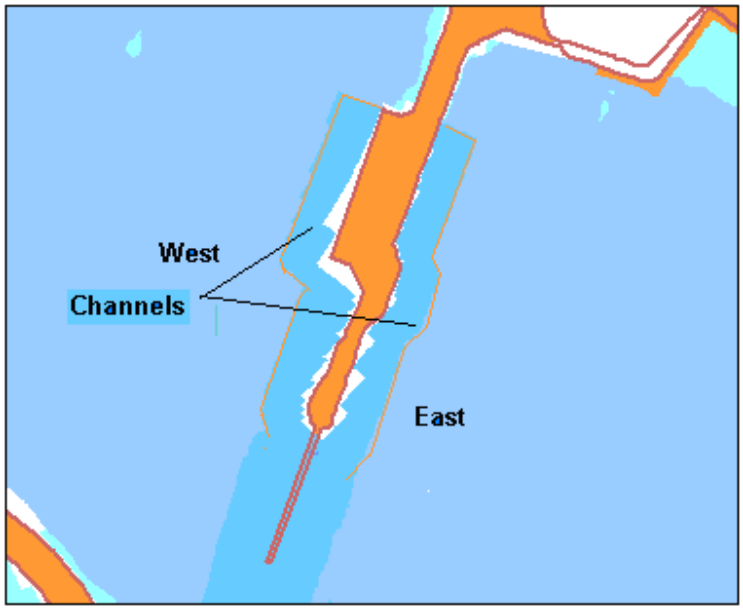

Figure 7.11 Channels layout

Channels width

Research and experience so far have shown that the required channel width depends particularly on environmental conditions as cross-currents and cross-currents gradients (variation of these cross-currents per unit length of channel), waves and swell, wind, visibility, but also on the accuracy of information regarding the ship's position and the easy 'readability' of this information to navigators. A minimum value for the width of one-way channel (width at full depth) would be 5 times the beam B of the biggest vessel in the absence of cross-currents. An average value for average conditions would be rather 7 or 8B. Actual one-way channel width in existing ports varies between 4 to 10B.
Considering no existence of cross-currents at these areas and that the maneuver area for ships is located some other place, we can calculate the width of the channels like 5B. Taking a B average value of 50 m we have a width of 250 m for each channel. So we will have two channels of 250 m width and 20 m constant depth.

Results for layout with the channels are shown in table 7.3. First, WL results were analyzed for both areas, and after that the same for the velocities.

		WL		Velocity	
		m0-bias (m2)	m0 difference [%]	m0-bias (m4/s2)	m0 difference [%]
West area	g	0.0030	18.92	0.615	21.25
	h	0.0020	47.03	0.518	33.67
	i	0.0021	43.24	0.369	52.75
East area	j	0.0064	-72.97	0.943	-20.74
	k	0.0055	-48.65	1.252	-60.31
	l	0.0102	-175.68	0.570	27.02
	m	0.0073	-97.30	0.747	4.35
	o	0.0104	-181.08	0.632	19.08
	p	0.0058	-56.76	2.060	-163.76
	b	0.0037	-	0.781	-

Table 7.3 New layout analysis: channels. Results for West and East area points: m0-bias and m0 difference

Water levels

West area: all the points have positive values for m0 difference parameter what means that the spectral energy for studied points is smaller than energy in point b (table 7.3). This difference between studied and point b energies are higher above all for the frequencies [0.009 - 0.012] Hz while for the other ones are approximately the same as point b (figure 7.12).
As we can see the values of mo difference in point i are very positive; then the situation in point i improves a lot due to the increase of depth.

East area: like happened for the situation without channels, the spectral energies for almost all the points are higher than in point b (figure 7.13). If we check table 7.3 we can see that the values for m0 difference are very negative. This difference is higher for the lower frequencies in the interval [0.0067 - 0.012] Hz.

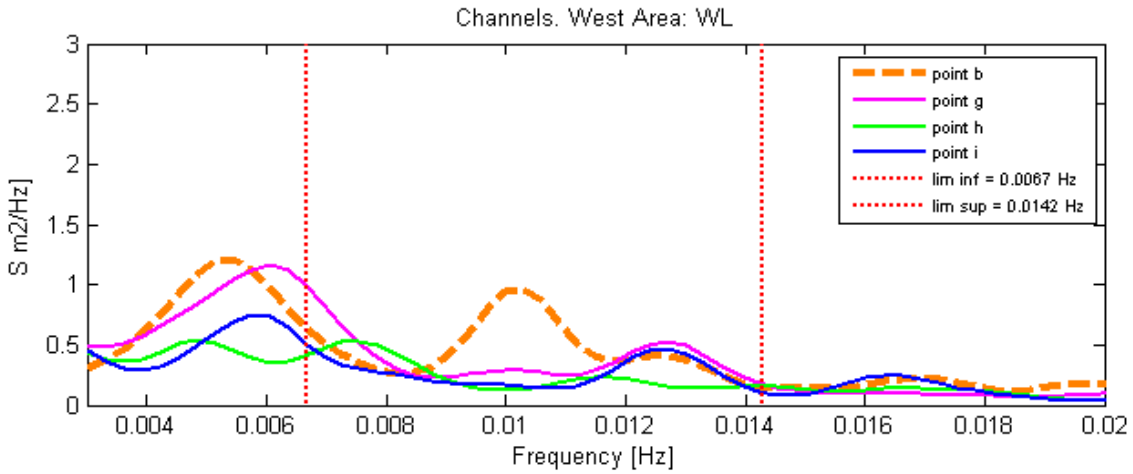

Figure 7.12 New layout analysis: channels. WL spectrums for West area points

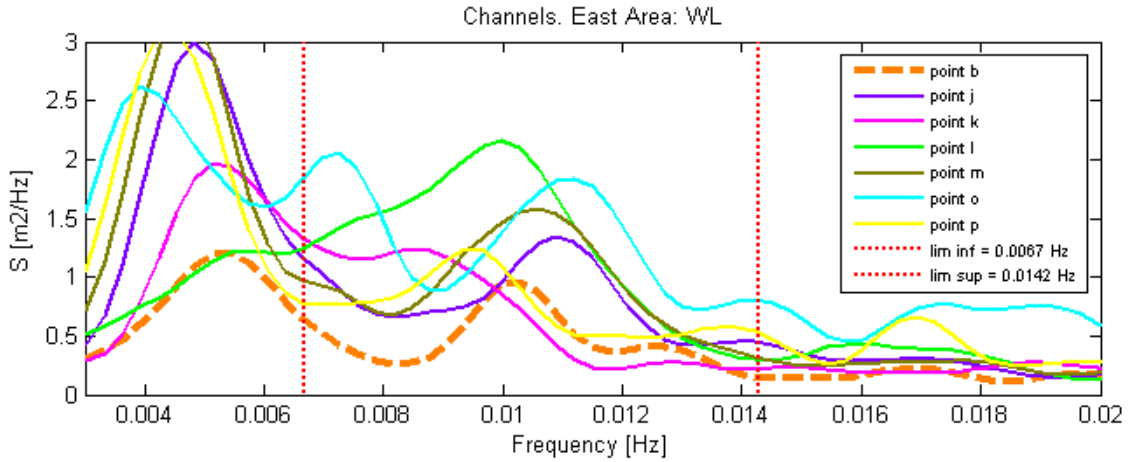

Figure 7.13 New layout analysis: channels. WL spectrums for East area points

Velocities

West area: table 7.3 shows positive values for points in west area for m0 difference parameter. In general for all the points, the spectral energies are smaller than in point b, although for the highest frequencies are quite close to point b (figure 7.14).

East area: for east area, we have positive or negative values depending on the point (table 7.3). Points l, m and o, have positive values for m0 difference, although very small values which means that these points energies are quite similar to point b energies (figure 7.15). For points j, k and p, happens the opposite: we have negative values for m0 difference, being very negative for point p.

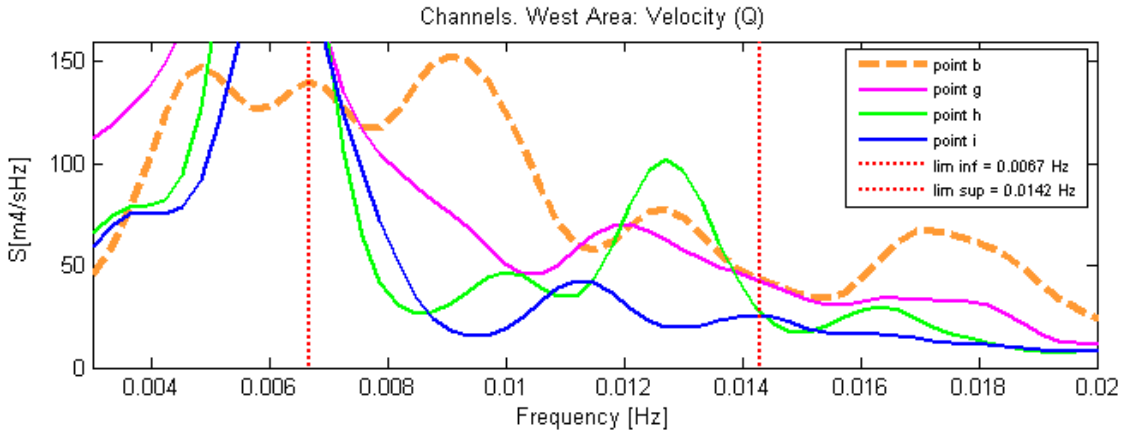

Figure 7.14 New layout analysis: channels. Velocity spectrums for West area points

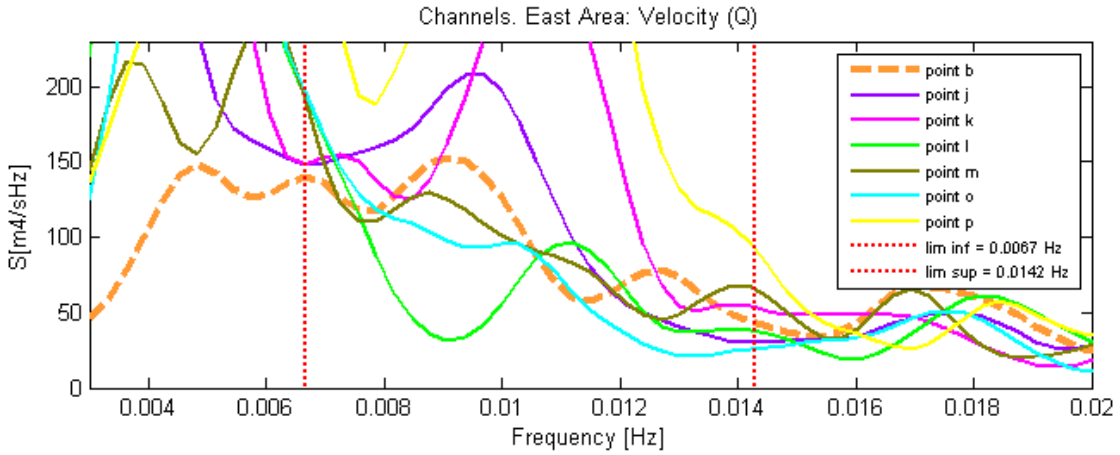

Figure 7.15 New layout analysis: channels. Velocity spectrums for East area points

7.3.3 No channels and channels simulations: comparison

Significant wave height

As we can see in table 7.4, the significant wave height is smaller for simulation with channels for all the points in all the areas: West, East and ore jetty area. This difference is more noticeable at the points included in the new channels as we hoped: the smallest differences are for points a, b, c and o (figure 7.16). For the rest of points, the difference in Hs is higher above all for these ones where the depth variation was higher like points j, k, l, m and p in east area and point i in west area (tables 7.4 and 7.5). A smaller depth makes the wave growth be higher because of the greater presence of different processes (shoaling, breaking....); there will be more interaction between waves and the bottom.

	Location	No Channels	Channel	Difference [%]
Ore jetty	a	0,452	0,421	6,86
	b	0,441	0,384	12,93
	c	0,439	0,38	13,44
West area	g	0,426	0,367	13,85
	h	0,372	0,309	16,94
	i	0,543	0,321	40,88
East area	j	0,796	0,525	34,05
	k	0,718	0,478	33,43
	l	0,701	0,552	21,26
	m	0,763	0,549	28,05
	o	0,687	0,643	6,40
	p	0,751	0,533	29,03

Table 7.4 No channels and channels simulations. Significant wave height comparison

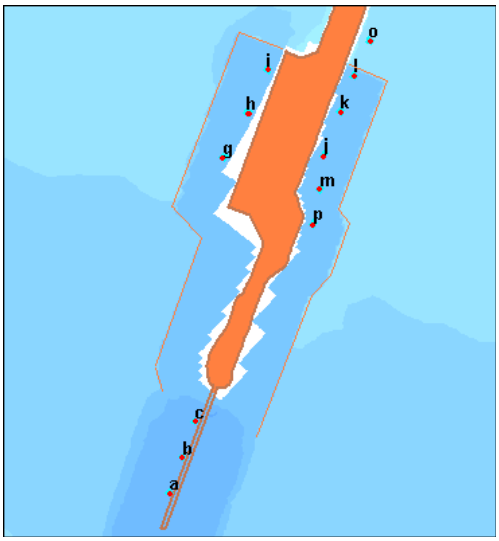

Figure 7.16 Points included in the new channels

Point	g	h	i	j	k	l	m	p
Actual depth (m)	13.46	13.42	3.5	7.55	7.86	8.99	9.38	8.45

Table 7.5 Actual depth of points included in the channels

Parameter "m0 difference" comparison

Table 7.6 shows the values of m0 difference for actual layout and simulation with channels; difference between situation with and without channel was calculated for each point.

		WL			Velocity (Q)		
		No channels [%]	Channels [%]	Difference	No channels [%]	Channels [%]	difference
West area	g	10.64	18.92	8.28	39.04	21.25	-17.78
	h	21.28	47.03	25.75	54.10	33.67	-20.43
	i	-100.00	43.24	143.24	83.64	52.75	-30.89
East area	j	-151.06	-72.97	78.09	32.45	-20.74	-53.19
	k	-163.83	-48.65	115.18	41.74	-60.31	-102.05
	l	-185.11	-175.68	9.43	47.75	27.02	-20.73
	m	-182.98	-97.30	85.68	44.22	4.35	-39.86
	o	-95.74	-181.08	-85.34	34.12	19.08	-15.04
	p	-119.15	-56.76	62.39	5.61	-163.76	-169.38

Table 7.6 No channels and channels simulations. Comparison m0 difference

Water levels

Like we saw in last section, the drop in significant wave height, was higher for the points included in the channels; then the drop in WL spectral energies will be higher for these points that for the ore jetty area (point b). What we get with the inclusion of the channels, is increasing the values of m0 difference for almost all the points (table 7.6); the relative differences between studied points spectral energies and point b increase and therefore the behavior in these areas (West and East) improves.

Velocities

In this case, the situation is completely different: the values of m0 difference parameter decrease with the inclusion of channels for all the points. In each area this variation is higher with the depth variation. These results means that the situation gets worse as relative differences for all studied points regarding point b decrease.
As we know, flow always try to follow the easiest way, what implies going through the biggest sections; so may be this increase in depth sections in West and East areas makes much more flow go through them and therefore increase the velocities in these areas.

Conclusions

The inclusion of channels in both areas, supposes an improvement water levels spectral energies regarding point b for all almost all the points in West and East area, and a worsening of the situation for the velocities. We will have to take into account these effects in the study of new areas in Saldanha Bay.

7.3.4 Selected point in West and East areas

After the analysis of both areas, a point of each area, among the previous studied, was selected how best location for the new jetty. This study is based on the results of section 7.3.2 as in section 7.3.1 we had different depth for each point.

West area: For WL, point h has the most positive value for m0 difference although values for point i are very similar (table 7.3). Spectral shape for both points are quite flat but almost all point i energies are smaller than point b (figure 7.12).
For the velocities, it is clear that point i has the best m0 difference value; m0 difference value is almost double positive than for points g and h (table 7.3). We have some discharge coming back from the coast, then as far we are from the coastline as higher is the discharge coming back and therefore the velocity; so may be points g, h and i have similar velocity gradients and the increase in points g and h in velocity energy is due to the outgoing discharge. This point requires deeper study. In spite of this supposition, we decided to recommend **point i** as best place for moored ships. Then, new jetty location is recommended to be built close to point i area, although the behavior in West area is better than point b for all the locations studied.

East area: For WL, points j, k and p have the best values of m0 difference although are negative values (table 7.3). As we can see in figure 7.13, these points are the ones which are closer point b energies.
Points with the best WL values for m0 difference parameter have the worst and negative values for the velocities (table7.3).
If we have to choose between both variables, it is more important to have low velocity energies as velocity gradients are the cause of surge motion. Point l has the lowest energy for velocities, indeed lower that point o located out of the channel. If we check point l position, we can see that is closer to the end of the channel and this smaller energy for velocity is surely due to that. We decided to do another simulation with longer channel (figure 7.17). Red rectangle was added to the old channel.

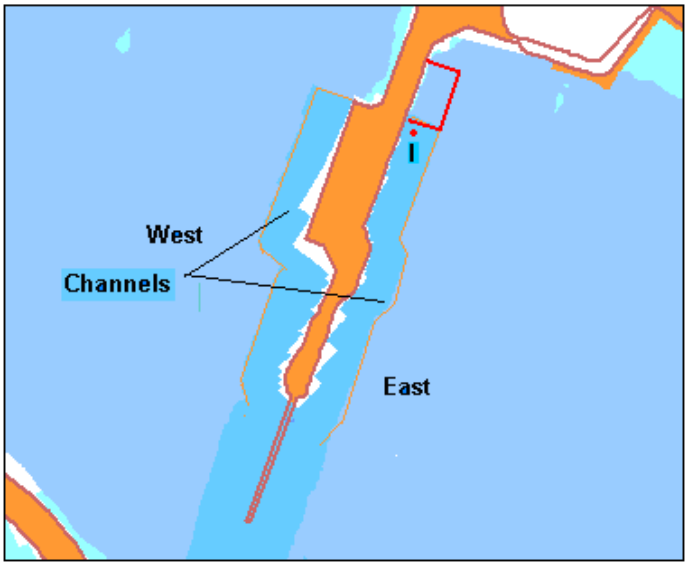

Figure 7.17 East area: New longer channel layout

		WL		Velocity	
		m0-bias (m2)	m0 difference [%]	m0-bias (m4/s2)	m0 difference [%]
l	no channel	0.0134	-185.11	0.444	47.45
	short channel	0.0102	-175.68	0.570	27.02
	long channel	0.0078	-110.81	0.768	1.66
m	long channel	0.0065	-75.68	0.778	0.38

Table 7.7 East area selected point. New longer channel results

As happened with the inclusion of the old channel, WL energy decrease and velocity energy increase for point l with the new channel (longer) (table 7.7, figures 7.18 and 7.19); the reasons are the same as section 7.3.3. For the new channel, point l velocity energy continue being smaller than point m, that was the only point included in the old channel, as well as point l, with positive value for m0 difference (table 7.3). On the other hand, point l has worst m0 difference value for WL than point m; but taking in account that velocity is more important variable than WL, we decided to choose **point l** as best location in east area for moored ships.

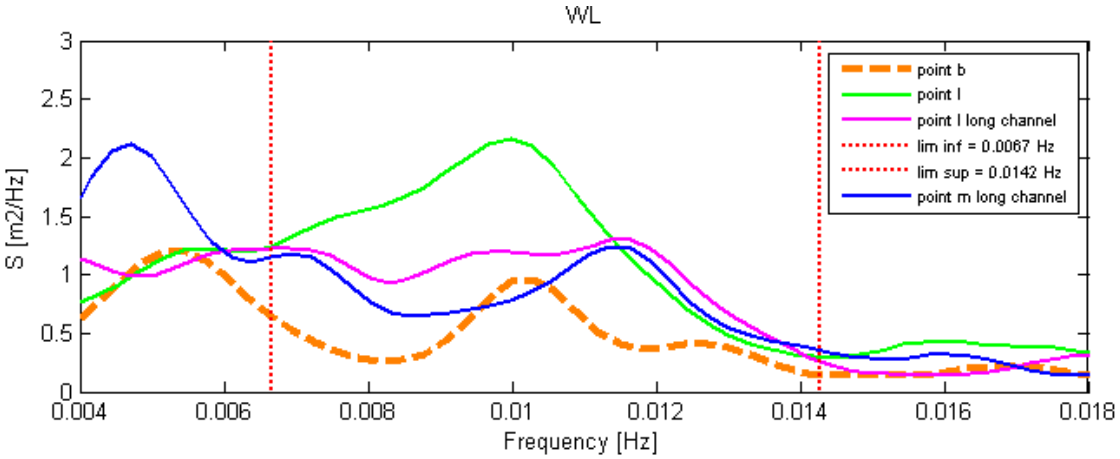

7.18 East area selected point. New longer channel: WL spectrums

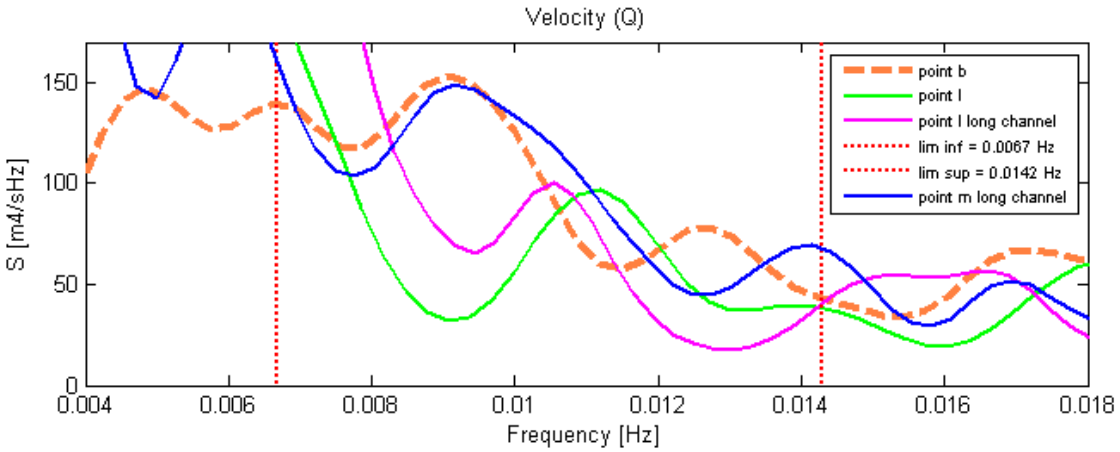

7.19 East area selected point. New longer channel: Velocity spectrums

7.4 Area 3 analysis

Last study was done for area 3 although briefer than for West and East areas. The variables selected and calculated, parameters used in the study and the way to do it, were the same as for West and East areas (see 7.2 and 7.3).

Point	q	r	s	t
Actual depth (m)	7.18	7.65	7.4	10.83

Figure 7.8 Actual depth of area 3 points

Next, results for area 3 simulation are given.

	WL		Velocity	
	m0-bias (m2)	m0 difference [%]	m0-bias (m4/s2)	m0 difference [%]
q	0.0023	51.06	0.221	74.00
r	0.0048	-2.13	0.168	80.24
s	0.0013	72.34	0.295	65.29
t	0.0029	38.30	0.261	69.29
b	0.0047	-	0.850	-

Table 7.9 Actual layout analysis: results for area 3 points: m0-bias and m0 difference

Water Levels

The m0 difference values are positive and high for all the points except for point r (table 7.9). The difference between studied and point b energies are higher above all for the frequencies [0.009 - 0.012] Hz while for the other ones are approximately the same as point b (figure 7.20). Only we have really big spectral energies at the lower frequencies of the interval for point r, being this, the reason of the negative values.

Velocities

Table 7.9 shows high positive values for points in area 3 for m0 difference parameters. The spectral energies are much smaller than in point b for all the frequencies at all the points (figure 7.21).

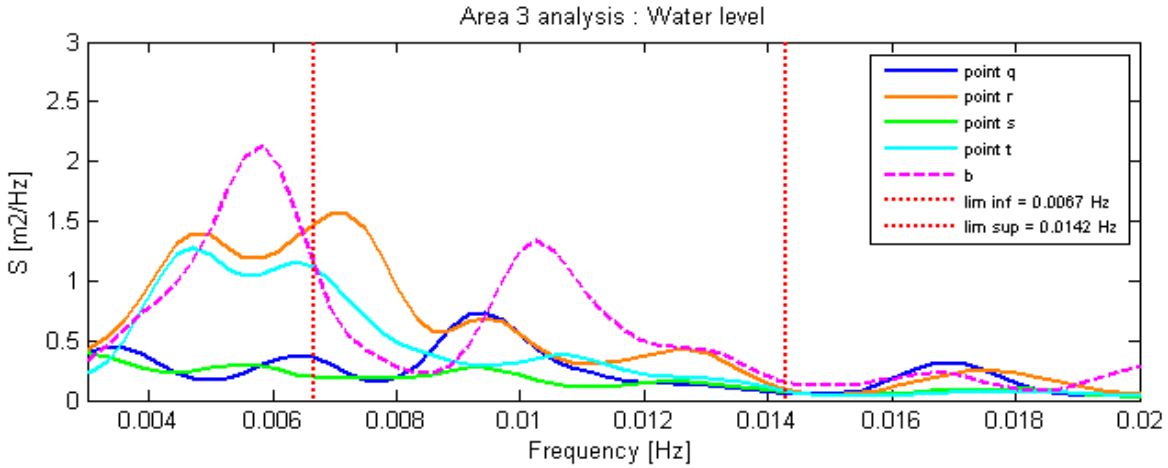

Figure 7.20 Actual layout analysis: WL spectrums for area 3 points

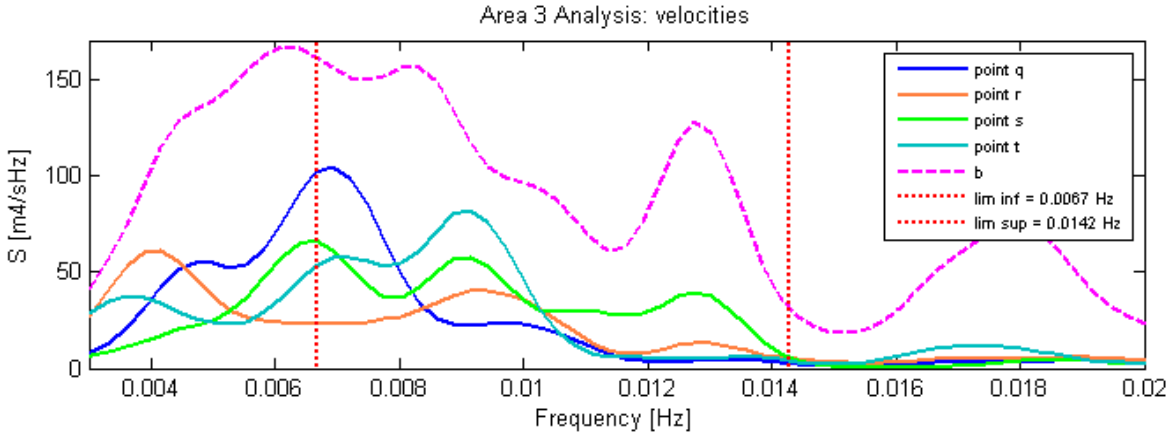

Figure 7.21 Actual layout analysis: Velocity spectrums for area 3 points

If we check both graphs (figures 7.20 and 7.21) we can see like the high WL energies at point r for [0.006 - 0.0085] Hz frequencies fit in the smallest energies for velocities; we can say for these frequencies, point r is near antinode (standing wave).
Similar situation happens with point q for [0.08 - 0.01] Hz.

7.5 Conclusions

For no channels simulations (actual layout), West area has a little bit smaller energies than at ore jetty area (point b) for WL, while for east area we can appreciate a high difference between studied points and point b, being the WL spectral energies for all the studied points in this area higher than in point b.
For velocities, both areas show a similar behavior; both have smaller energies than point b, although East area has some point with no very good results for the parameters analyzed.
Taking all said before into account, we can conclude from the analysis without channels, West area is better location than East for the new jetty.

With the inclusion of the channels in the layout we get to increase the difference for water levels spectral energies (more positive m0 difference parameter) between studied points and point b, for all the points in West and East area (see 7.3.4). In spite of this increase, WL spectral energies for East area, continue being higher than point b. The behavior for West area points is indeed better than the situation without channels.
For velocities, the worsening of the situation with the inclusion of the channels, makes spectral energies for East area points be higher than for point b; we have switched the situation: from being in a acceptable situation without channels, we are now in worse conditions than point b. The situation for West area velocities does not change so much as for East area, from no channels to channels simulations.
In this case, it is clearer that West area is better location for the new jetty than East.

Although the analysis was done just for storm 3, brief analysis was carried out with storm 2 for the actual layout. Conclusions obtained are quite similar to analysis with storm 3 (appendix E).

For Area 3 just a brief study was done. This area shows good results for both, WL and velocities, being much better than West results for velocities. This area seems a good option for location of the new jetty as well; but a deeper study has to be carried out with inclusion of channels to check the effects on both variables and compare with West area results.

Next, graphs with WL and velocity spectrum for point b and best points in West and East area for new jetty location, are shown (figures 7.22 and 7.23). Results from simulation with channels was used to get spectrums for points b and i, while for point l was used the simulation with the longer channel for east area (figure 7.17). At point i energies for both, WL and velocities, are smaller than point b for all the frequencies. It does not happen this to point l in East area, as WL energies are higher than point b energies for all the frequencies; moreover velocity energies for point l are quite close or indeed higher than point b for the highest frequencies of the interval. It is clear than point i in West area is much better location for the new jetty.

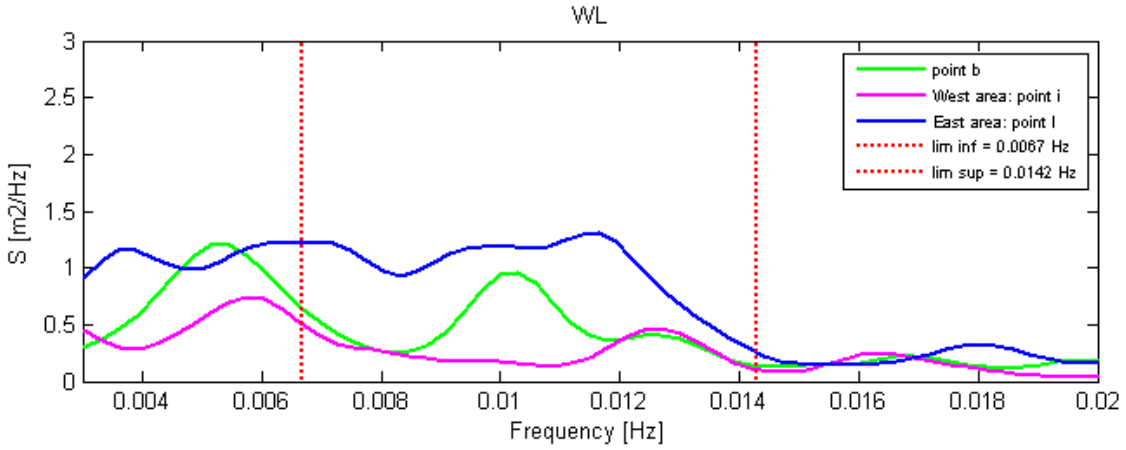

Figure 7.22 Analysis new jetty location. Points b, i and l WL spectrums

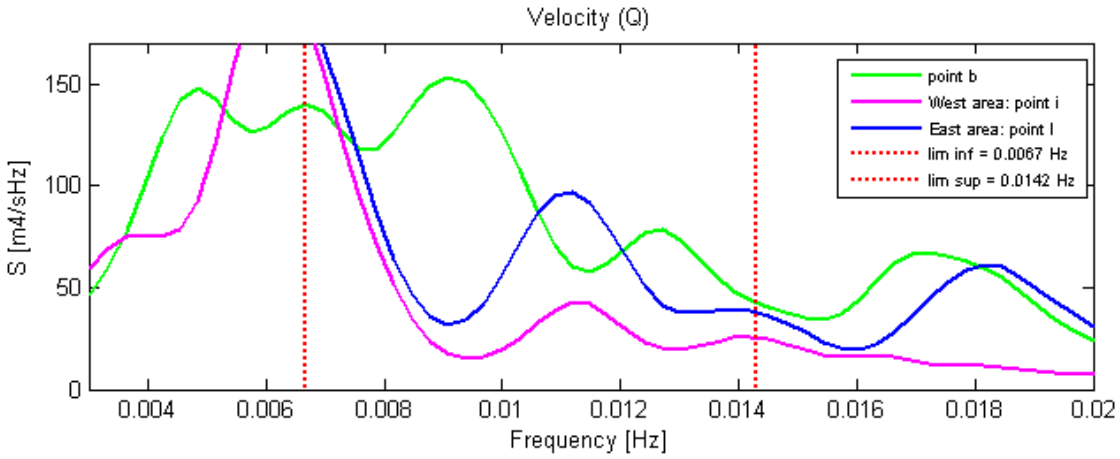

Figure 7.23 Analysis new jetty location. Points b, i and l velocity spectrums

Chapter 8

Conclusions and recommendations

8.1 Conclusions

8.1.1 Main research objectives

Hydrodynamic model

The numerical model SURFBEAT is suitable for application in harbor areas, since the energy levels simulated by the program have good agreement with the measured data.

Sensitivity analysis

Overall sensitivity of the model is quite high, above all for the lowest frequencies. Slight changes in certain parameters, like directional parameters (mean direction and directional spreading), can mean all the difference. It is demonstrated then, that the wave direction and spreading are very important for the determination of the wave action inside the port areas and consequently the wave forces.

New buoy and jetty location

Research carried out gives a general idea of the energy distribution in Saldanha Bay.
A new buoy location is given for East and West area from the studied points, trying to locate it as closer as possible from antinodes.
It is proved that the energy in West area is smaller than East area for both, WL and velocity and smaller than ore jetty area as well. We can conclude East area is not a good location for a new jetty and it is recommended to focus on West area for the new location. On the other hand, area 3 seems a good location for new jetty as well, but large study has to be carried out.

8.2 Recommendations

Hydrodynamics

For the exact calibration of the free parameters of the SURFBEAT model, as the wave height to depth breaking parameter (γ) and the friction coefficient, deeper research must be done in order to establish the optimum value. It is recommended to place a cross-shore array of pressure gauges or a similar device at shallow water and far from the harbor entrance. Then the procedure suggested by Gallagher et al [1998] can be applied (appendix F).
Probably the inclusion of different values of the wave height to depth breaking parameter (γ) in the same domain would be recommendable.

Grid definition

The proper distribution of energy needs a very fine grid structure and very gentle smoothing. The energy flow under diffraction is certainly not accurate if sharp bends occurs in a fairly coarse grid geometry. Some recommendations to make the grid, are given in appendix F.

Measurements

The main problem in Saldanha Bay study was the lack of data. For an accurate study is recommended the presence of more gauges in the area. Two directional gauges to record short and long waves, one at offshore location in Saldanha Bay area and another one inside the small bay. With the first one will be possible to get information at the sea boundary (short and long wave height and directional information) very useful for calibration procedure. Further, directional and long wave measurements at other locations (like gap situated between the islands and the breakwater, and the midpoint of the main bay) could point out whether the prediction for the long waves at this point is realistic.

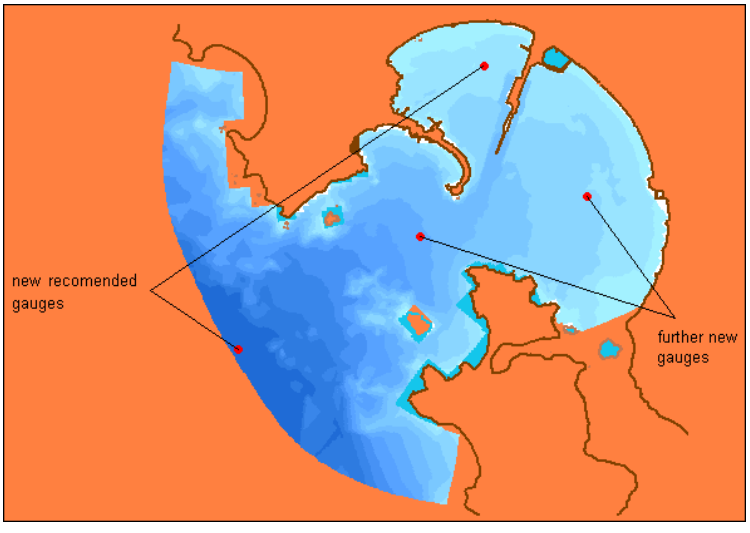

Figure 8.1 New recommended gauges

Further research

Further research the observed forerunners in Saldanha Bay, by looking at storm tracks and distances to the bay, to study the cause and origin of generation.

Further research, at East and West area with the new measurements (new gauges) to verify the conclusions of this report; if these ones are correct, focus on the study in West area studying more locations and with more storms (different mean direction).
Area 3 can be a good location for the new jetty as well, but a study has to be carried out for more points and with the inclusion of a channel.

Appendix A

A.1 Circular caissons

Figure A.1 Photograph showing the jetty construction

A.2 Stationary pattern: standard deviation - time graph

Standard deviation – time graph

Selected storms periods have to be approximately stationary to get real results which can be compared with the simulated ones. A “standard deviation – time” graph was obtained for each storm to check that the standard deviation keeps constant during the selected periods. This kind of graph was used for the simulated series as well to study when the simulations are approximately stationary.
For each time-step, standard deviation of the next 20 minutes interval data (serie) was calculated (figure A.2); in this way we can represent for each time-step the pair of data (t, σ) (figure A.3).

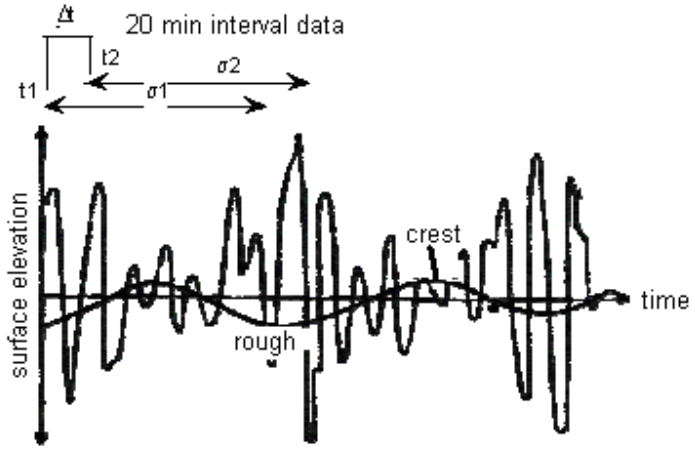

Figure A.2 Standard deviation for each 20 minutes interval data

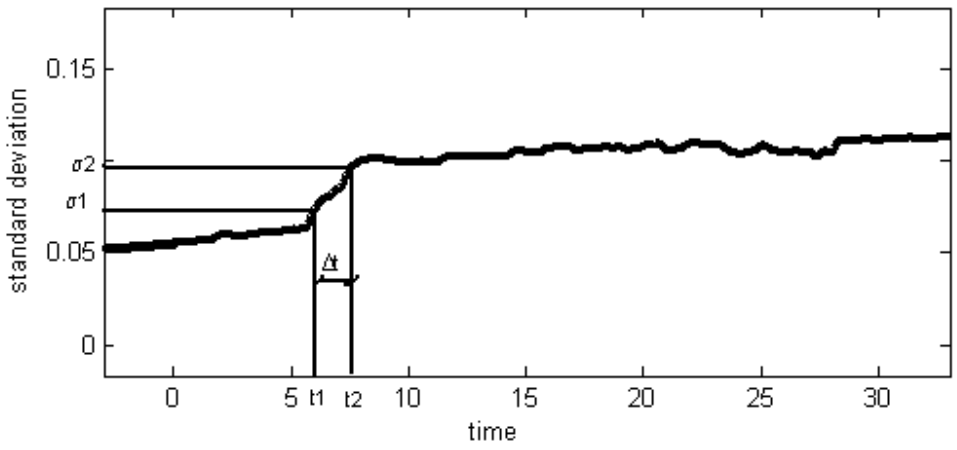

Figure A.3 standard deviation - time graph example

Appendix B

B.1 Delft-RGFGRID

The purpose of the Delft-RGFGRID program is to create, modify and visualise orthogonal, curvilinear grids for the Delft3D-FLOW module.
Curvilinear grids are applied in finite difference modelling to provide a high grid resolution in the area of interest and a low resolution elsewhere, thus saving computational effort.
Grid lines may be curved along land boundaries and channels, so that the notorious 'stair case' boundaries, that may induce artificial diffusion, can be avoided.
Curvilinear grids should be smooth in order to minimise errors in the finite difference approximations. Finally, curvilinear grids for Delft3D-FLOW have to be orthogonal, which saves some computationally expensive transformation terms. Extra effort in the model setup phase, results in faster and more accurate computations.

Delft-RGFGRID is designed to create grids with minimum effort, fulfilling the requirements of smoothness and orthogonality. The program allows for an iterative grid generation process, starting with a rough sketch of the grid by splines. Then, the splines are transformed into a grid that can be smoothly refined by the program. Whenever necessary, you can orthogonalise the grid in order to fulfil the Delft3D-FLOW requirement of orthogonality.
Various grid manipulation options are provided in order to put the grid lines in the right position with the right resolution. For instance, a grid line can be 'snapped' to a land boundary. The surrounding grid smoothly follows. More detail is brought into the grid after every refinement step.
Existing grids may be modified or extended using this program. Grids can be locally refined by insertion of grid lines. The resulting local 'jump' in grid sizes can be smoothed by a so called 'line smoothing'.
Bathymetry data can be displayed on the screen, so that internal gullies can be taken into account while drawing the design grid. Existing model grids can be loaded and displayed on the screen, while creating new grids to be pasted later to the original. Before each modification or edit action, the grid is saved to the so-called 'previous state' grid. Pressing *'Esc'* after an edit action, or selecting *Operations*, *undo*, copies the previous state grid back to the grid. If desired, the previous state grid can be displayed together with the actual grid.
Grid properties such as smoothness, resolution, orthogonality etc, can be displayed to check the grid quality. Graphical output can easily be created in various formats.

B.2 Narrow banded spectrum

Delft-3D can only be used in cases where the wave spectrum is narrow-banded both with respect to frequency and with respect to direction:

- Frequency: Surfbeat calculates celerity for the different groups created; so if the spectrum is not narrow-banded in frequency, celerity for waves in each group will be more different than cg, and error made will be higher.

- Direction: if we really have high direction variation in waves, the mean direction, in which all the waves groups are propagated in surfbeat, will be further from reality and the error made will be higher.

Appendix C

C.1 Jonswap spectrum

	m0 value	peak energy	peakedness parameter
storm 1	0.628	25.07	3.90
storm 2	1.629	54.36	1.58
storm 3	1.585	60.12	1.50
storm 4	0.831	55.15	4.26

Table C.1 Storms peakedness parameter

Next graphs show measured spectrum at Wave Rider and Jonswap spectrums for each storm. We have two Jonwap spectrums for each one: both have the same m0 value that measured one; first was obtained by dividing Jonswap spectrum energy values for Jc (equation 4.17). Then,we obtainend the second one, changing peakedness parameter (γ) value till Jonswap spectrum energy peak was the same as Wave Rider energy peak.

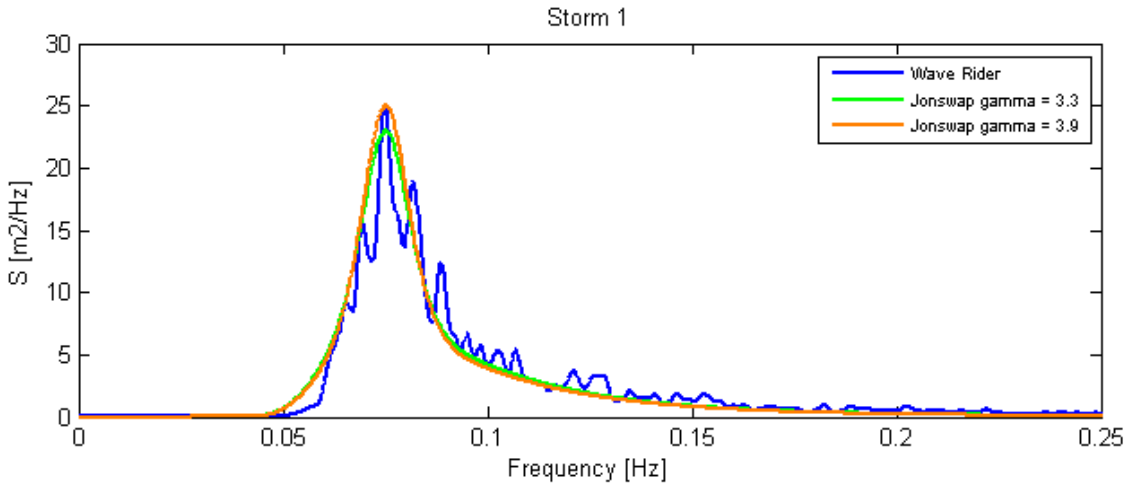

Figure C.1 Storm 1: measured (Wave Rider) and Jonswap spectrums

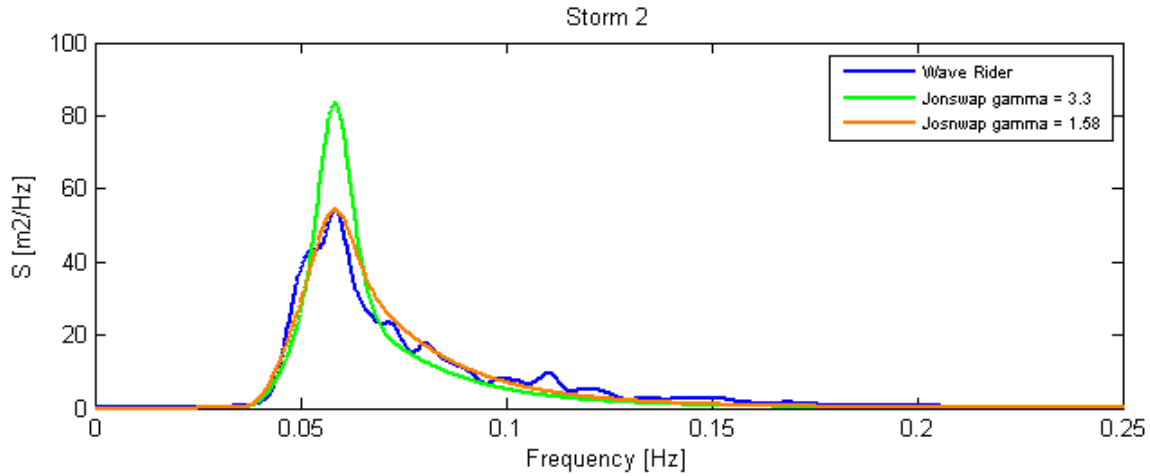

Figure C.2 Storm 2: measured (Wave Rider) and Jonswap spectrums

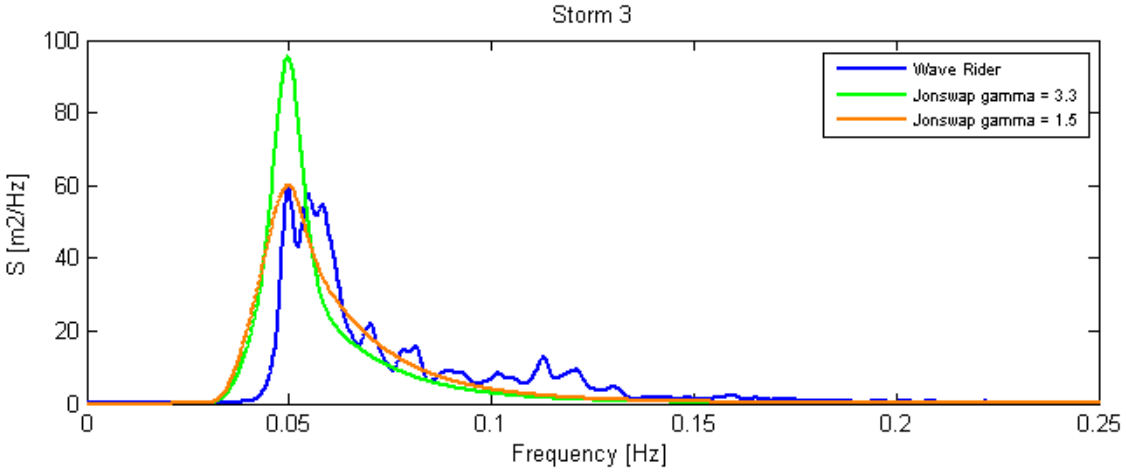

Figure C.3 Storm 3: measured (Wave Rider) and Jonswap spectrums

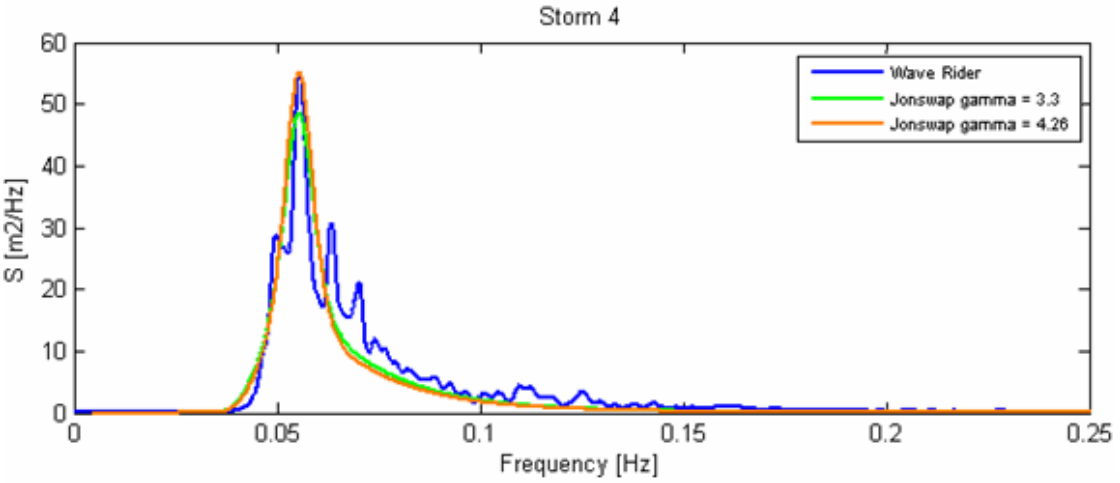

Figure C.4 Storm 4: measured (Wave Rider) and Jonswap spectrums

C.2 Wave component file

In this section we will describe the structure of the file 'wavcmp' that prescribes the Fourier components of the incoming short and long wave signals. The following records must be provided in the free format; after the prescribed number of values in each record, any comment can be added as only the required values per record are read.

N_{comp}			
f_{split} [Hz]			
f_1 [Hz]	a1 [m]	φ1 [eg]	Θ1 [deg]
...	....	....	...
....	....	....	....
f_Ncomp [Hz]	aNcomp [m]	φNcomp [eg]	ΘNcomp [deg]
nmskf	nmskl	mmskf	mmskl
timtap [sec]			

Table C.2 Wave components file structure

- N_{comp}: is the number of spectral components.
- f_{split}: is the splitting frequency between the long and short waves. Only the components which have a frequency lower than f_{split} will be prescribed at the boundary as free waves. The other components are used to determine the incoming high frequency wave energy field which will generate forces waves in the model.
It's assumed for he frequencies of the wave components that fj < fp if j<p.

- nmskf is the grid number in eta dir below which the wave forces are gradually and artificially reduced to zero at the lower boundary.
- nmskl is the grid number in eta dir below which the wave forces are gradually and artificially reduced to zero at the upper boundary.
- mmskf is the grid number in ksi dir below which the wave forces are gradually and artificially reduced to zero at the left boundary.
- mmskl is the grid number in ksi dir below which the wave forces are gradually and artificially reduced to zero at the right boundary.

By using -1 for one or more of these four parameters the reduction of the wave forces does not take place near the corresponding boundary.

- Timap is the time in seconds that is used by the taper for the incoming signals. It is advised to define timtap at least several times as large as the period of atypical group in the signal.

Wave components file are calculated at each point of flow sea boundary using the energy spectrum obtained from the wave run.

amplitude (aj)
If we use an equidistant grid (with grid size Δf) for the frequency, the energy in one frequency bin can be approximated by $\Delta f \; E\left(j \; \Delta f \right) = 0.5 \; a_j{}^2$ where a_j is the amplitude assigned to the bin. Like Δf and E are know from the flow boundary energy spectrum, a_j can be calculated.

frequencies (f_j)
Like we are using an equidistant grid, frequencies can be got easily.

Phase (φj)
The phase values are random. The phase φj of the j-th component is drawn from a uniform distribution on [0-2π].

Directions (Θj)
One direction is assigned to each frequency bin. This direction is determined by using the directional spreading function for the frequency bin to define a probability density function and then randomly draw from the distribution.

1000			
4.6			
0.03			
0.134	0.005	56.461	0
0.1344	0.005	149.887	0
0.1349	0.006	33.853	0
0.1353	0.006	161.981	0
0.1358	0.006	312.895	0
0.1362	0.006	140.982	0
0.1367	0.007	91.002	0
0.1371	0.007	127.577	0
0.1376	0.007	267.472	0
0.138	0.007	234.3	0
....	.....	.....	.....
.....	.....	....	.....
0.5816	0.003	252.704	0
0.582	0.003	315.014	0
-1,	-1,	-1,	-1
30			

Table C.3 Wave component file example

C.3 Grid cell size definition

It is very important to define the right cell size; a rough grid, can make us lose information about the higher frequencies; less information as more rough is the computational grid. As example, in figure C.5 we can see two simulated spectrums for different grid cell sizes for storm 1: for the simulation with the rough grid (average grid cell size of 100 m) we do not have energy for frequencies higher than 0.02 Hz. The model, with such a rough grid, can only simulate the slowest waves groups as for the faster wave groups it has a few points to represent them.
After different simulations, an average grid cell size of 30 m was selected for the simulations (accurate grid).

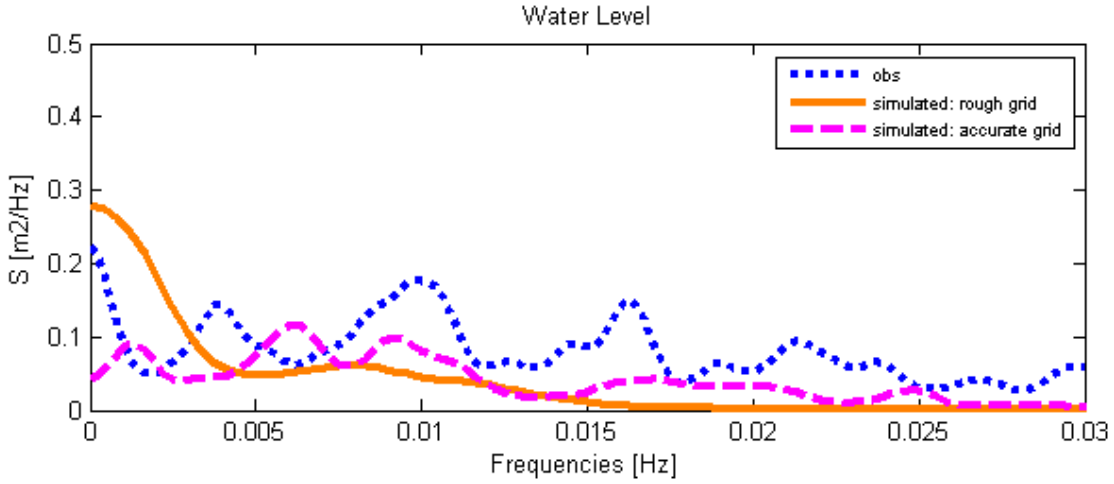

Figure C.5 Grid cell size definition: water level spectrums

C.4 Breaker index parameter (γ)

Losada [1999] proposed a relation between γ and the foreshore slope (equation C.1). A slope value of 0.035 corresponds to γ = 0.55; so like the slope in Saldanha Bay is about 0.015, was decided to use a value of γ = 0.45 for the first simulation.

$$\gamma = 0.35 + 5.8 \ \tan(\alpha) \qquad \text{(C.1)}$$

Appendix D

D.1 Breaker index parameter (γ)

The γ parameter is defined as the wave height to water depth ratio, which is related to the wave depth-breaking condition; then this parameter controls the breaking area near the coast.

$$Hs = \gamma h \qquad (d.1)$$

where Hs is significant short wave height and h is the depth (bound wave - bed).

Surfbeat uses equation d.1 to simulate the breaking wave process nearshore. Given a significant short wave height and depth, as higher is γ parameter as nearer from the coast will break wave groups. As we can see in figure d.1, with a higher value of γ , the slope of the curve will be higher as well; then the curve will reach the incoming significant wave height before and therefore closer to the coast. This wave breaking closer to the coast makes the length (area) of short waves growth larger so we will have higher Hs and therefore more energy.

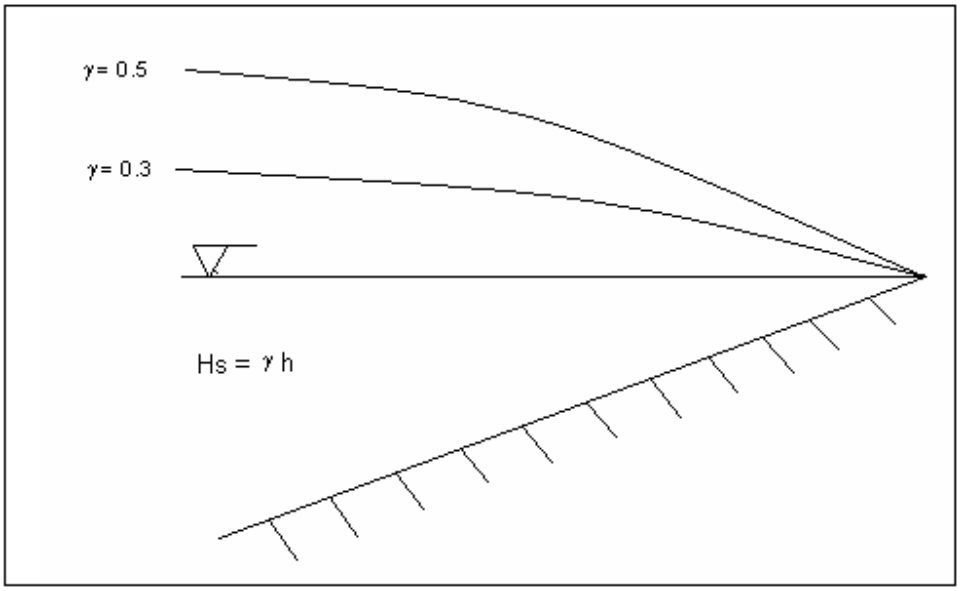

Figure D.1 Surfbeat breaker index parameter equation

Appendix E

E.1 New buoy location: study points selected

Point	x[m]	y[m]	z[m]
1	406283	345452	10.03
2	406780	345162	10.29
3	406722	345706	8.9
4	406304	345007	11.06
5	405362	346207	8.83
6	405559	346580	8.6
7	404985	346450	7.36
8	404892	345876	9.03
9	405957	346388	8.01
10	406515	345276	10.15
W1	405310	346028	9.4
W2	405200	346165	8.32
W3	405168	346079	8.49
W4	405284	346313	8.61
W5	405136	345989	8.66
W6	405223	346234	8.52

Table E.1 New buoy location: study points coordinates
R.E.F point (405714 , 345821). Figure 6.3

E.2 New jetty location: study points selected

Point	x[m]	y[m]	z[m]
a	405170	343523	26.29
b	405170	343706	25.47
c	405237	343890	26.72
g	405384	345281	13.46
h	405519	345505	13.42
i	405612	345733	3.5
j	405913	345286	7.55
k	405993	345509	7.86
l	406069	345693	8.99
m	405899	345107	9.38
o	406145	345881	8.1
p	405854	344923	8.45
q	402289	345668	7.18
r	402756	345504	7.65
s	402172	345435	7.4
t	402696	345128	10.83

Table E.2 New jetty location: study points coordinates

R.E.F point (405714 , 345821). Figure 6.3

E.1 Storm 2: actual layout analysis

Analysis for actual layout was done with storm 2 to check if the response of the bay was similar to storm 3 results.
As we can check in 5.3.2, dissipation for storm 3 is higher than storm 2 at the small bay (figures 5.16 and 5.17), above all on the left side at the gap between the island and the breakwater where the differences for significant wave height between both storms are the highest. If we remember, storm 3 has a direction of 224º (figure 5.16) then more southern than storm 2. It causes that the waves can not enter so direct into the main bay, neither the cause-jetty area (figure 7.1). Therefore, it is expected to have higher energy (water levels) for storm 2 at East and West areas. Tables E.3 and E.4, show the results for WL and velocities in both areas for both storms. As we can see, m0 difference parameter for WL is smaller for all the points for storm 2; it means that the spectral energy for WL is higher in East and West areas than at the ore jetty. In spite of being all these values negatives, as for situation with storm 3, these values are more negative for points at East area. On the other hand, values for velocities are very similar to values with storm 3.
Taking into account the effects of the channels on WL and velocities, we can expect values for WL similar to ore jetty area for West area and worst for the East area, and same results for velocities that the case with storm 3. From this analysis we can conclude that west area continues being the best option for new jetty.

		WL		Velocity	
		m0-bias (m2)	m0 difference [%]	m0-bias (m4/s2)	m0 difference [%]
West area	g	0.0033	-50.00	0.425	35.31
	h	0.0031	-40.91	0.316	51.90
	i	0.0062	-181.82	0.128	80.52
East area	j	0.0064	-190.91	0.354	46.12
	k	0.0101	-359.09	0.199	69.71
	l	0.0063	-186.36	0.441	32.88
	b	0.0022	-	0.657	-

Table E.3 Storm 2. Actual layout analysis: no channels. Results for West and East area points: m0-bias and m0 difference

		WL		Velocity	
		m0-bias (m2)	m0 difference [%]	m0-bias (m4/s2)	m0 difference [%]
West area	g	0.0042	10.64	0.518	39.04
	h	0.0037	21.28	0.390	54.10
	i	0.0094	-100.00	0.139	83.64
East area	j	0.0118	-151.06	0.574	32.45
	k	0.0124	-163.83	0.495	41.74
	l	0.0134	-185.11	0.444	47.75
	b	0.0047	-	0.850	-

Table E.4 Storm 3. Actual layout analysis: no channels. Results for West and East area points: m0-bias and m0 difference

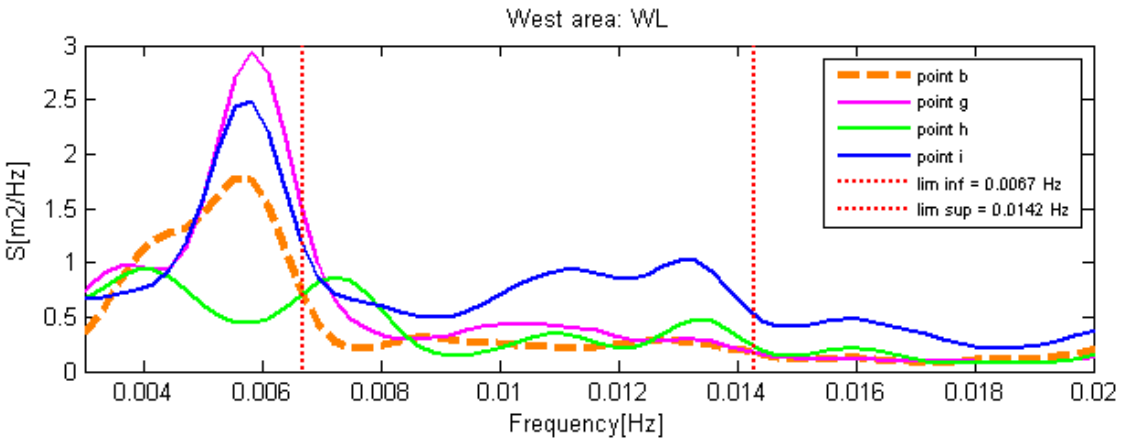

Figure E.1 Actual layout analysis: no channels. WL spectrums for West area points

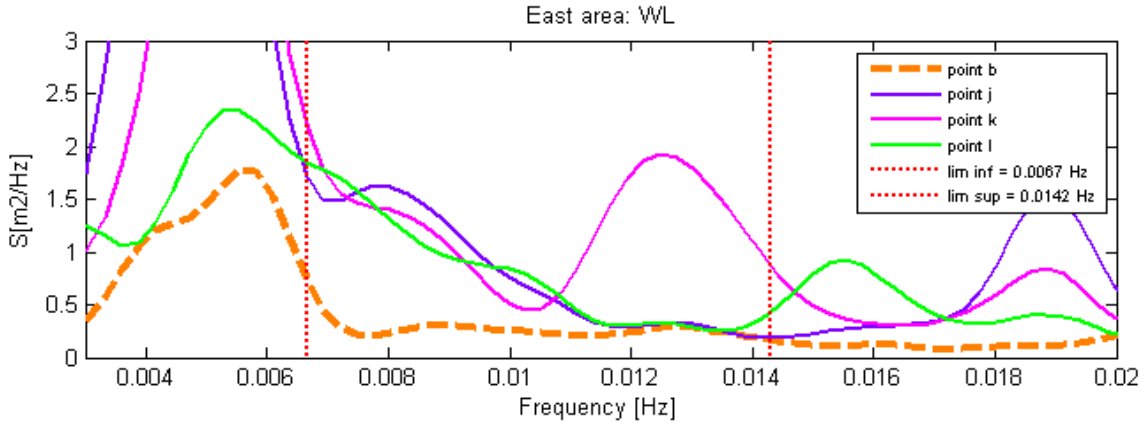

Figure E.2 Actual layout analysis: no channels. WL spectrums for East area points

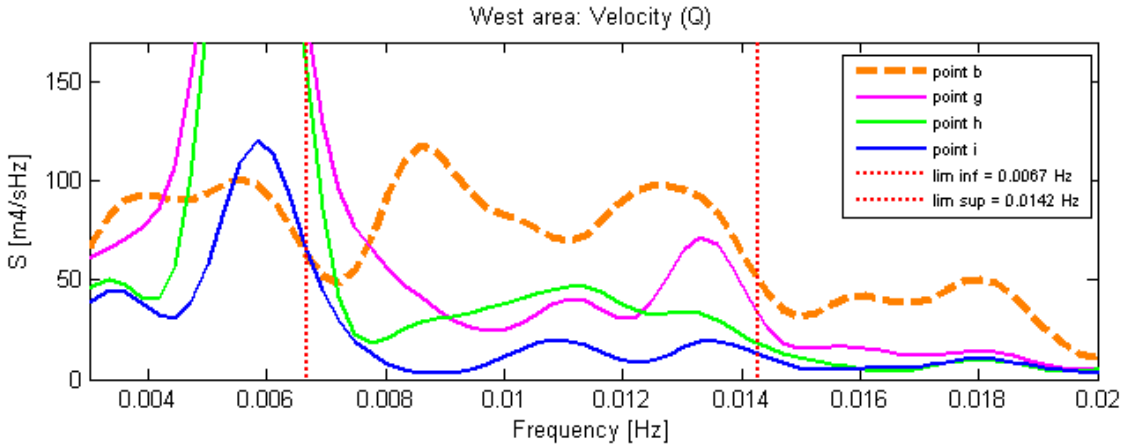

Figure E.3 Actual layout analysis: no channels. Velocity spectrums for West area points

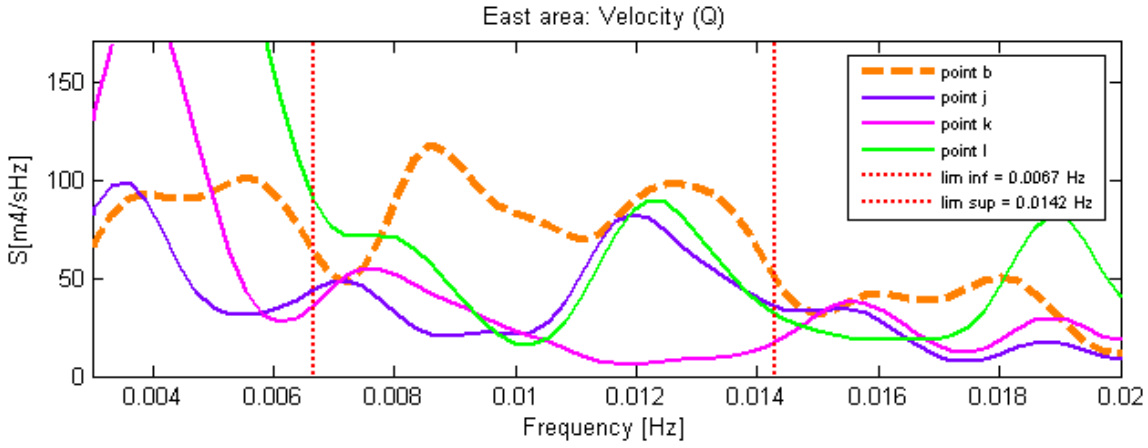

Figure E.4 Actual layout analysis: no channels. Velocity spectrums for East area points

Appendix F

F.1 Breaking index parameter (γ): accurate calculation procedure

The idea is to place a cross-shore array of pressure gauges or a similar device at shallow water and far from the harbor entrance. In this way, we can measure long and short significant wave height and depth in each measure point. Known significant wave height and depth, we can obtain value of γ from equation f.1 for each point and calculate an average value for the bay.

$$Hs = \gamma\, h \qquad (f.1)$$

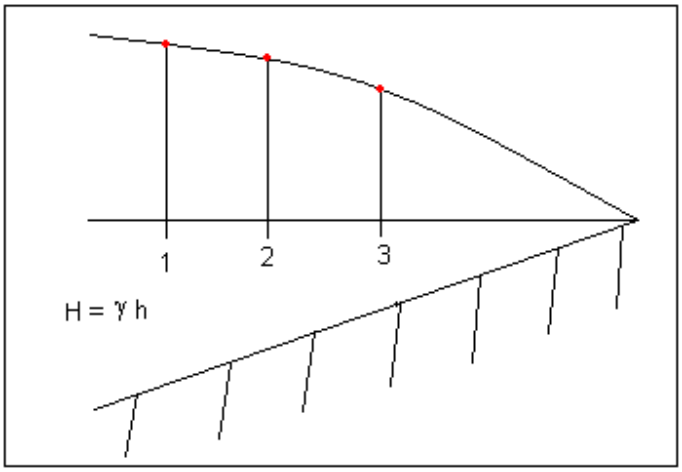

Figure F.1 Breaking index parameter (γ): accurate calculation procedure

F.2 Some notes to future modelers

Some general notes have been added explaining the rudimentary procedure to follow to make a grid for an area. Please read the mean Delft 3D manual and tutorials First before starting modeling with Surf Beat. This way you can familiarize yourself with the staggered grid used and the files needed for a FLOW calculation.

1. Determine carefully which area is to be modeled. Check whether the upward sea boundary has at least intermediate water depth conditions. If you are unsure of the longshore size of you grid, make it larger then necessary in this direction to make future extensions possible. It is quite some work to make a detailed grid from scratch it is important to think this stage through including extensions to the grid you might want to make for future simulations.

2. Make the grid using splines in the rgf- grid generator featured by Delft 3D. Keep in mind that as much boundary points as possible should lie on the same grid line. Make sure the grid direction corresponds to the land boundaries for almost all locations. The time needed to make this will certainly save you a lot of time later on. The FLOW or Surf Beat grid can be curve-linear. It is advised to keep the grid rectangular and curve-linear of shape.

3. Make the Swan grid file with the Surf Beat grid as passive grid. This way you can make sure the Swan grid fits the size of the FLOW grid file. Also ensure the grid is larger in all directions.

4. The .dep files are now to be created for both Swan and Surf Beat corresponding to both grids previously mentioned.

5. Open flow and swan .dep files in notepad and use CTRL+h to replace all the -999.000 values to corresponding minimum depths. Do the same with negative values for flow .dep file. The Flow program sometimes behaves strangely when maintaining these values.

6. The morf-file is probably set up to run a dummy calculation first to obtain the correct dimensions and set up of the com-file. After this is done one HISWA calculation will be performed. Then the main Surf Beat calculation is started using the number of steps defined in the bottom of the morf-file. Calculation times defined in the Flow module are ignored. Please note that the storage times should be larger than the period you want to model.

7. Analyze your results using the MATLAB-Delft 3D interface and your own scripts. Inspect water level in d3d quickplot on the map file for numerical instabilities or strange behavior in the bi-chromatic wave.